NREL/TP-451-5755 • UC Category: 273 • DE93018213

Polycrystalline Thin Film Materials and Devices

Final Subcontract Report
16 January 1990 – 15 January 1993

R. W. Birkmire, J. E. Phillips,
W. N. Shafarman, S. S. Hegedus,
B. E. McCandless, T. A. Yokimcus
Institute of Energy Conversion
University of Delaware
Newark, Delaware

NREL technical monitor: B. von Roedern

National Renewable Energy Laboratory
1617 Cole Boulevard
Golden, Colorado 80401-3393
Operated by Midwest Research Institute
for the U.S. Department of Energy
under Contract No. DE-AC02-83CH10093

Prepared under Subcontract No. XN-0-10023-1

August 1993

NOTICE

Printed in the United States of America
Available from:
National Technical Information Service
U.S. Department of Commerce
5285 Port Royal Road
Springfield, VA 22161

Price: Microfiche A01
Printed Copy A07

Codes are used for pricing all publications. The code is determined by the number of pages in the publication. Information pertaining to the pricing codes can be found in the current issue of the following publications which are generally available in most libraries: *Energy Research Abstracts (ERA); Government Reports Announcements and Index (GRA and I); Scientific and Technical Abstract Reports (STAR)*; and publication NTIS-PR-360 available from NTIS at the above address.

Printed on recycled paper

DISCLAIMER

Preface

Results and conclusions of the final phase (III) of a three year research program on polycrystalline thin film heterojunction solar cells are presented. The research consisted of the investigation of the relationships between processing, materials properties and device performance. This relationship was quantified by device modeling and analysis. The analysis of thin film polycrystalline heterojunction solar cells explains how minority carrier recombination at the metallurgical interface and at grain boundaries can be greatly reduced by the proper doping of the window and absorber layers. Additional analysis and measurements show that the present solar cells are limited by the magnitude of the diode current which appears to be caused by recombination in the space charge region.

Developing an efficient commercial scale process for fabricating large area polycrystalline thin film solar cells from a research process requires detailed understanding of the individual steps in making the solar cell and their relationship to device performance and reliability. The complexities involved in characterizing a process are demonstrated with results from our research program on $CuInSe_2$ and CdTe processes.

Summary

Objectives

The objectives of this research are to obtain the understanding of the materials processing, properties and performance of polycrystalline thin-film $CuInSe_2$ and CdTe solar cells that are needed to achieve the goals for efficiency, reliability and cost for flat plate thin-film photovoltaic systems set by DOE for the National Photovoltaics Program. A further objective of this program is to support the development of a competitive U.S. photovoltaic industry through collaboration with engineers and scientists at other laboratories.

Discussion

This is a report on the final phase (Phase III) of a three year phased research program of integrated investigations of processing, properties, and performance of polycrystalline thin film $CuInSe_2$ and CdTe based heterojunction solar cells.

Analysis of the process used for fabricating research solar cells and its relationship to material properties and device performance will become increasingly important as thin film polycrystalline solar cells are commercialized. In order to effectively characterize a process, an integrated research approach is required so that material properties and device performance can be coupled with the process analysis. In the case of CdTe solar cells, we have used evaporated CdTe solar cells as a model system and developed a self consistent picture, based on materials and devices measurements, of the effects of processing on the evolution of a CdTe cell which can be applied to other processing methods. For $CuInSe_2$ formation by selenization, a clear understanding of the process is beginning to emerge.

Both H_2Se and elemental selenium are used to form copper indium diselenide. Equilibrium thermodynamic calculations were performed and show that the higher order Se_x species (Se_5, Se_6, Se_7) are important at temperatures below 800K whereas Se_2 becomes the predominant species at temperatures above 900K. A kinetic model is presented for the decomposition of H_2Se. The reaction is found to be first order at short times, but the reverse reaction of Se_x with H_2 assumes importance at higher conversions and longer times. The constants in the kinetic model are calculated from the data available in literature and from our experiments.

Copper-indium bilayers have been selenized in 1) a tubular reactor with flowing H_2Se at atmospheric pressure and, 2) an evaporator using a Se source. In both systems, the selenizations were carried out at temperatures ranging from 150°C to 400°C for 60 minutes. Additionally, in the tubular reactor, copper-indium bilayers were selenized at 400°C for 1-45 minutes. The operating conditions in

the tubular reactor were selected to ensure that the decomposition of H_2Se to Se_x species was less than 1%. The reaction pathways to $CuInSe_2$ formation using either H_2Se or Se proceed through the formation of a $Cu_{11}In_9$ alloy and the indium selenide phases (In_2Se and InSe). The only different precursors between the two reacting systems are the copper selenide phases which were observed in the selenization in the PVD reactor. The reaction with Se proceeds faster than the reaction with H_2Se.

Investigation of the relationship between CdTe post processing and the properties of the CdS and CdTe layers show that different optimization conditions are required for devices with different CdS thickness. For the $CdCl_2$ heat treatment step, reducing the treatment time improved yield and performance of devices with CdS less than 2000Å thick. Results for devices prepared with $CdCl_2$ vapor treatment show that the quantity of $CdCl_2$ and the delivery method are other important parameters to consider. The $CdCl_2$ heat treatment step recrystallizes the CdTe grains uniformly from the CdTe surface to the CdS/CdTe interface but produces non-uniform CdS and CdTe interdiffusion, the extent of which influences the device J_{sc}. Interdiffusion may also influence the V_{oc}, depending on the electronic properties of the resulting Cd(STe) and Cd(TeS) layers. Devices with CdTe films having 6 μm lateral grain size have been fabricated but with no enhancement observed in the V_{oc}, which suggests that once grain size of ~1 μm is achieved, another V_{oc}-controlling mechanism dominates. Devices with very thin (<1000Å) CdS may also be sensitive to contamination or other properties associated with the TCO superstrate, since the junction is located closer to the TCO in those devices. With a post deposition process amenable to thin CdS in place, further improvement in device performance is likely to emerge from choice of a suitable TCO superstrate in conjunction with TCO/CdS preparation.

Several approaches to fabricating $CuInSe_2$ thin film solar cells in a superstrate configuration have been investigated. The $CuInSe_2$ films were grown on glass/ITO/CdS substrates by both three source evaporation and selenization using elemental Se. The ratio of the Cu/In in the $CuInSe_2$ film was varied from 0.5 to 1.3. The results are discussed in terms of device performance, $CuInSe_2$ film growth and alloy formation, and starting substrate.

I-V measurements over a wide range of temperatures and light intensities have been made on thin film $CuInSe_2$ based solar cells. These cells have been fabricated both at IEC and Siemens Solar Industries. The $CuInSe_2$ has been formed by several methods including elemental evaporation and selenization of Cu-In layers with H_2Se or elemental Se. The measurements have been analyzed and it has been found that all the devices have a non-linear series resistance which dominates the I-V behavior at lower temperatures. However, at higher temperatures and at V_{oc}, the behavior can be represented as a simple diode with an activation energy equal to the bandgap of the $CuInSe_2$ (~1.0eV) and with a diode quality factor between 1 and 2. This diode represents the behavior of the primary $CuInSe_2/CdS$ junction, which is basically the same in all devices. But, when the standard diode behavior is subtracted from the I-V measurements to reveal the contribution of the non-linear series resistance, it is found that this contribution is different for each device.

I-V measurements over a similar range of light intensities and temperatures have been made on a University of South Florida CdTe solar cell. When a small voltage dependent current collection effect is accounted for, under illumination this device can also be represented by a simple diode with an activation energy of about 1.4eV and a diode quality factor of 1.6. This is very similar to results obtained from IEC's CdTe devices.

All of the I-V measurements are available to other researchers via the Internet or e-mail.

The regular retesting of CdTe devices over time to determine the stability of the output assumes that the testing itself does not introduce degradation. To test this assumption on IEC's CdTe devices, six samples with three different types of contacts to the CdTe were given repeated I-V tests. There were substantial changes in output due to testing with devices that had either the Cu/Au or the ZnTe/Au contact. There was little change in the devices that had the harder and more robust ZnTe/Ni contact. It appears that the probes used for current-voltage testing scratch the surface of the soft contacts, causing lowered fill factors due to both contact removal and device shunting.

List of Contributors for Phase III

Robert W. Birkmire	Principal Investigator
James E. Phillips	Principal Investigator
William N. Shafarman	Principal Researcher
Steven S. Hegedus	Principal Researcher
Brian E. McCandless	Principal Researcher
Takashi Yoshida (Fuji)	Visiting Scientist
Satoshi Yamanaka	Post Doctoral Fellow
Linda Moulton	Post Doctoral Fellow
Sandeep Verma	Graduate Student
Wayne A. Buchanan	Technical Support
Herbert O. Wardell	Technical Support
Sarah K. Buchanan	Technical Support
Sally I. Gordon	Technical Support
Ronald Dozier	Technical Support
Kevin Hart	Technical Support
Shannon Fields	Technical Support
Laurie Adkins	Student
Frank Prenot	Student
Michael Goetz	Student
Joseph Shan	Student
Elaine A. Koronik	Document Preparation

David Albin (NREL)
Scot Albright (Photon Energy Inc.)
Rajeewa Arya (Solarex Corp.)
Anthony Catalano (Solarex Corp.)
Ting Chu (Univ. of South Florida)
Chris Eberspacher (Siemens Solar Industries)
Kim Mitchell (Siemens Solar Industries)
Keith Emery (NREL)
Fouad Abou-Elfotouh (NREL)
Mowafak Al-Jassim (NREL)
Zolton Kiss (EPV)
Peter Meyers (Solar Cells, Inc.)
Alvin Compaan (Univ. of Toledo)
Terry Peterson (EPRI)
Angus Rockett (Univ. of Illinois)
Ajeet Rohatgi (Georgia Tech)
Axel Schonecker (Fraunhofer Institute, Germany)
James Sites (Colorado State Univ.)
Jarmo Skarp (Microchemistry, Finland)
Rommel Noufi (NREL)
Andrew Tennant (NREL)

Table of Contents

List of Figures

List of Tables

1.0 INTRODUCTION

1.1 BACKGROUND

Modules utilizing copper-indium-diselenide ($CuInSe_2$) and cadmium telluride (CdTe) have emerged as promising candidates for meeting the DOE long range efficiency, reliability and cost targets for flat plate photovoltaic energy systems (1).

Under the NREL Polycrystalline Thin-Film Task, the Institute of Energy Conversion (IEC) has been conducting an integrated program of investigation of $CuInSe_2$-solar cells (2). IEC has established a two-step physical vapor deposition (PVD) process and characterization capabilities for fabricating and analyzing state-of-the-art $CuInSe_2$ materials and devices. In addition, IEC has established processes to produce device quality $CuInSe_2$ by the selenization of copper and indium layers with both H_2Se and elemental Se.

IEC also initiated a chemical reaction engineering analysis of the formation of device quality $CuInSe_2$ by selenization of copper and indium metal layers, a process which promises to be more readily translated from laboratory scale solar cells to large area module manufacturing.

These results, along with those obtained by others under the NREL Polycrystalline Thin-Film Task indicate that further improvements in performance and cost potential of $CuInSe_2$ modules can be expected from continued investigations of processing, material properties and device behavior.

Research conducted by IEC on CdTe has also shown that PVD is capable of producing near state-of-the-art CdTe materials and devices and that sequential post-deposition treatments are critical for achieving high efficiencies regardless of CdTe deposition technique. Recent results obtained by IEC and others under the NREL Polycrystalline Thin-Film Task indicate that further research is likely to lead to achievement of practical efficiencies greater than 15% and long term stability for thin-film CdTe modules.

Accordingly, a continued research effort with the objective of obtaining the understanding of materials processing, properties and performance of polycrystalline thin-film solar cells needed to achieve the goals for performance, cost and reliability set by DOE for the National Photovoltaics Program is needed. A further objective of such a program is to support the development of competitive U.S. photovoltaic industry through collaboration with other research groups and the training of engineers and scientists in photovoltaic technology.

1.2 TECHNICAL APPROACH

In order to achieve these objectives IEC has undertaken a phased three year program to carry out the following integrated research tasks:

Task 1 - $CuInSe_2$ Based Materials and Devices

A. Characterize and optimize selenization of Cu/In films with a primary goal of establishing capability to fabricate state-of-the-art $CuInSe_2$ materials and devices by selenization and explore the use of alternatives to H_2Se.

B. Increase open circuit voltage in $CuInSe_2$-based solar cells, through investigations of reducing space charge recombination by alloying with gallium and/or sulfur and reducing the space charge width in the $CuInSe_2$ by optimizing doping levels in the $CuInSe_2$ and window layers.

C. Examine interface recombination as a limiting mechanism for open circuit voltage by fabricating and characterizing $CuInSe_2$ heterojunctions with ZnSe, ZnO, or other thin, n-type materials.

D. Identify the controlling mechanisms and demonstrate approaches for improving open circuit voltage in superstrate $CuInSe_2$ devices.

E. Quantify losses due to multidimensional junction effects and relate them to material processing and properties.

Task 2 - CdTe Based Materials and Device

A. Characterize and optimize fabrication of state-of-the-art CdTe material and devices using physical vapor deposition to deposit CdTe.

B. Develop and characterize thermally stable, transparent contacts to CdTe.

C. Develop a quantitative model of the effects of sequential post-deposition processing, from systematic studies of the following relationships: $CdCl_2$/high temperature heat treatment step and restructuring of CdTe; contacting/low temperature heat treatment and type conversion of CdTe; chemical treatments with bromine-methanol (or hydrazine).

D. Develop and optimize high transparency n-type window layer/heterojunction partners for increased short circuit current. Tin oxide and thin (<50nm) CdS will be investigated for realizing short circuit currents in excess of 25 mA/cm^2.

Other window layers, including ZnCdS, will be used to study heterojunction interface mechanisms limiting open circuit voltage.

Task 3 - $CuInSe_2$ and CdTe Cells with Thin Absorber Layers

A. Fabricate and characterize $CuInSe_2$ solar cells with $CuInSe_2$ absorber layers 1 micron or less in thickness and CdTe solar cells with CdTe absorber layers 0.3 micron or less in thickness. The effects of thin absorber layers on cell efficiency will be investigated. Losses in short circuit current, open circuit voltage and fill factor due to reduced thickness will be quantified with particular emphasis on recombination losses at ohmic contacts, optical losses due to decreased optical path length and shunts.

B. Develop and assess approaches for minimizing thickness-related losses, with particular emphasis on use of back surface reflection and texture to enhance optical absorption in thin $CuInSe_2$ and CdTe cells.

C. Fabricate and optimize the efficiency of thin absorber layer $CuInSe_2$ and CdTe solar cells.

1.3 OUTLINE OF REPORT

In this report we describe the significant results and conclusions reached at the end of the third year of the program. Also included is research that has been done in collaboration with other scientists at various universities and industrial organizations. The report is divided into three basic sections: solar cell deposition and processing, solar cell measurement and analysis, and collaborative research and development.

Section 2, 'Device Fabrication and Process Analysis' is devoted to explaining how the materials that compose the solar cells are made and analyzed as well as describing the device fabrication steps for both $CuInSe_2$ and CdTe solar cells. Section 2.1 covers the materials processing while Section 2.2 is devoted to device fabrication.

Section 3, 'Solar Cell Measurements and Analyses', describes both the device measurements and the analysis techniques that help determine the modes of current collection and junction behavior that are present in $CuInSe_2$ and CdTe based solar cells. Section 3.1 describes the current-voltage analysis techniques, while Sections 3.2 and 3.3 are devoted to the analysis of $CuInSe_2$ and CdTe solar cells respectively.

Finally Section 4, 'Research and Development Collaboration' describes the materials and device processing, measurements, and analysis done in collaboration with other research organizations.

2.0 DEVICE FABRICATION AND PROCESS ANALYSIS

Understanding the process for depositing thin films and post-deposition processing are critical issues as thin film devices move to the manufacturing stage. In this section, the processes involved in film growth and device fabrication for $CuInSe_2$ and CdTe based solar cells are discussed.

2.1 PROCESS ANALYSIS OF $CuInSe_2$ MADE BY SELENIZATION

Selenization of Cu-In layers to Form $CuInSe_2$ Films

Cu-In layers were reacted in both H_2Se and elemental Se to form $CuInSe_2$ films. The Cu-In layers were deposited by electron beam evaporation on soda lime glass sputter coated with 1 μm of Mo. The Cu/In ratio was varied from 0.8 to 1.1 where the thickness of the Cu was fixed and In varied to give a $CuInSe_2$ film of nominally 2 μm. Devices were made using $CuInSe_2$ films formed by reaction with both H_2Se and Se with efficiencies about 10% where 1 μm evaporated CdS was used as the window layer.

Previously, we reported on the development of a closed reaction system where either Se or H_2Se is transported via thermo syphon (3). In the design of this system, we identified critical areas requiring additional experimental data. The reaction chemistry leading to the formation of $CuInSe_2$ films had not been well characterized and when using H_2Se, the gas phase species and relative concentrations due to H_2Se pyrolysis were not identified.

H_2Se Dissociation

To evaluate $CuInSe_2$ film growth and to provide the information needed to design an efficient commercial scale reaction system, thermodynamic and kinetic data on the decomposition of H_2Se were evaluated. H_2Se is a colorless, extremely toxic gas which has received wide attention as a selenium source in the formation of $CuInSe_2$ thin films. The decomposition products of H_2Se have been identified as polymeric Se_x species (4,5). If H_2Se is used for selenization, both H_2Se and the product selenium species are available for reaction with the copper/indium layers to form $CuInSe_2$. The general consensus in the literature dealing with the thermolysis or pyrolysis of hydrogen selenide is that the following overall reaction governs its decomposition (5,6):

$$H_2Se \longleftrightarrow H_2 + 1/2Se_2$$

The reaction is endothermic with an enthalpy change ΔH^o_{298} of 9.7 kcal/mole and a free energy change ΔG^o_{298} of 14.46 kcal/mole (5). Only a limited amount of research on the reaction order and rate constants for this reaction has been performed (6).

Thermodynamics of H_2Se Dissociation

Whereas the stoichiometry and structure of gas phase Se species in equilibrium with molten selenium has been measured by mass spectroscopy techniques (4), the products of the decomposition of hydrogen selenide have not been measured. The dissociation of H_2Se may be considered as occurring by the following series of independent chemical reactions.

$$xH_2Se(g) \longleftrightarrow xH_2(g) + Se_x(g) \tag{1}$$

Where x is 1, 2, 3, 5, 6, and 7.

Tabulated free energies of formation (4) can be used to calculate the decomposition of H_2Se at equilibrium. The equilibrium constant K_y is related to the Gibbs free energy change of the reaction by:

$$k_y = \frac{y_{H_2}^{\ x}\, y_{Se_x}}{y_{H_2Se}^{\ x}} = \exp(-\Delta G^\circ_{rxn} x/RT) \tag{2}$$

where;

y = gas phase mole fraction.

Equation 2 assumes ideal gas behavior at the temperatures and pressures of interest and at a total pressure of 1 atmosphere. If we select as a basis 1 mole of undissociated H_2Se, then nx number of moles will react in the xth reaction. We can set up the equilibrium relations based on equation 2 for each of the chemical equations (x = 1, 2, 3, 5, 6, 7).

It is helpful to define:

$$n_{H_2} = \Sigma x n_x \tag{3}$$

$$n_{H_2Se} = 1- \Sigma x n_x \tag{4}$$

$$n_t = 1+ \Sigma n_x \tag{5}$$

where, x = 1, 2, 3, 5, 6, 7;

e.g.

$$y_{H_2Se} = \frac{n_{H_2Se}}{n_t}$$

The general relationship is:

$$\exp\left(\frac{-\Delta G^{o}_{rxnx}}{RT}\right) = \frac{n_x \, (n_{H_2})^x}{n_t \, (n_{H_2Se})^x} \qquad (6)$$

The Gibbs free energy for each reaction is calculated from the elemental Gibbs free energy and the enthalpy of formation data tabulated in K.C. Mills (4). The six non-linear equations are numerically solved at temperatures from 300 to 1400K. The resultant fraction of H_2Se dissociated is plotted as a function of temperature in Figure 2.1 for:

- Se_2 as the sole selenium species;
- Se_2, Se_3, Se_5, Se_6, Se_7 as the product selenium species.

Our data and that of Pearson is shown on the plot as well as some much older data from Flogel and Pruner (5). Over the range of typical selenization temperature (600K - 800K), there is satisfactory agreement with experimental data.

The thermodynamics of H_2Se dissociation suggests that 80% of the H_2Se species decomposes to primarily Se_7, Se_6 and Se_5 around 300K. Se_2 becomes increasingly important at temperatures above 800K and is the dominant species present at temperatures above 950K. Analysis of the data at 700K suggests that Se_2 and Se_6 are the dominant species.

The thermodynamic analysis does not give any information as to the rate of dissociation of H_2Se. In the next section, we present a model to consider this issue.

Kinetics of H_2Se Dissociation

We have performed pyrolysis experiments in the temperature range 673K - 723K using the apparatus drawn in Figure 2.2 (7). The experimental procedure was similar to that used by Pearson. In a typical experiment the system was pumped down to pressures less than 10μm. The 15 wt% H_2Se mix was admitted to the vacuum manifold through a mass flow controller to a pressure of about 700 torr. The valve to the preheated pyrolysis bulb was then opened for about 5 sec. and the amount of H_2Se charged was obtained from the difference in pressure measurements. The H_2Se remaining in the vacuum manifold was pumped out. The reaction time was started when the H_2Se was charged to the pyrolysis bulb and stopped when the gas was released through the traps. The H_2Se and its dissociation products were pumped through the two traps. H_2Se and the selenium species were condensed in liquid N_2 traps. Argon and H_2 were removed from the system by pumping. The pyrolysis system was then isolated and the cold traps were dropped. The pressure of unreacted H_2Se trapped in the cold traps was measured after about five minutes to allow the H_2Se to evaporate. The primary difference between our experiments and Pearson's was that Pearson

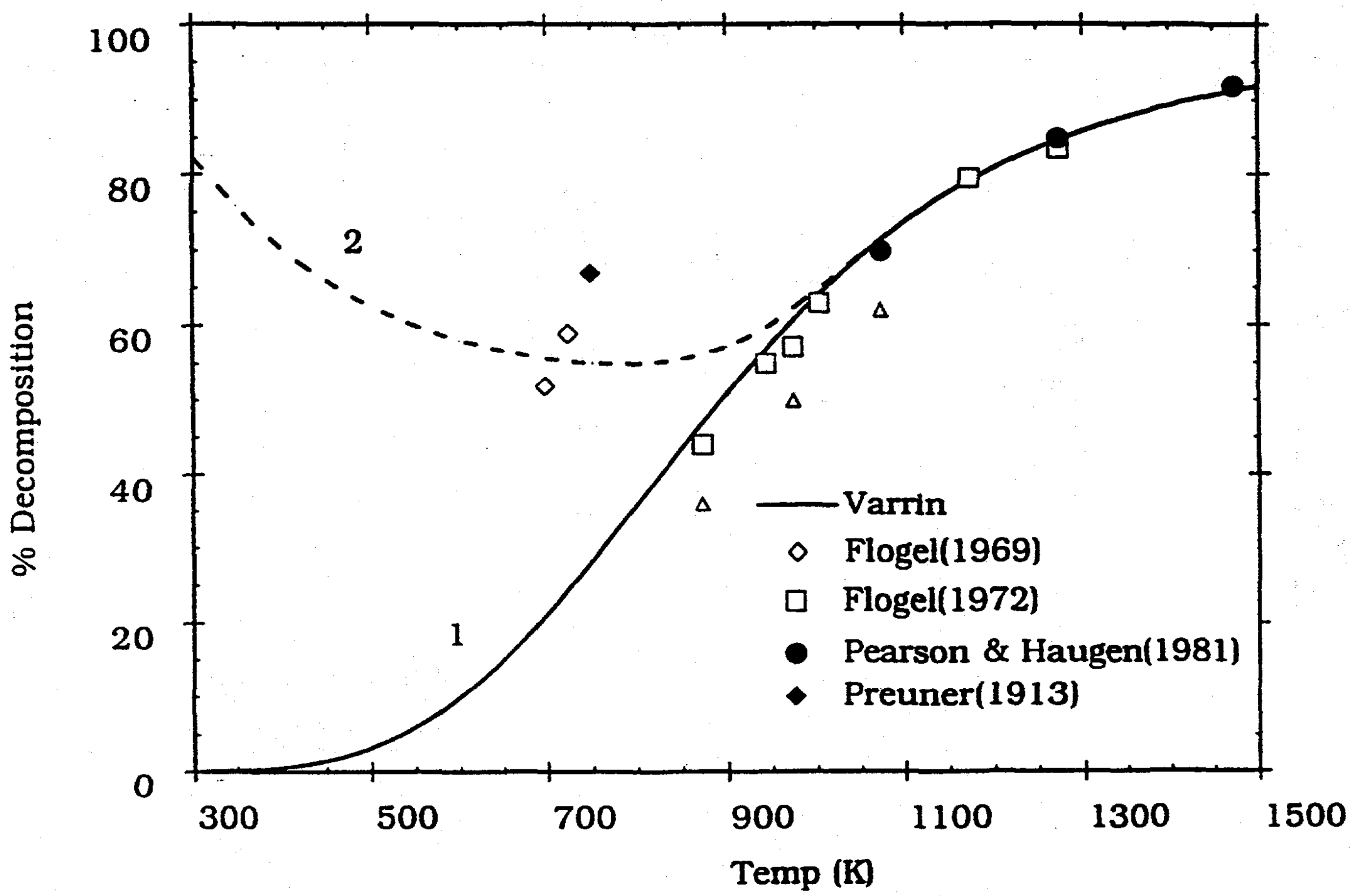

Figure 2.1 The predicted equilibrium dissociation of H_2Se assuming 1) Se_2 as the product species, 2) Se_2, Se_3, Se_6 as the product species, 3) Se_2, Se_3, Se_6, Se_7 as the product species and, 4) Se, Se_2, Se_3, Se_5, Se_6, Se_7, as the product species.

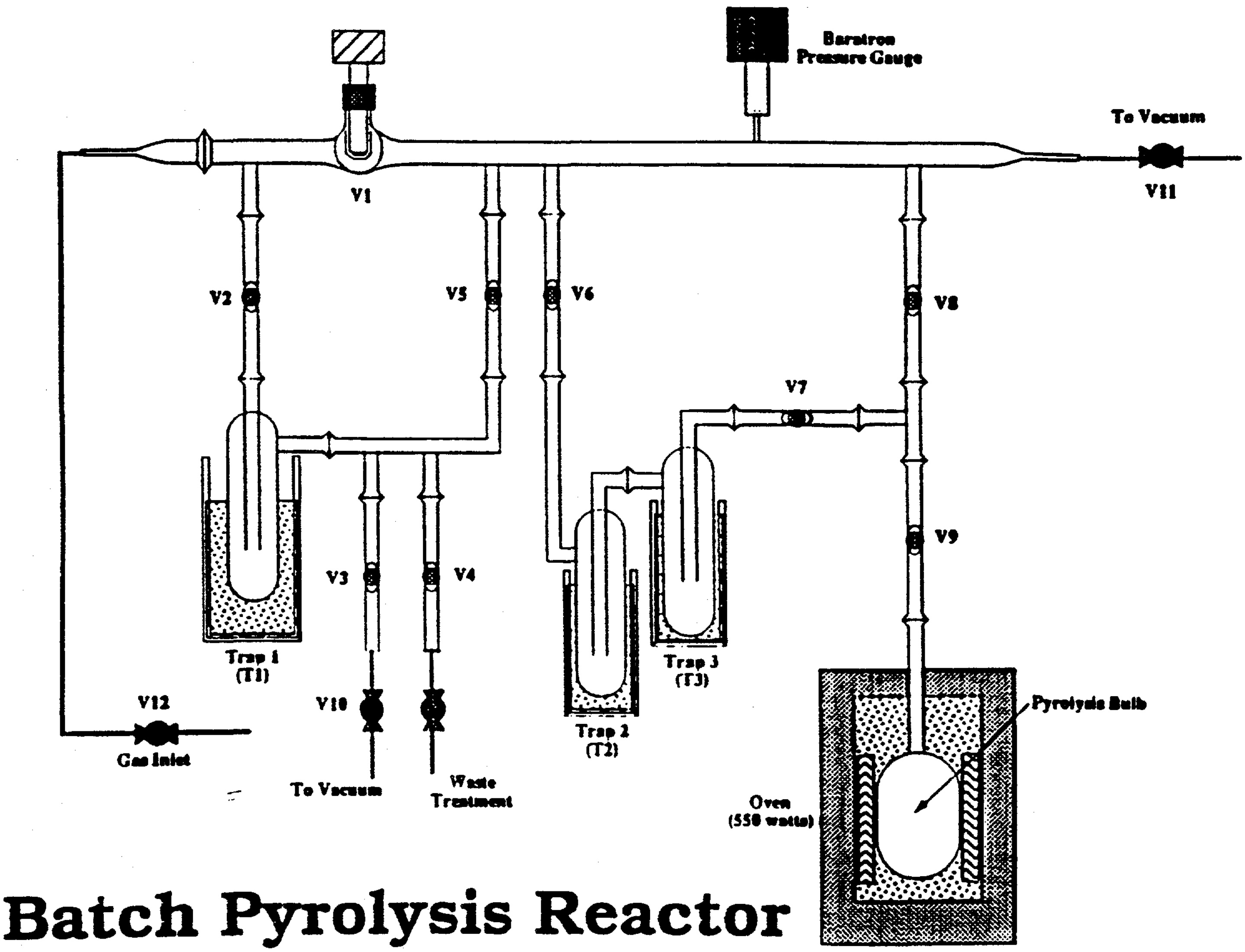

Figure 2.2 A schematic of the batch pyrolysis reactor used for our experiments.

used triple distilled vacuum outgassed H_2Se whereas we used the 15 wt% H_2Se in Argon gas as received from the manufacturer.
Since we (or Pearson) could not measure concentrations of Se_x species as a function of time, we based our analysis on the following chemical equations:

$$H_2Se <--> H_2 + 1/2\ Se_2 \tag{7}$$

$$H_2Se <--> H_2 + 1/6\ Se_6 \tag{8}$$

The thermodynamic analysis predicts the importance of both these species in the temperature ranges examined in the pyrolysis experiments.

Applying the law of conservation of mass to the batch pyrolysis reactor using reactions 7 or 8 yields:

$$dC_{H_2Se}/dt = k_f\ C_{H_2Se} - k_r\ C_{H_2}\ C_{Se_2}{}^{1/2} \tag{9}$$

$$dC_{H_2Se}/dt = k_f\ C_{H_2Se} - k_r\ C_{H_2}\ C_{Se_6}{}^{1/6} \tag{10}$$

At short times, the reverse reaction terms will be small so the rate of change of H_2Se conversion may be assumed to be first order in the H_2Se conversion.

$$dC_{H_2Se}/dt = k_f\ C_{H_2Se} \tag{11}$$

Integrating (13) gives:

$$\ell n \frac{C_{H_2Se}\ (t)}{C_{H_2Se}\ (t=0)} = -k_f t \tag{12}$$

Figure 2.3 presents the short time best fit to the above functional form H_2Se dissociation at 723K for Pearson's data and our

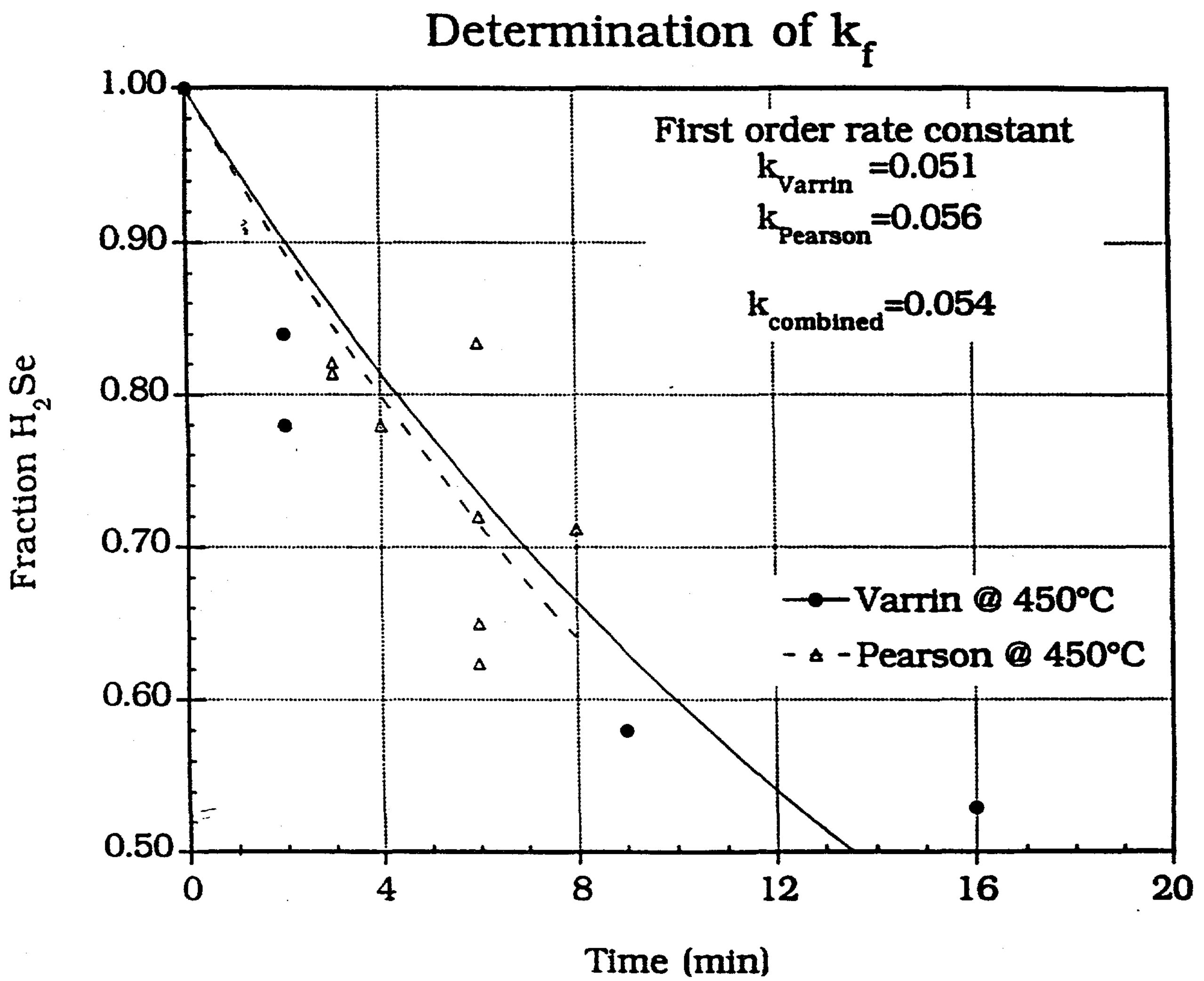

Figure 2.3 Determination of k_f by the short time best fit to equation 12 for the two data sets.

experimental data. A similar set of plots at 673K and 698K allows us to evaluate the forward reaction rate constant, k_f, for both independently obtained data sets and also for the combined data set. The values are shown in Table 2.1. At 673K there is a large discrepancy between our data and Pearson's value of k_f. If we assume an Arrhenius form for k_f, its temperature dependence is:

$$k_f = k_{fo} \exp(-E_a/RT) \tag{13}$$

Figure 2.4 is a plot of ln k_f vs 1/T. This leads to a value of k_{fo} = 1.0 x $10^9 sec^{-1}$, E_a = 39.96 kcal/mol which compares well with Pearson's reported value of k_{fo} = 3.8 x $10^{10} sec^{-1}$, E_a = 46.4 kcal/mol.

To explain the decomposition at longer times, the reverse reaction of H_2 with Se_x needs to be considered.

If we assume the initial concentration of hydrogen and the Se_x species to be zero, we can express the equations (10 and 11) in terms of conversion of the reaction, α.

$$\frac{d\alpha}{dt} = \frac{2}{3} k_f(1-\alpha)(1+\frac{\alpha}{2}) - k_r\frac{\sqrt{2}}{3} \alpha^{3/2}(1+\frac{\alpha}{2})^{1/2} \tag{14}$$

$$\frac{d\alpha}{dt} = \frac{6}{7} \quad k_f(1-\alpha)(1+\frac{\alpha}{6}) - \frac{6}{7}^{5/6} k_r \alpha^{7/6}(1+\frac{\alpha}{6})^{5/6} \tag{15}$$

k_r may be estimated from the following relation:

$$\frac{k_f}{k_r} = k_y$$

where k_y is given by equation (2).

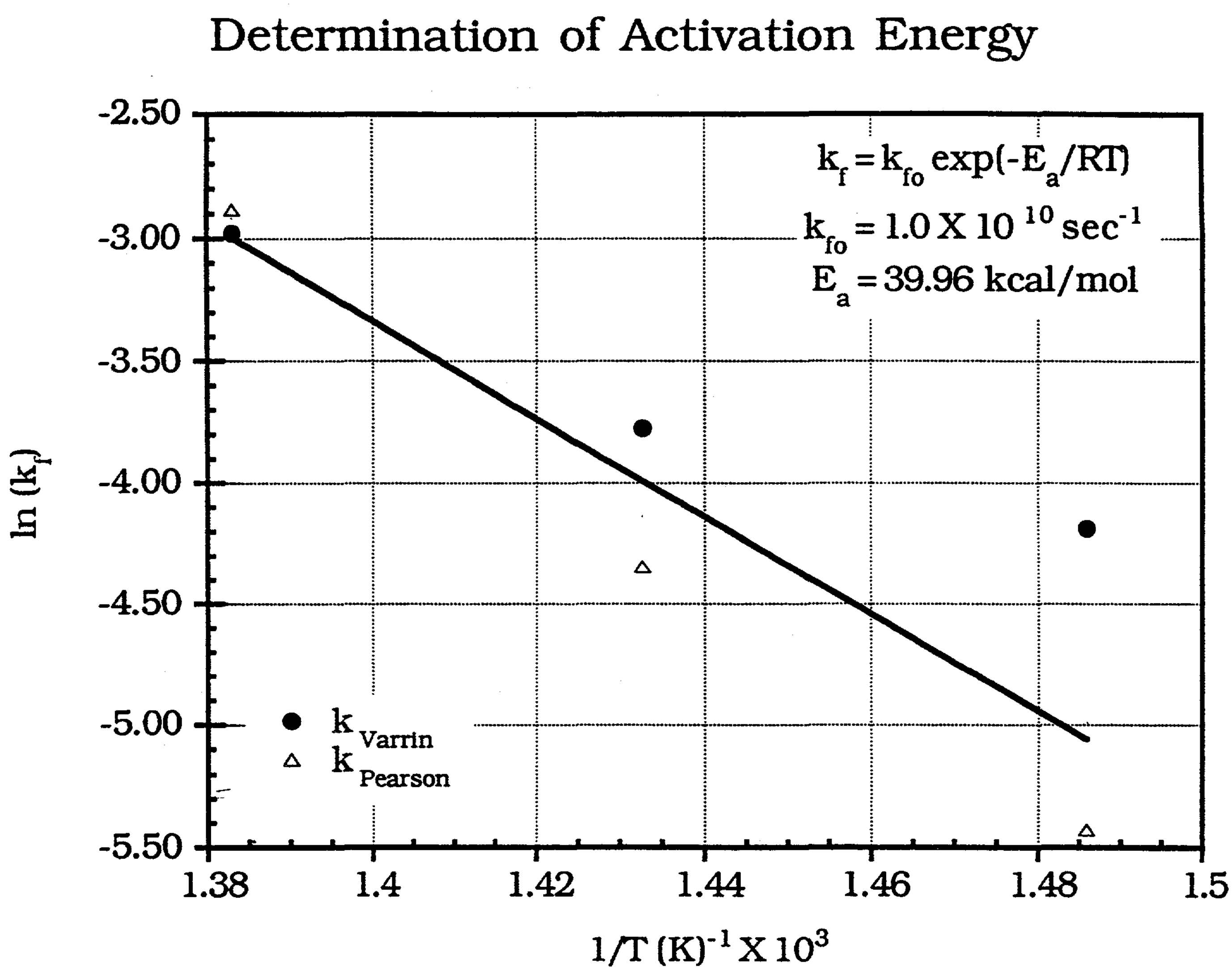

Figure 2.4 Determination of the activation energy for the forward rate constant k_f by a best fit to equation 13.

Table 2.1 A summary of the forward rate constant k_f calculated for the two data sets.

k_f	Varrin's data	Pearson's data	Combined
673K	0.0152	0.0047	0.0068
698K	0.023	0.013	0.016
723K	0.051	0.056	0.054

The above differential equation was then numerically solved to generate α as a function of time at a fixed temperature. Figure 2.5 shows the model curve generated at 450°C. The bold curve is generated considering Se_2 as the product species and the dashed curve was generated for Se_6 being the sole selenium product. The model curves underestimate the decomposition of H_2Se leading to speculation that more than one Se species may be present in the product.

To summarize, at equilibrium, over the temperature range important for selenization of copper indium bilayers, the gas phase consists of about 50% Se_2 and Se_6 and 50% H_2Se. At 450°C, it takes about 10 minutes to reach equilibrium, which is about the same time that it takes to form $CuInSe_2$. At short times (less than 10 minutes) the rate of dissociation of H_2Se is directly proportional to its concentration. The reverse reaction becomes increasingly important as time increases. The forward rate constant k_f was calculated to be $1.0 \times 10^9 \exp(-Ea/RT)$ where Ea = 39.96 kcal/mol. Kinetic experiments on the pyrolysis of H_2Se show that a reasonable fit to the data can be obtained by assuming Se_6 as the decomposition product.

Reaction Chemistry for Formation of $CuInSe_2$

The selenization process can be considered in two stages: the deposition of copper, indium and, in some cases, selenium followed by the reaction in a H_2Se and/or Se environment. Past attempts at establishing the reaction pathways to selenization have considered the binary selenides Cu_2Se and In_2Se_3 as the $CuInSe_2$ film precursors (9,10). These compounds were then (8,9,10) presumed to interdiffuse or react to form $CuInSe_2$ although the process was not quantified.

The reaction pathways and the precursors to formation of $CuInSe_2$ have been reevaluated for copper-indium bilayers selenized in 1) a tubular reactor with flowing H_2Se at atmospheric pressure and, 2) an evaporator using a Se source. The reacted films were then analyzed and the reaction schemes were evaluated for the two reacting systems. $CuInSe_2$/CdS solar cells were fabricated with efficiencies of about 10%.

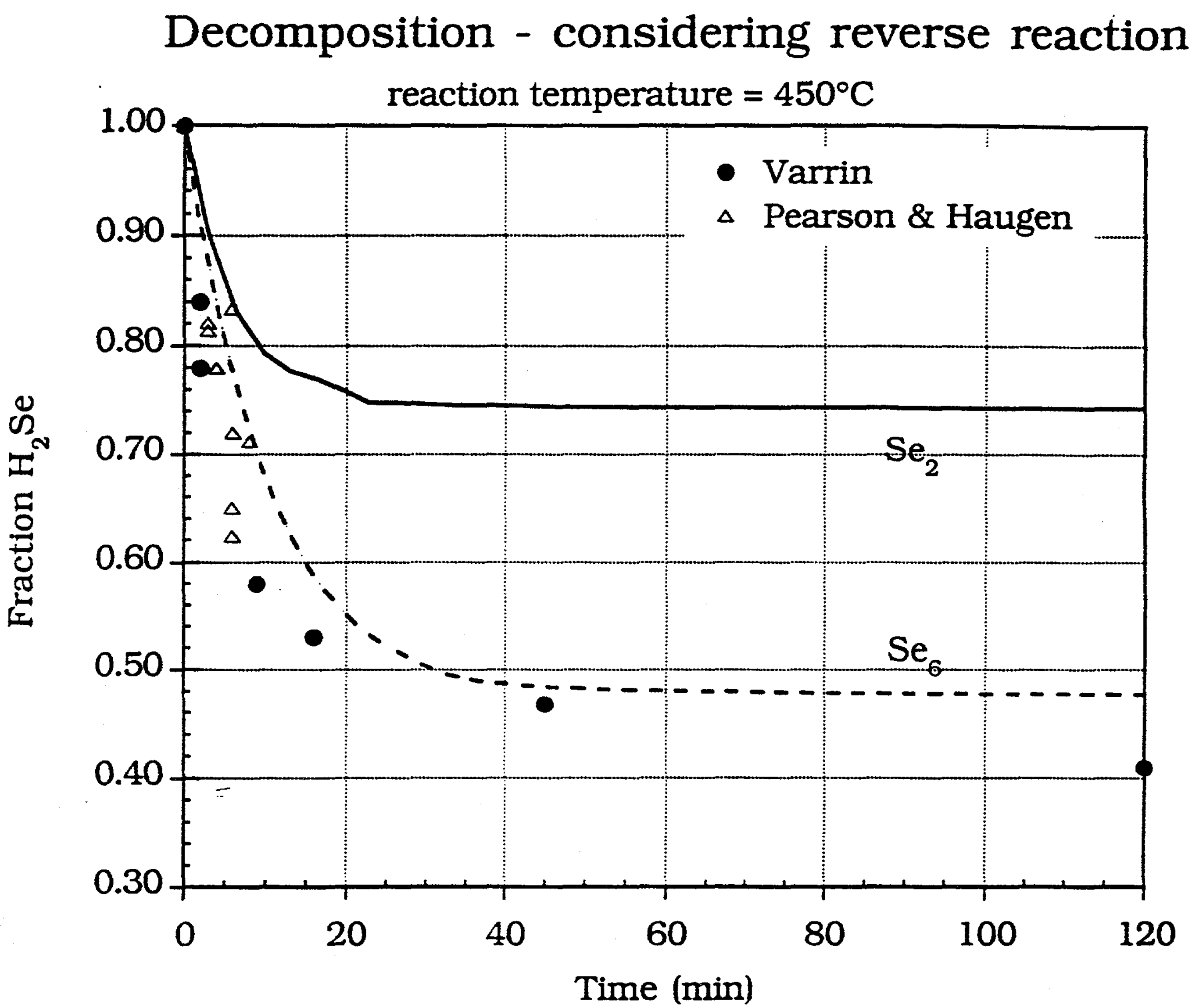

Figure 2.5 The model curves generated by consideration of the reverse reaction: 1) the bold curve considers Se_2 as the dissociation product, 2) the dashed curve considers Se_6 as the dissociation product.

In the tubular reactor Cu-In bilayers were selenized at 150°C, 250°C, 350°C and 400°C for 60 minutes in 1.7 mole % H_2Se in argon (Fig. 2.6). All substrates were annealed in vacuum for 20 minutes at 150°C prior to selenization and then selenized for an hour at atmospheric pressure. The ramp up times to reaction temperature were from 2 to 3 minutes. Based on published rate data (11) our calculations indicate that, in the absence of any contaminants, the decomposition of H_2Se for the temperature profile and the flow rate in the reactor is less than 1%. Experimental observations of the lack of condensation of Se on the cold surfaces of the reactor tube reinforce the assumption that the dominant reaction species is H_2Se. The selenization reactor was pumped out to pressures less than 2×10^{-6} torr prior to each run and residual gas analysis was used to ensure consistent starting conditions.

The Cu-In bilayers were also selenized in H_2Se gas at 400°C for 1-45 minutes. The tubular reactor has a push pull feed-through allowing the introduction of the substrate to the heated zone after the gas flow rate has been established.

At the end of the reaction time, the substrates were withdrawn from the heated zone, the H_2Se flow rate was stopped and the reactor was purged with argon. This procedure enables us to carry out a series of experimental runs with a reaction time resolution of about 30 seconds.

The Cu-In bilayers were also selenized by physical vapor deposition (PVD) using Se at substrate temperatures of 150°C, 200°C, 250°C, 300°C and 400°C. About a micron of Se was deposited on the Cu-In bilayer at room temperature prior to the reaction. The substrate temperature was ramped up at a rate of ~50°C per minute and the films were reacted in a Se flux of ~10 Å/sec. for about an hour at a pressure of 5×10^{-5} torr.

The as-deposited Cu-In bilayers and selenized Cu-In films were examined by optical microscopy and scanning electron microscopy (SEM) to characterize their morphology. The elemental composition of the selenized films was determined by energy dispersive X-ray spectroscopy (EDS).

The films were analyzed by XRD to investigate the phases present. Phase identification in the XRD patterns was carried out by comparison of the standard d-spacings with JCPDS card files. $CuIn_2$ and $Cu_{11}In_9$ were identified using computer generated XRD patterns from the crystal structure of these compounds (12). Identification of In_2Se is based in the XRD pattern of an In layer selenized at 250°C and a computer generated XRD pattern for the crystal structure of the In_2Se phase (13,14). High resolution scans were used to resolve closely spaced peaks such as the In_2Se and the CuSe peaks at d-spacings of 3.199Å and 3.173Å, respectively. For a qualitative assessment of the relative amounts of the phases in the reacted films, the ratio of the most intense peaks for different

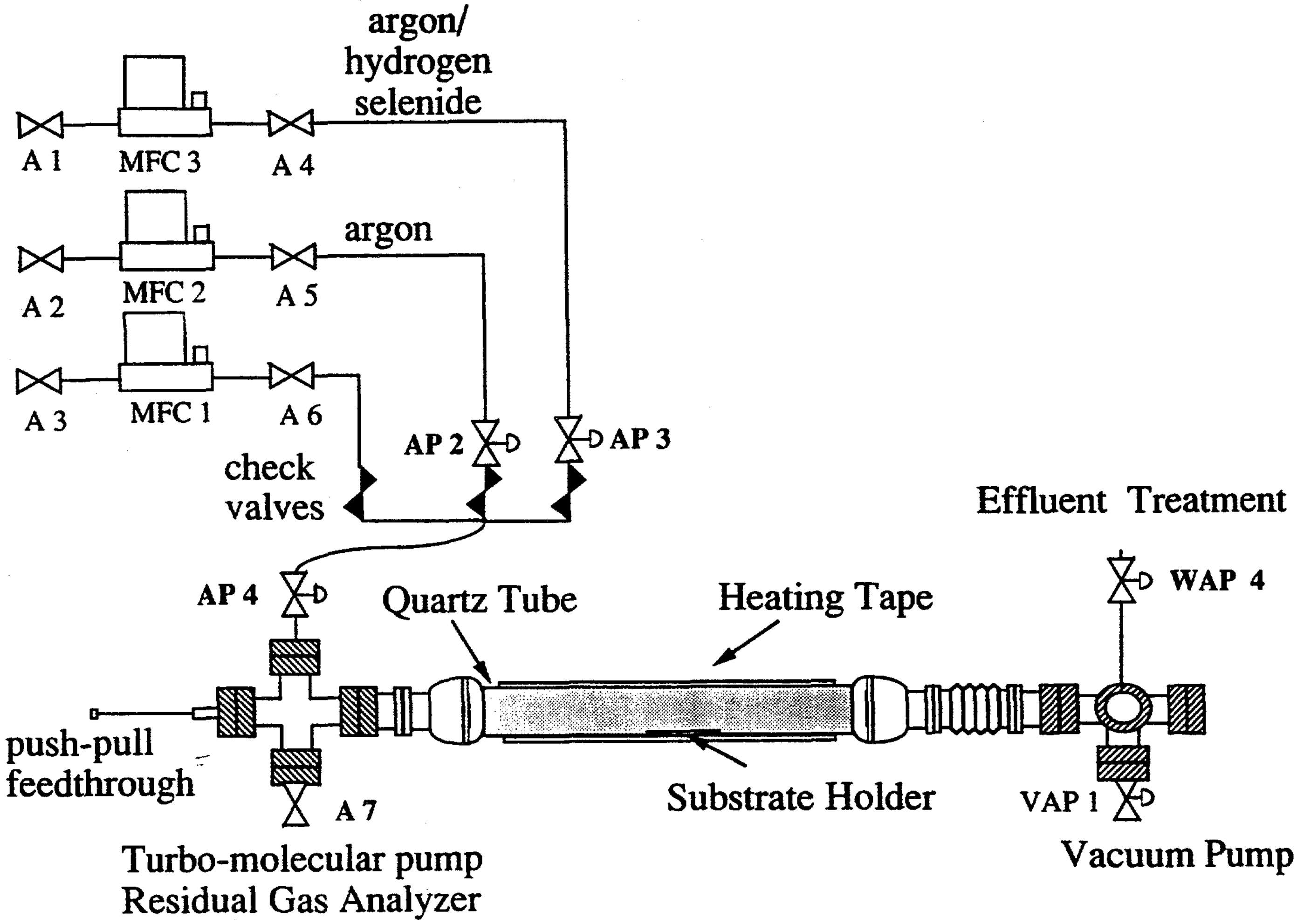

Figure 2.6 Schematic of the tubular reactor

phases were used since the relative intensities within each phase were about the same for different samples.

Table 2.2a presents a summary of the experimental results for the selenization of the Cu-In bilayer in H_2Se and Table 2.2b shows a similar summary for the reaction in Se. Figure 2.7a presents the XRD patterns for the bilayers selenized in the tubular reactor from 150-350°C for 60 minutes. Figure 2.7b is a plot of the XRD patterns selenized in the PVD reactor from 150-400°C for 60 minutes. Figure 2.7c presents the XRD patterns for the films reacted in the tubular reactor at 400°C for 1-45 minutes. When $CuInSe_2$ was observed, it was preferentially oriented along the (112) direction.

<u>Time 60 Minutes, Temperature 150 - 350°C</u>

In_2Se is the only selenide observed in the Cu-In bilayers reacted in H_2Se at 150°C. The presence of the $Cu_{11}In_9$ phase and In is consistent with the phases observed in a heat treated film at similar conditions. The selenized bilayer when examined under the SEM resembles the as-deposited structure of the Cu-In layer. Indium appears to be preferentially selenized to In_2Se while copper exists as the stable $Cu_{11}In_9$ phase. At 150°C, reaction with Se or H_2Se results in the formation of In_2Se. It should be noted that no Cu-Se phases were detected although Cu reacts with Se at room temperature.

The bilayer reacted at 200°C in Se indicates the presence of $Cu_{11}In_9$, InSe, In_2Se and CuSe. The film resembles the bilayer selenized at 150°C with the as-deposited indium peanut structure being preserved. Small sub-micron grains appear over these peanuts.

The bilayer selenized in H_2Se at 250°C reveals the presence of $Cu_{11}In_9$, In_2Se and perhaps $CuInSe_2$ and In at the detection limit. The selenized film morphology is smooth and specular and is significantly different from the as-deposited film. The bilayer selenized in Se shows $CuInSe_2$ as the dominant phase along with $Cu_{11}In_9$, InSe, In_2Se and $Cu_{(2-x)}Se$. It is interesting to note that a Cu-Se phase is observed when reacting with Se while only In-Se phases are observed in the reaction with H_2Se.

Cu-In bilayers selenized in Se at 300°C consists of $CuInSe_2$, InSe and perhaps $Cu_{11}In_9$ at the detection limit. The film appears to be extremely smooth with submicron grains.

The bilayer selenized at 350°C in H_2Se shows that $CuInSe_2$ is the dominant phase along with InSe, In_2Se and $Cu_{11}In_9$. The presence of $Cu_{11}In_9$ indicates that the reaction to $CuInSe_2$ has not proceeded to completion at 350°C in about an hour and SEM examination showed that the film had segregated into islands.

Table 2.2a Summary of results for the selenization of Cu-In bilayers in the tubular reactor using the H_2Se gas source

Temperature (°C)	Time (min.)	Cu-In Pre-Treatment	H_2Se gas concn (mole%)	Phases Observed			$\frac{I_{CuInSe_2}(112)}{I_{Cu_{11}In_9}(313)}$
				metals	binary selenides	ternary selenides	
150	60	Yes	1.7	$Cu_{11}In_9$, In	In_2Se		0
250	60	Yes	1.7	$Cu_{11}In_9$	In_2Se	$CuInSe_2$	0.08
350	60	Yes	1.7	$Cu_{11}In_9$	In_2Se, InSe	$CuInSe_2$	16.4
400	1	No	3.4	$Cu_{11}In_9$, In	In_2Se		0
400	2	No	3.4	$Cu_{11}In_9$	In_2Se, InSe	$CuInSe_2$	1.4
400	5	No	3.4	$Cu_{11}In_9$	In_2Se, InSe	$CuInSe_2$	4.2
400	10	No	3.4		InSe, In_2Se_3	$CuInSe_2$	-
400	15	No	3.4		InSe, In_2Se_3	$CuInSe_2$	-
400	30	No	3.4		InSe, In_2Se_3	$CuInSe_2$	-
400	45	No	3.4		InSe	$CuInSe_2$	-
400	45	No	3.4			$CuInSe_2$	-

Table 2.2b Summary of results for the selenization of Cu-In bilayers in the PVD reactor using the elemental Se source

Temperature (°C)	Time (min.)	Phases Observed			$\frac{I_{CuInSe_2}(112)}{I_{Cu_{11}In_9}(313)}$
		metals	binary selenides	ternary selenides	
150	60	$Cu_{11}In_9$, In	In_2Se		0
200	60	$Cu_{11}In_9$	In_2Se, InSe, CuSe		0
250	60	$Cu_{11}In_9$	In_2Se, InSe, CuSe, Cu_7Se_4	$CuInSe_2$	4.0
300	60	$Cu_{11}In_9$	InSe	$CuInSe_2$	37.5
400	60			$CuInSe_2$	-

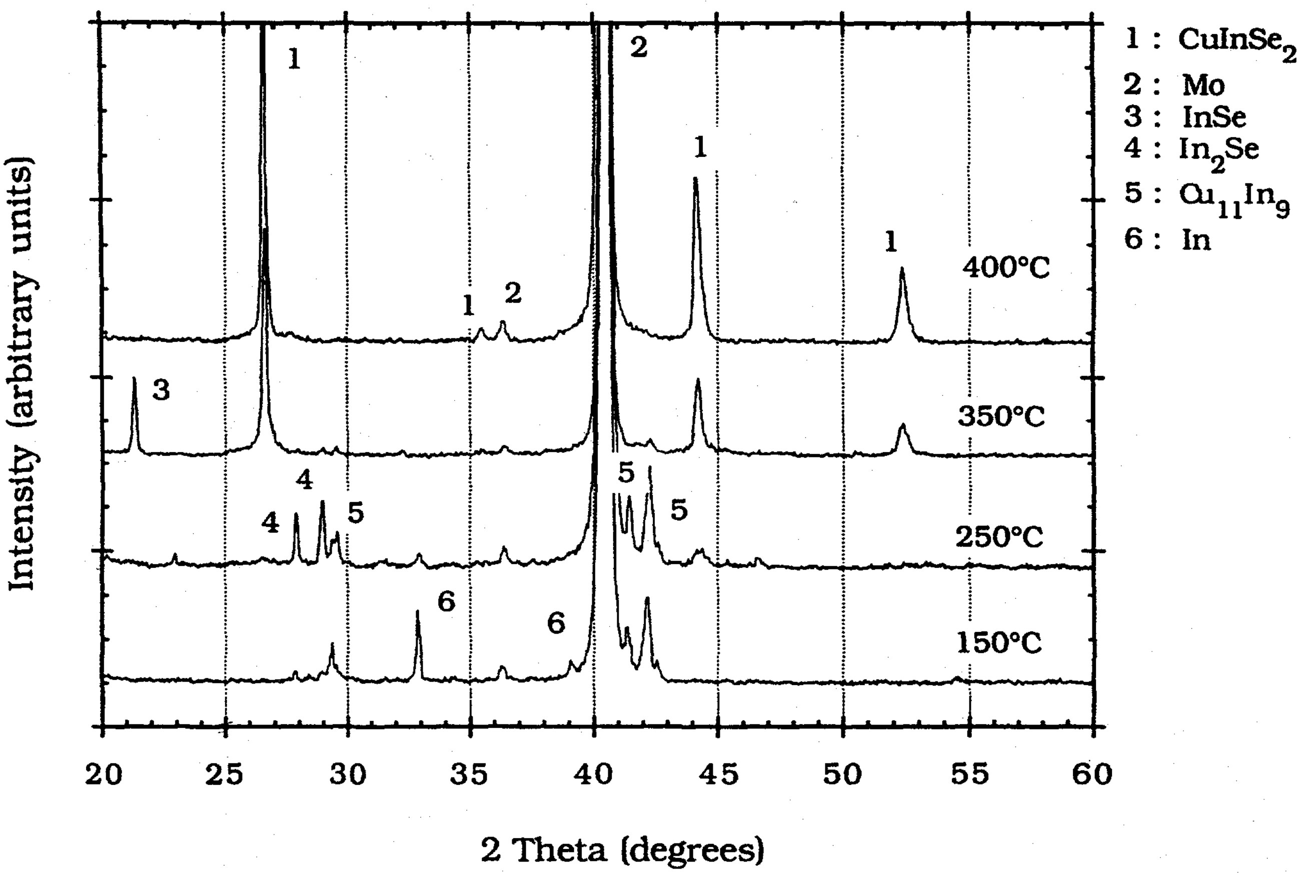

Figure 2.7a Selenization in the Tubular Reactor. Time 60 minutes, temperature 150-400°C.

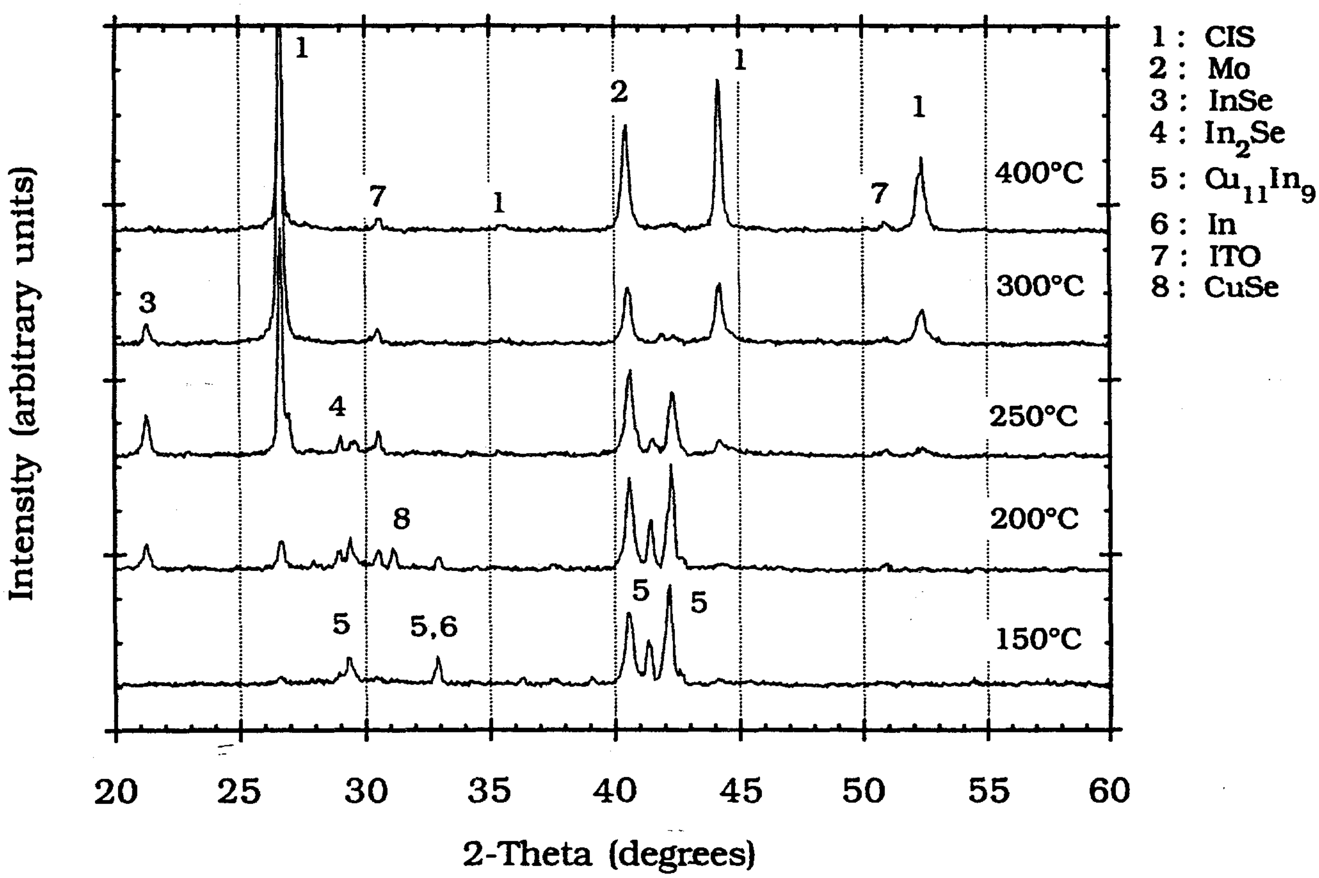

Figure 2.7b Selenization in the PVD Reactor. Time 60 minutes, Temperature 150-400°C.

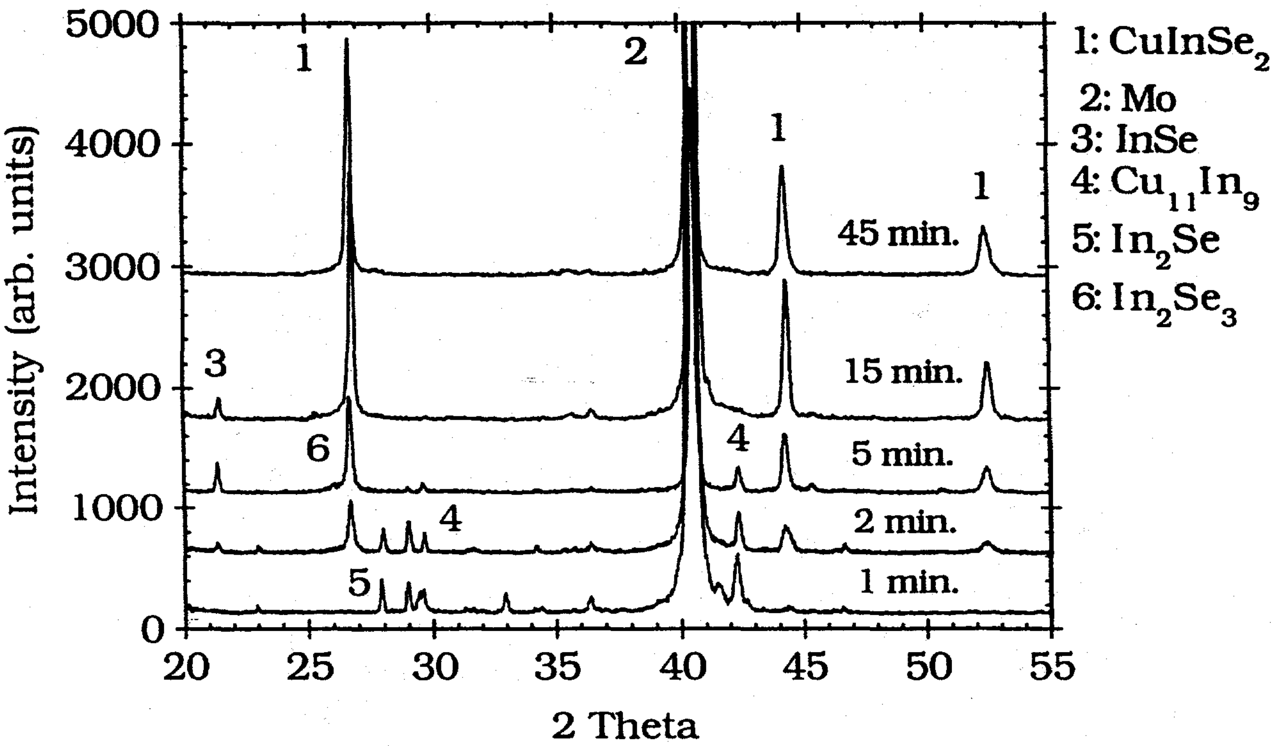

Figure 2.7c Selenization in the Tubular Reactor. Temperature 400°C, Time 1-45 minutes.

At 400°C, $CuInSe_2$ is the only phase observed in the Cu-In bilayer selenized in either H_2Se or Se. The morphology of the Cu-In bilayer selenized in H_2Se is segregated similar to those at 350°C. The morphology of the bilayer selenized in Se consists of a 1μm nodular structure (Fig. 2.8a).

Temperature 400°C, Time 1-45 Minutes

The Cu-In bilayer selenized in H_2Se for 1 minute alloys to form the $Cu_{11}In_9$ and In, while some of the In reacts to form In_2Se in segregated areas.

By 2 minutes at 400°C, $CuInSe_2$ is detected along with $Cu_{11}In_9$ and, In_2Se and InSe in segregated regions. By 5 minutes, $CuInSe_2$ is the dominant phase. $Cu_{11}In_9$, In_2Se and InSe are also observed and the film composition is homogeneous across the surface. The film is completely converted to $CuInSe_2$ by ~45 minutes. Figure 2.8b shows the surface morphology of a Cu-In bilayer selenized at 400°C for 45 minutes in H_2Se.

Based on the experimental results from the tubular reactor in which we carried out reactions both at lower temperatures for 60 minutes and for 1-45 minutes at 400°C, the intermediate (In-Se and $Cu_{11}In_9$) and the final ($CuInSe_2$) phases formed are the same for both sets of experiments. Since it was not possible to perform a series of short-time runs at 400°C in the PVD reactor, we are assuming that the phases formed at lower temperatures for 60 minutes are the same as would be observed at 400°C for shorter times. Thus, the phases observed at lower temperatures in the PVD reactor are presumed to be the precursors to the $CuInSe_2$ film formation at 400°C.

The reaction pathways to $CuInSe_2$ formation in H_2Se have been shown to proceed through the formation of $Cu_{11}In_9$ and In-Se phases. For reaction in Se, the reaction pathway includes Cu-Se phases. We can consider the reaction pathways in the two systems to be occurring analogous to a classic series reaction A -> B -> C. A represents the unreacted metals In and $Cu_{11}In_9$, B includes the binary selenides and C refers to the $CuInSe_2$. For the 1st order series reaction, the concentration of A decreases exponentially with time, B goes through a maximum at a time which is a function of the two rate constants, and C increases with time. Although we do not have quantitative measurements on the relative amounts of the different phases as a function of time, there is a definite qualitative agreement with the available data. For the two reacting systems the pathways are:

	A	-->	B	-->	C
Tubular reactor	$Cu_{11}In$, In		In_2Se, InSe, In_2Se_3		$CuInSe_2$
PVD reactor	$Cu_{11}In_9$, In, Se		In_2Se, InSe, CuSe, Cu_7Se_4		$CuInSe_2$

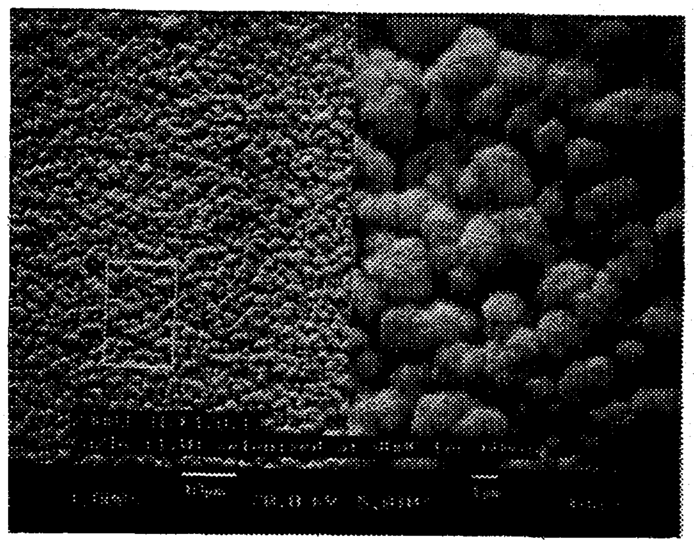

Figure 2.8a SEM micrograph of a Cu-In bilayer reacted at 400°C for 60 minutes in the PVD reactor.

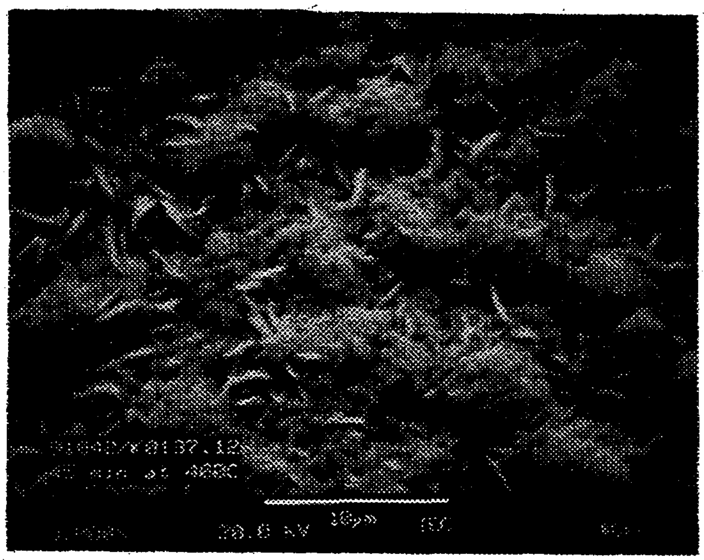

Figure 2.8b SEM micrograph of a Cu-In bilayer reacted at 400°C for 45 minutes in the tubular reactor.

It appears, on a preliminary examination, that the binary selenides which form the $CuInSe_2$ precursors govern the final film morphology. The presence of Cu-Se phases in the reaction scheme involving Se leads to a specular film with the grains being about a micron in size. The film selenized in H_2Se had no discernible grain structure or size with the occasional presence of dendrites on the film surface. It is also interesting to note that CuSe is formed at a temperature lower than Cu_7Se_4 which suggests that Cu is the faster diffusing species and diffuses to a Se-rich area. If Se diffuses to a Cu-rich area, we would have expected to find formation of Cu_7Se_4 at earlier times.

Selenization in the PVD reactor with Se proceeds faster than in the tubular reactor with H_2Se. At 250°C, a comparison of the XRD patterns of the reacted bilayers shows that while $CuInSe_2$ is the dominant phase for the film reacted in Se, it is barely detectable in the film reacted in H_2Se gas. The faster reaction in the PVD reactor could be due to either 1) reaction with Se being faster than the reaction with H_2Se gas, or 2) the presence of the copper selenide phases in the reaction with Se vapor.

To summarize the precursors to $CuInSe_2$ formation in the tubular reactor are different from those in the PVD reactor as copper selenide phases were observed only in the latter. The rate of formation of $CuInSe_2$ has been determined to be faster in the PVD reactor. A preliminary set of reaction pathways have been proposed analogous to a classic series reaction. A more detailed quantitative analysis would require information on the distribution of the chemical species in the film as a function of time.

2.2 WINDOW/HETEROJUNCTION LAYERS FOR $CuInSe_2$

Investigation of the use of chemical bath deposited cadmium sulfide to enhance the performance of $CuInSe_2$/CdS devices has continued. However, despite improvements in the CdS deposition process device results have not improved. The low V_{oc} appears to be caused by the morphology of the evaporated $CuInSe_2$. Alternative baths for the deposition of CdS and CdSe have also been investigated. Finally, modifications to the ZnO layer deposited on the CdS have been made to incorporate higher resistivity ZnO between the CdS and low resistivity sputter-deposited ZnO:Al.

Chemical Bath Deposition of Cadmium Sulfide

Chloride-Based Bath

Substantial improvement in the chemical deposition of cadmium sulfide has been obtained since modifications were made by improving the purity of the DI water system. Analysis of the water showed that calcium, zinc, sodium, and potassium ions were present in the DI water used for CdS solution growth. These ions are believed to have acted as nucleation sites in the CdS reactant bath, accelerating the homogeneous formation of CdS in the bath, depleting the bath constituents, and severely limiting the deposition of CdS on the substrate surfaces.

Improved DI water purity in combination with increased bath temperature and ammonia concentration has resulted in the deposition of films with thicknesses of up to 180 nm on Corning 7059 glass. The films are specular with little powder formation on the surface. Current reactant bath conditions used are as follows:

2×10^{-3} M $CdCl_2$
5×10^{-3} M NH_4Cl
2×10^{-2} M $(NH_2)_2CS$
1.5 M NH_4OH
T = 85-90°C

A growth rate curve for these deposition parameters is shown in Figure 2.9. Film thicknesses are believed to be approximately 20% greater when deposited on glass with textured SnO_2. The optical transmission and reflection of a 7059/CdS sample, approximately 120 nm, are shown in Figure 2.10. The film was deposited under the above conditions with a deposition time of 8 minutes.

$CuInSe_2$/CdS/ZnO:Al cells were fabricated with solution grown CdS using the improved DI water purity. The device parameters of the best efficiency cell for three pieces from $CuInSe_2$ run #32279 with CdS deposition times of 2, 3, and 4.5 minutes are given in Table 2.3 along with the results for a piece from the same $CuInSe_2$ run with an evaporated (CdZn)S/ITO window. The J_{sc} of the three cells with solution grown CdS increases in a manner consistent with the bath time and CdS thickness.

The quantum efficiencies of these cells are shown in Figure 2.11. The thicknesses estimated from the response at 400nm are 300-600 nm as given on the figure and are consistent with the growth curve for CdS on glass. This confirms that the CdS thickness can be controlled over the range of interest for high efficiency cells using this modified deposition bath with higher purity DI water without being limited by homogeneous CdS formation in the bath.

The cells with solution grown CdS all have significantly lower V_{oc}'s and fill factors than the cell with evaporated (CdZn)S. In addition, all the cells with solution grown CdS are soft in reverse bias, starting to break down at around -0.2V. This can be seen in Figure 2.12 where the dark and light J-V curves of the best cell on 32279.33 are shown. Air heat treatments, which are used to improve cells with evaporated (CdZn)S, result in increased shunting and lower V_{oc} and fill factor on cells with the solution grown CdS. Both this breakdown and the low V_{oc}'s may be due to non-uniform coverage of the solution grown CdS caused by the highly textured morphology of the evaporated $CuInSe_2$.

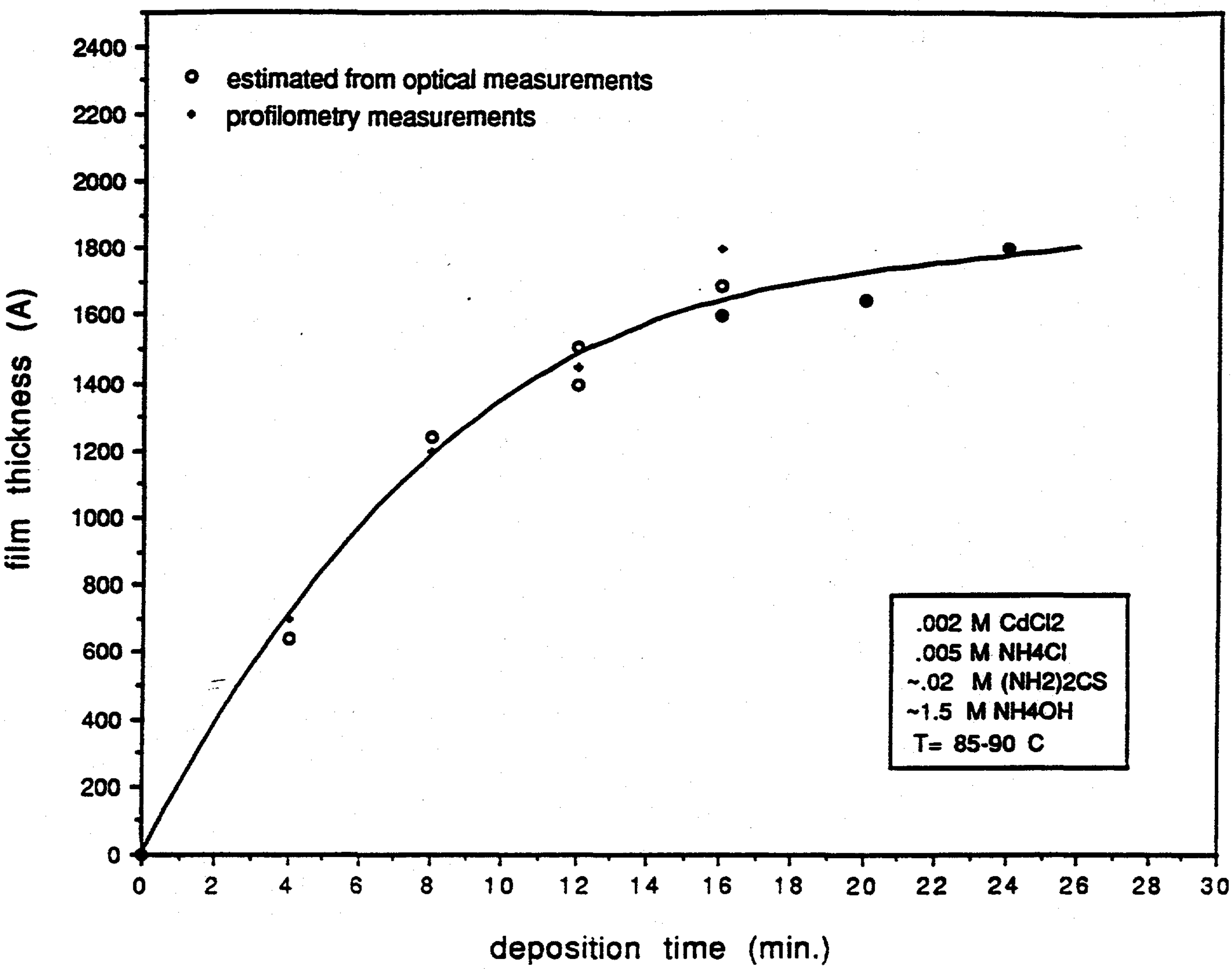

Figure 2.9 Growth rate of CdS on 7059 glass by chemical bath deposition (chloride bath).

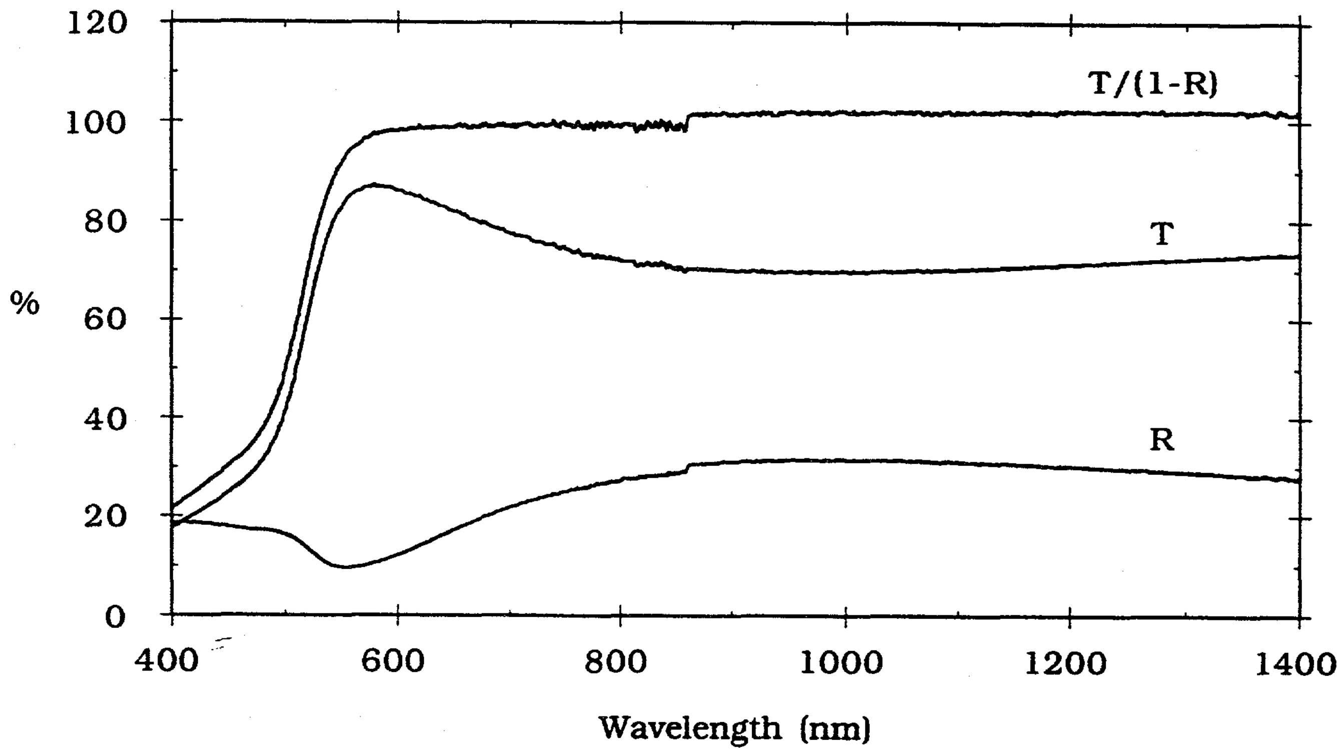

Figure 2.10 Optical transmission and reflection of chemically deposited CdS on 7059 (~120 nm). Sample #70210.2.

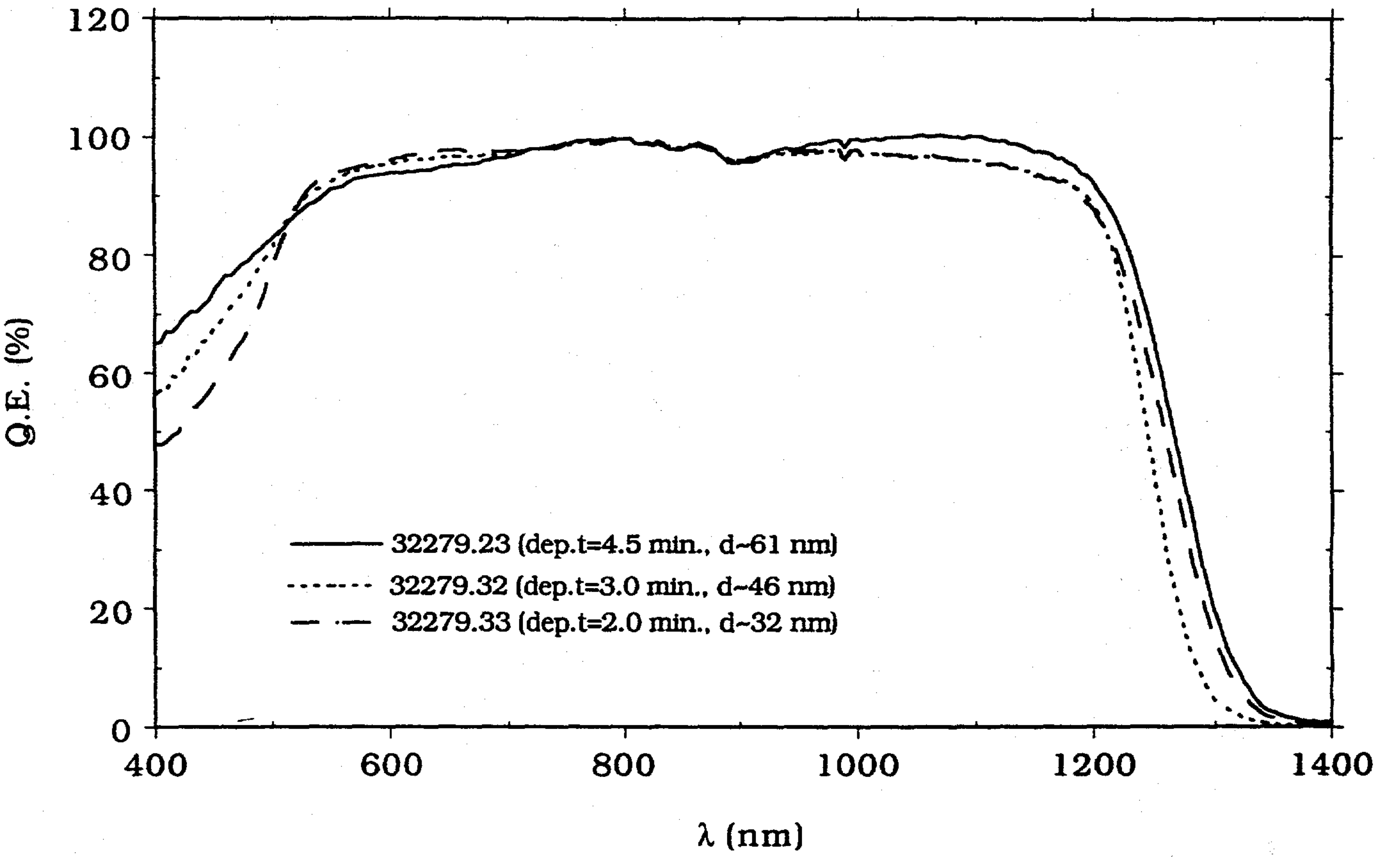

Figure 2.11 Quantum efficiencies of $CuInSe_2$ devices with chemically deposited CdS. QE 32279.

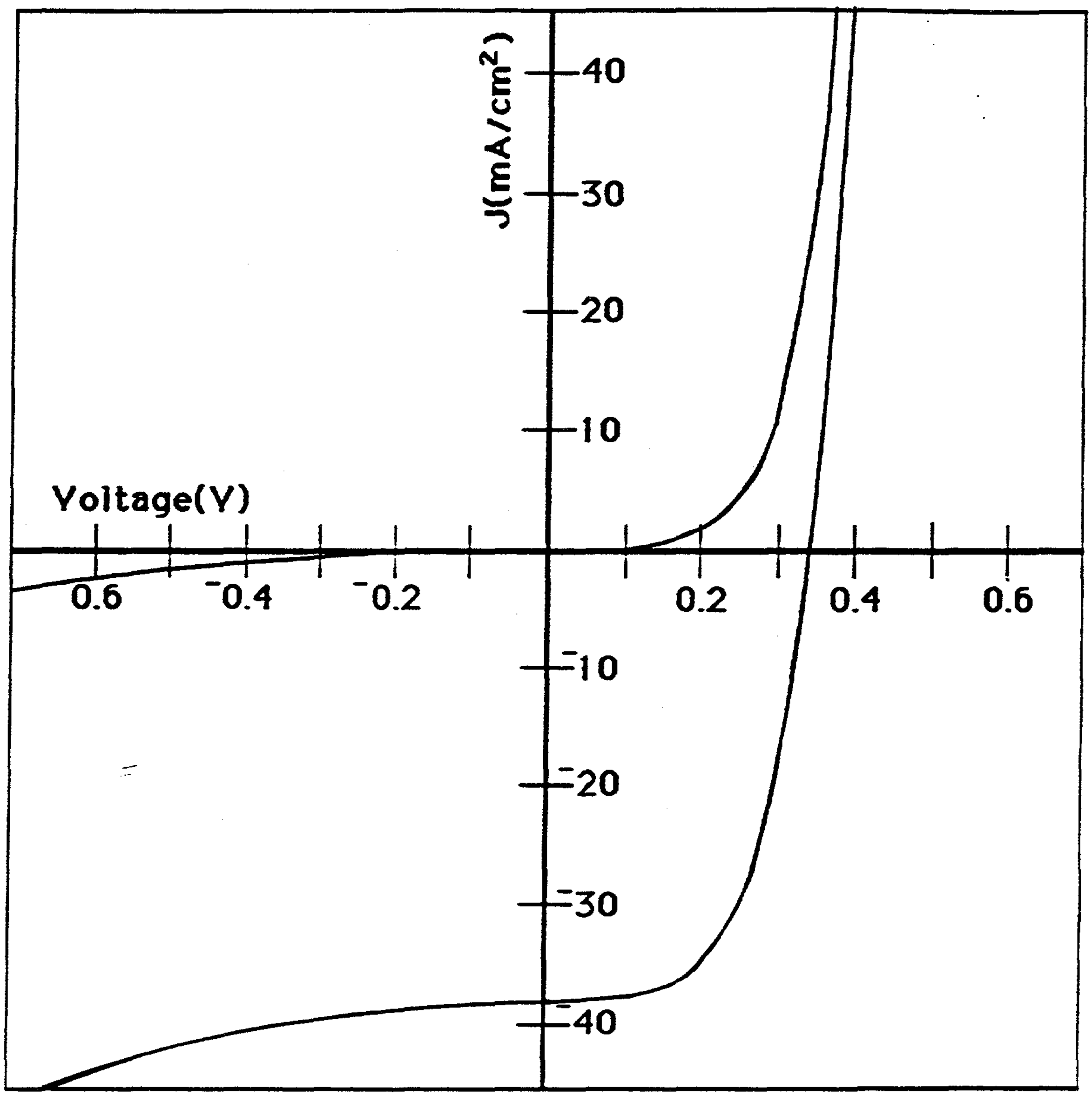

Figure 2.12 J-V curves of $CuInSe_2$/CdS Device 32279.33 Cell 7.

Table 2.3 Best Efficiency $CuInSe_2$ Cell Results with Solution Grown CdS Deposited at 3 Bath Times.

piece #	CdS time (min)	V_{oc} (V)	J_{sc} (mA/cm^2)	FF (%)	$dV/dJ@V_{oc}$ (Ω-cm^2)	$dJ/dV@J_{sc}$ (mS/cm^2)	Eff (%)
23	2	0.347	36.8	57.3	2.0	3.8	7.33
32	3	0.367	37.8	60.6	1.7	1.7	8.40
33	4.5	0.347	38.4	57.2	1.8	3.3	7.62
22	evap	0.431	34.9	69.5	1.5	2.4	10.47

Further evidence of problems caused by the morphology of the $CuInSe_2$ with the solution grown CdS was observed on cells delineated by photolithography. The completed cells have holes etched through the ZnO and CdS layers, reducing the cell area. In the worst cases, as much as 30% of the cell area has been removed resulting in very poor cell performance with low J_{sc} and V_{oc}. These holes occur where there are sharp growth defects protruding from the $CuInSe_2$. This causes non-uniform coverage of the photoresist which then breaks down during the subsequent steps used to remove the ZnO and CdS. These growth defects, which have been discussed previously (15), can be as high as 5-7 μm above the $CuInSe_2$ surface but do not create a problem with thick evaporated CdS layers.

$CuInSe_2$ films were etched to smooth the surface before depositing solution grown CdS and fabricating devices. Experiments were done with both bromine/H_2O (cell #32282.33) and bromine/methanol (cell #32290.21) etches. The bromine/H_2O etch smooths the surface and effectively removes all growth defects. In each case the problems with photolithography caused by the growth defects were greatly reduced but the devices were still shunted with low V_{oc}. This suggests that the morphology alone is not responsible for the poor performance and the surface or grain boundary chemistry may be critical. However, it should be noted that the cell performance with the Br/H_2O etch is very non-reproducible even with window layers based on evaporated (CdZn)S.

<u>Acetate-Based Bath</u>

Solution grown CdS films were also deposited from a bath using acetate-based reactants, rather than the standard chloride-based reactants. Typical deposition conditions were similar to those of the chloride bath method with the pH in the 9-9.5 range. The bath was heated to 85°C and was composed of the following reactants at indicated concentrations:

0.002 M $Cd(C_2H_3O_2)_2$
0.02 M $NH_4(C_2H_3O_2)$
0.008 - 0.02 M $(NH_2)_2CS$
~1.4 M NH_4OH

Growth rates for this bath composition were much slower than with the chloride bath. The growth rates are shown in Figure 2.13 for CdS deposited on glass substrates at 2 different thiourea/cadmium acetate ratios (R). The growth is directly proportional to R which was varied by changing the thiourea concentration. The homogeneous reaction of CdS in the bath was suppressed as R increased and the CdS precipitate in solution was greatly reduced in both amount and particle size with R=10. At this ratio, bulk precipitate in the solution was very fine and the glass substrates appeared specular with no powder on the surface.

$CuInSe_2$/CdS/ZnO cells were fabricated with solution grown CdS from this acetate bath. The CdS layer was ~55 nm thick. There was no improvement in cell performance over typical cells with the chloride based CdS deposition. The best cell had V_{oc}=0.30V, J_{sc}=40mA/cm^2, and 5.0% efficiency.

<u>Zinc Oxide</u>

Sputtered Bilayer ZnO

Experiments were done to investigate the effect of a high resistance ZnO layer between the solution grown CdS and the doped low resistance ZnO layer. Presently ZnO is RF sputter deposited from a ZnO-Al_2O_3(2% by weight) target which yields films with resistivity 1-2x10^{-3}Ω-cm. By sputtering in an oxygen-argon mixture instead of just argon the resistivity can be increased to 1 Ω-cm. Cells fabricated with the high resistivity sputtered ZnO layer between the CdS and low resistivity ZnO showed no improvement. Results in reference (16) indicate an increase in V_{oc} and FF with an intrinsic ZnO layer which has an optimum resistivity of ~10^4 Ω-cm. This cannot be achieved with the Al-doped target and will require an alternative deposition procedure.

Chemical Bath Deposition of ZnO

A method for the deposition of ZnO by solution growth was developed. Zinc ions from a zinc salt were complexed in an alkaline aqueous bath, analogous to the chemistry used for cadmium in solution growth of CdS. Specifically, ammonia and triethanolamine (TEA) were used as complexing agents for zinc. The deposition bath was heated to 85-90°C, had a pH of ~10, and consisted of the following reactants at indicated concentrations:

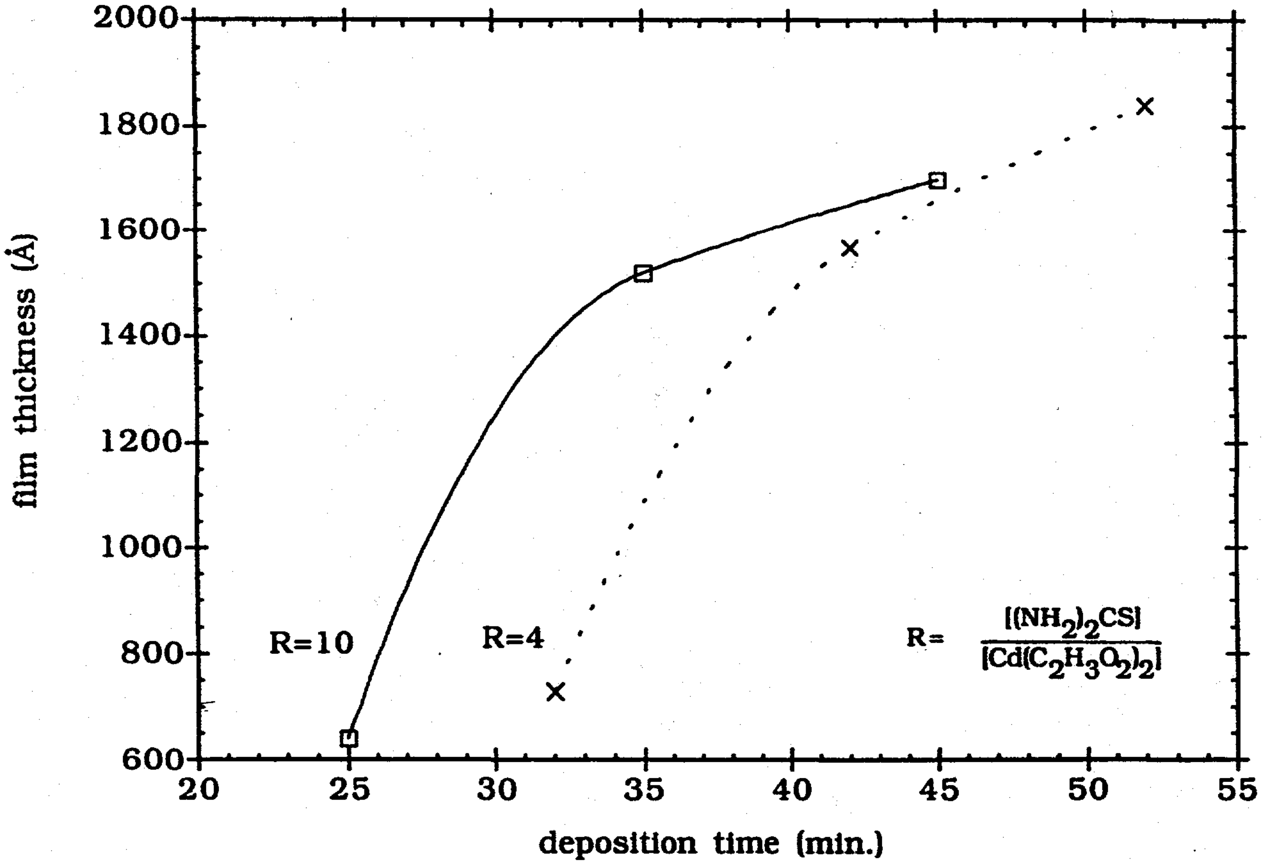

Figure 2.13 Growth rate of CdS on 7059 glass in acetate baths with varying [thiourea][cadmium acetate] ratios.

$ZnCl_2$	0.03 M
NH_4OH	1.12 M
TEA	0.45 M
NaOH	0.15 M

Similar to solution grown CdS and CdSe, the ZnO preferentially deposited on textured surfaces, and it was difficult to obtain a continuous film on 7059 glass. Therefore, the resistivity of the films was not determined. Fairly smooth, visible films were deposited on both ITO and $CuInSe_2$ within 40 minutes at the above bath conditions.

$CuInSe_2$/solution grown CdS/ZnO and $CuInSe_2$/ZnO cells were fabricated with a 2 layer ZnO structure, consisting of solution grown ZnO followed by sputtered Al-doped ZnO, to investigate the effect of the undoped ZnO layer. The $CuInSe_2$/CdS/ZnO showed no improvement with low V_{oc}, <0.3V. The $CuInSe_2$/ZnO cells had even lower V_{oc}, <0.2V, as has been observed previously.

Chemical Bath Deposition of Cadmium Selenide

The general bath chemistry used for solution growth of CdS was used as the basis for the chemical deposition of CdSe. The chemistry was modified to accommodate the need for Se^{-2} ions by introducing sodium selenosulfate (Na_2SeSO_3), rather than thiourea, into the bath. The sodium selenosulfate is not commercially available and had to be prepared in the laboratory by refluxing selenium powder in a sodium sulfite (Na_2SO_3) solution.

An acetate-based chemistry replaced the standard chloride-based bath usually used at IEC for CdS solution growth. Also, trisodium citrate (TSC) was added as a complexing agent for the selenium ions in order to control the rate of deposition and precipitation in the reaction bath. Sufficient quantities of the reactants were mixed together to provide the following final concentrations:

$Cd(C_2H_3O_2)_2$	0.01 M
NH_4OH	2.1 M
Na_2SeSO_3	0.016 M
TSC	0.03 M

The reactants were mixed at room temperature, the substrates immersed, and the bath heated to ~85°C while rigorously stirred. The pH at 85°C ranged from 9.0 to 9.5 and typical deposition times were 40-60 minutes. Reflective brownish-red films were obtained on 7059 glass and ITO substrates.

CdSe films were deposited onto $CuInSe_2$ by this method and a device was fabricated, yielding V_{oc}=0.24 V, J_{sc}= 29 mV, FF=35%, and EFF=2.82%.

2.3 FABRICATION OF CdTe SOLAR CELLS

CdTe Solar Cells

In this section the relationships between the CdTe device fabrication process, the physical properties of the layers, and the device performance are addressed. It is shown that shorter post-deposition treatments of devices with CdS less than 2000 Å thick lead to high yield and moderate performance. The effects of CdS heat treatments prior to CdTe deposition are evaluated.

A new process using $CdCl_2$ vapor in place of the $CdCl_2$ surface layer was developed. This process promotes uniform grain growth in CdTe, leaves the CdTe surface free of residue, and results in uniform spatial device efficiency.

Detailed materials analysis of the CdS/CdTe structure will be used to show: 1) the grain enhancement observed on the CdTe surface extends down to the CdS/CdTe interface; 2) the interdiffusion of CdS and CdTe is a complex process which may limit the device V_{oc}; and 3) that the changes in short wavelength spectral response compared to initial CdS transmission are due to Te diffusion into the CdS.

Alternative contacts to CdTe were fabricated. Work on ZnTe:Cu contacts was completed. Devices with graphite ink contacts were fabricated.

Film Preparation

CdTe/CdS devices were prepared using evaporated CdTe in a superstrate configuration on ITO and SnO_2 transparent conductive oxide (TCO) samples. CdS was deposited by physical vapor deposition (PVD) and solution growth. Contact to CdTe was made with Cu/Au films deposited by electron-beam (e-beam) evaporation.

Transparent Conductive Oxide

ITO 2500 Å thick with a sheet resistance of ~20 ohm/sq was sputtered at room temperature onto cleaned Corning 7059 glass substrates.

SnO_2 coated glass substrates were provided by the following sources:

Solarex (SLX)
Asahi (ASH)
Libbey Owens Ford (LOF)
Cherry Electric (CHE)

The SnO_2 samples were characterized by optical microscopy, optical transmission, and x-ray diffraction prior to use in CdS/CdTe devices. The normalized optical transmission, T/(1-R), for representative SnO_2 samples used in this work are shown in Figure 2.14.

CdS

CdS was deposited by PVD and solution growth at thicknesses from 800 Å to 2000 Å. Optical transmission and reflection were routinely measured on as-deposited films before and after heat treatment.

Undoped CdS films were deposited by PVD from an effusion source bottle using high purity General Electric CdS powder. For these depositions, the substrate temperature was 130°C and the CdS source bottle temperature was 790°C, yielding a deposition rate of ~0.03 μm/min.

CdS films were deposited by solution growth using the chemistry described in section (2.1).

CdTe

CdTe films were deposited by PVD from an effusion source using CdTe powder made by grinding 99.999% pure CdTe ingots purchased from Alfa Products. The powder was ground to A.S.T.M. 100 mesh giving 150 μm maximum particle size. The following deposition conditions were used to deposit 2 - 2.5 μm thick CdTe films: substrate temperature = 250°C; CdTe effusion source charge temperature = 750°C; deposition time = 100 minutes; and bell jar base pressure = $1x10^{-5}$ Torr.

Post Deposition Processing

After CdTe deposition the samples were chemically and thermally treated to improve their properties for devices. The processing steps are summarized below:

1. $CdCl_2$ coating from $CdCl_2$:CH_3OH solution
2. Dry in inert atmosphere at > 100°C
3. Heat treat in Ar/O_2 mixture at 400 - 420°C
4. Rinse $CdCl_2$ off in DI water
5. Dry in inert atmosphere at > 100°C
6. Contact deposition
7. Device optimization

Cu/Au contacts with evaporated 100 Å Cu and 500 Å Au were used throughout this work. Devices were given an air heat treatment at 160 - 180°C for 1 hour followed by immersion in 0.01 % Br_2-CH_3OH solution for 5 seconds.

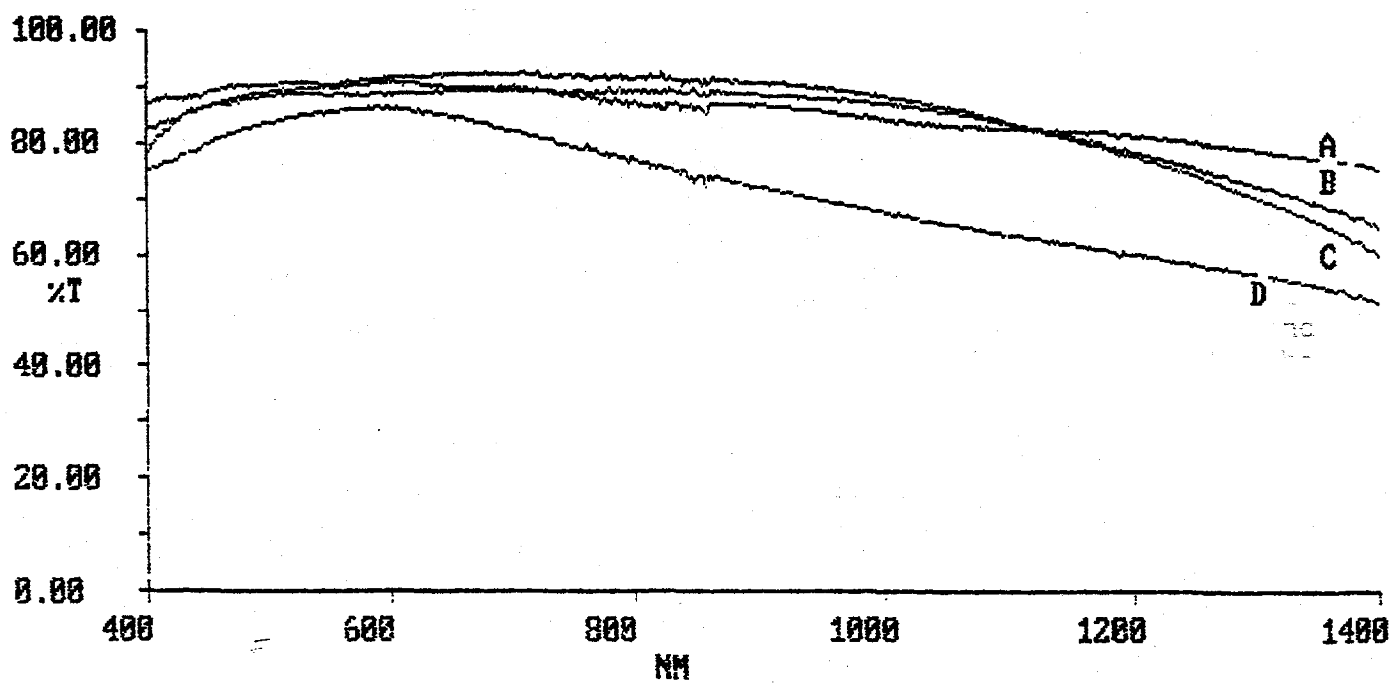

Figure 2.14 Normalized optical transmission, T/(1-R), of glass/SnO_2 superstrates supplied by the following manufacturers: a) Asahi; b) Solarex Corporation; c) Cherry Electric; and d) Libby Owens Ford.

Devices with Evaporated CdS

The most critical step for consistently achieving high efficiency is the heat treatment at 400 - 420°C with $CdCl_2$. In previous work (17), it was shown that CdS/CdTe devices treated for 30 minutes at 400°C with $CdCl_2$ exhibited a decrease in V_{oc} as the CdS thickness was reduced below 2000 Å. Accompanying this was an increase in the percentage of shorted devices obtained across a 1" x 1" sample. To improve the yield of non-shorted devices with thin CdS, the heat treatment time was reduced from 30 minutes to ~15 minutes. The J-V parameters obtained for the best device on structures with different CdS thicknesses are shown in Table 2.4.

Table 2.4 J-V parameters of CdS/CdTe devices with thin evaporated CdS.

Sample	TCO	d CdS (Å)	V_{oc} (mV)	J_{sc} (mA/cm^2)	FF (%)
746.21	ITO	3500	747.7	17.92	67.92
721.12	ITO	2400	778.5	17.95	75.92
747.21	ITO	1500	768.1	19.32	70.18
748.21	ITO	800	504.5	23.04	54.46
733.13	LOF	2000	725.2	18.23	59.75
722.23	SLX	2500	729.3	19.87	67.13
752.11	SLX	1300	527.2	20.35	42.23
731.22	SLX	800	422.6	20.47	56.09

This data, taken with the relatively high device yield shows that pinhole defects are not a critical issue with evaporated CdS for films greater than ~500 Å thick.

The influence of CdS processing on the performance of CdTe/CdS devices was also evaluated. Devices were fabricated using 2000 Å thick evaporated CdS layers which were heat treated prior to the CdTe deposition. The CdS films were heat treated at three temperatures (410°C, 450°C, and 480°C), in two groups: 1) with a $CdCl_2$ surface coating in Ar/O_2 and 2) in 4% H_2/Ar without $CdCl_2$. In all cases, the heat treatment sharpened the CdS optical transmission edge. After CdTe deposition, devices were completed by a $CdCl_2$ surface treatment at 410°C for 30 minutes followed by a rinse and evaporation of Cu/Au contacts and optimization. The device results for the best device one each piece are summarized in Table 2.5.

Table 2.5. J-V parameters for devices with different CdS pre-treatments using 2000 Å thick CdS on ITO.

Sample	CdS Treatment Temp	Atmosphere	V_{oc} (mV)	J_{sc} (mA/cm^2)	FF (%)
742.11	410	H_2/Ar	731	18.39	62.3
742.22	450	H_2/Ar	737	16.37	62.8
742.21	480	H_2/Ar	744	17.83	57.2[a]
742.12	410	$CdCl_2$:Ar/O_2	652	17.48	54.2
742.13	450	$CdCl_2$:Ar/O_2	700	17.73	58.7
742.23	480	$CdCl_2$:Ar/O_2	582	18.36	52.7[a]

[a]) J-V trace exhibited curvature for $V > V_{oc}$.

Comparing the spectral response for each set shows that the devices with $CdCl_2$ treated CdS retain the sharp CdS bandedge short wavelength cutoff after processing, but those with H_2/Ar treated CdS exhibit a very shallow edge (Figures 2.15 and 2.16) which is produced by the diffusion of Te into the CdS layer. No change in the short wavelength cutoff in spectral response is observed for increasing CdS treatment temperature in either case.

Devices with Solution Grown CdS

Reduction of heat treatment time and improvement of the CdS deposition chemistry allowed devices to be made with thin solution grown CdS. Previous experience with solution grown CdS in CdS/CdTe cells using this process produced mostly shorted devices. Table 2.6 lists device parameters for CdS/CdTe cells made with solution CdS on various substrates.

Solution grown CdS was pre-treated under the same conditions used for the evaporated CdS, but the effects were never reproducible, for example, in some cases the $CdCl_2$ treatment darkened the CdS film and softened the CdS bandedge, a result which has never been observed for evaporated CdS.

For CdS films of the same thickness, the V_{oc} is lower on devices made with solution grown CdS than with evaporated CdS.

Contacts

Previously, optimal conditions were identified for fabricating ZnTe contacts for CdS/CdTe cells (18), providing an alternative to Cu/Au contacts. Another alternative contact, graphite ink,

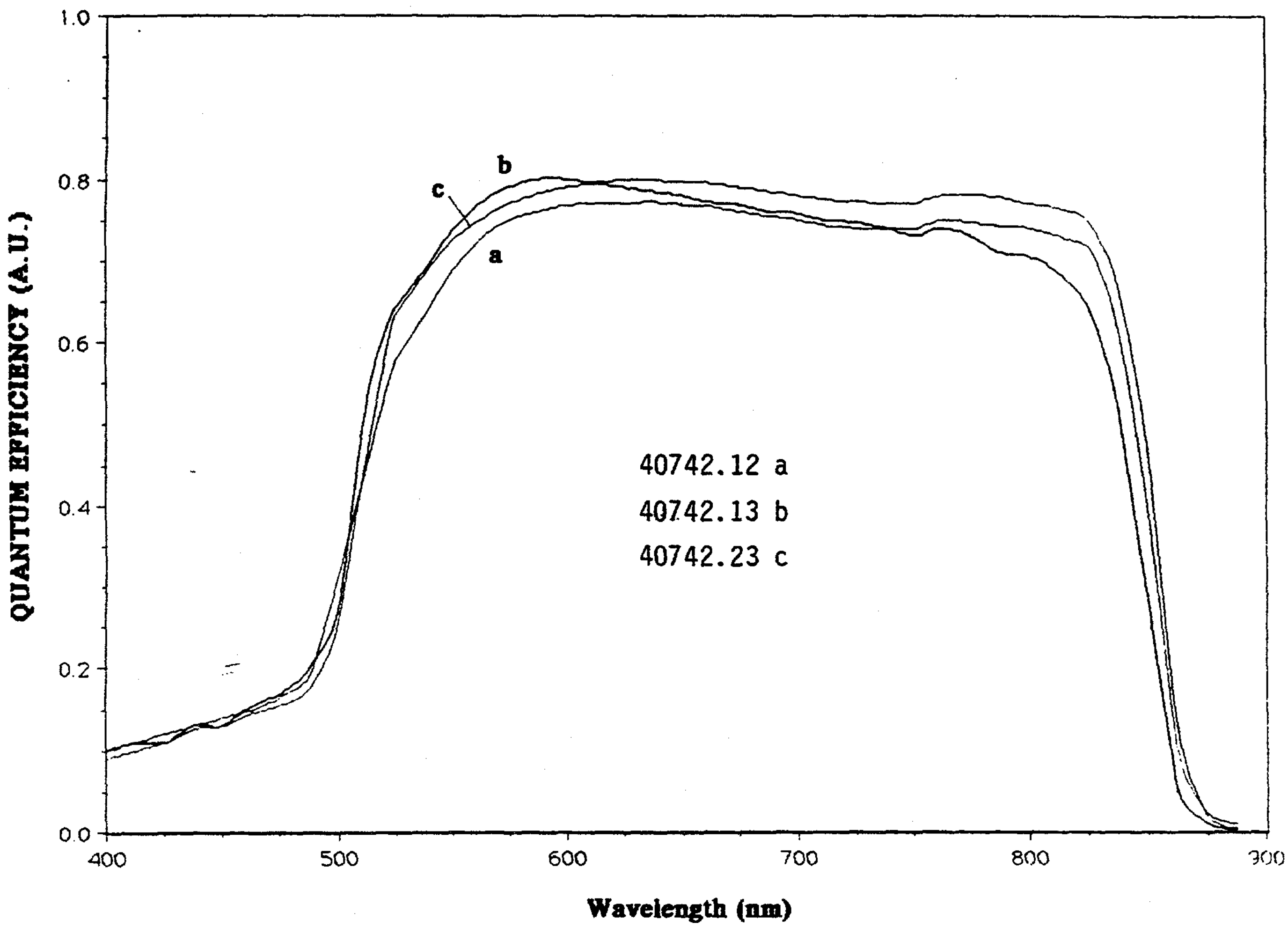

Figure 2.15. Spectral response of CdS/CdTe devices with CdS heat treated with $CdCl_2$ prior to CdTe deposition: a) 410°C for 30 minutes; b) 450°C for 30 minutes; and c) 480°C for 20 minutes.

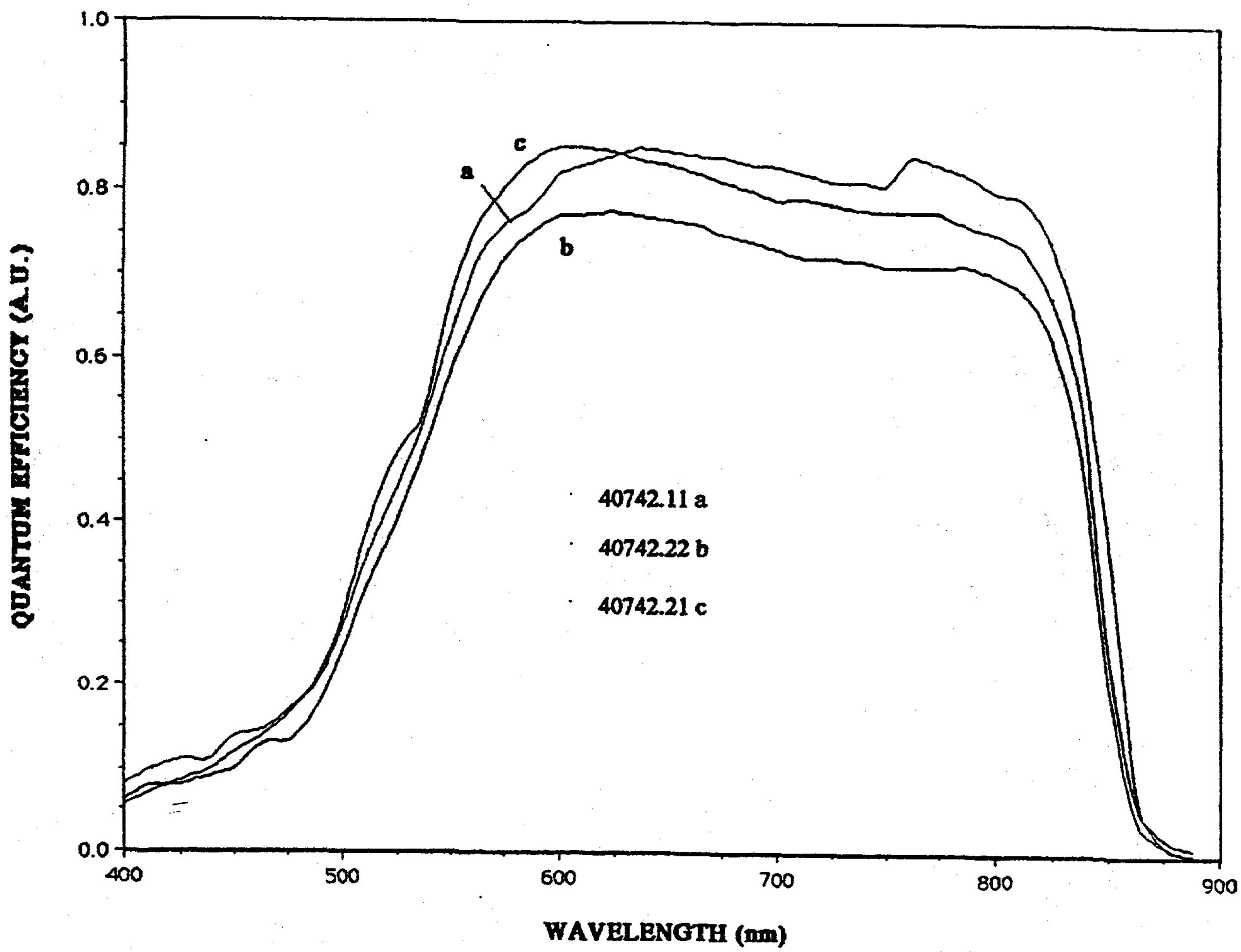

Figure 2.16 Spectral response of CdS/CdTe devices with CdS heat treated with H_2/Ar prior to CdTe deposition: a) 410°C for 30 minutes; b) 450°C for 30 minutes; and c) 480°C for 20 minutes.

Table 2.6 J-V parameters of CdS/CdTe devices with thin solution grown CdS.

Sample	TCO	d CdS (Å)	V_{oc} (mV)	J_{sc} (mA/cm^2)	FF (%)
739.31	ITO	1100	447	22.45	55.2
736.13	ASH	1200	340	20.58	50.9
732.32	SLX	1600	543	22.57	54.4
732.23	CHE	1600	670	20.10	58.6
732.22	CHE	1600	607	19.03	56.5[a]
732.12	CHE	800	602	21.60	56.4
732.11	CHE	800	595	21.87	59.06[a]

a) device had ZnTe:Cu/Cu/Au contact

was examined on a small number of samples. For the evaluation, vapor treated CdS/CdTe was used to provide a clean surface requiring no other preparation. J-V data is shown in Table 2.7 for devices contacted with Cu/Au, undoped graphite ink (Acheson 505SS), doped ink, and undoped ink deposited on a thin Cu layer. The samples were dried at 100°C for 10' then were heat treated at 150°C in argon for 30 minutes prior to testing. Ag paste was added to make low resistance contact to the graphite surface.

Table 2.7. J-V parameters for CdS/CdTe devices with graphite contacts.

Sample	Contact	V_{oc}	J_{sc}	FF
737.232	Cu/Au	701	18.0	64.6
737.232	C	619	15.7	44.9
737.232	C+100ppm $CuCl_2$	661	17.1	51.6
737.232	C+Te+$HgCl_2$	702	11.1	40.9
737.322	Cu/C	702	17.4	62.9
737.323	Cu/C	689	19.0	56.7
733.231	C	691	10.7	49.2

$CdCl_2$ Processing

Alternative approaches to the 400°C/$CdCl_2$ heat treatment were investigated to evaluate: 1) the chemistry involved in the recrystallization; 2) the effects on device performance; and 3) the efficacy of other halides in restructuring the CdTe.

$CdCl_2$ melts at 568°C and boils at 960°C (19). From equilibrium sublimation data for $CdCl_2$ vapor over $CdCl_2$ solid from 618°C to 967°C (20) the $CdCl_2$ vapor pressure extrapolated to the 400 - 410°C range used for processing CdTe/CdS cells is around 1.5 x 10^{-2} torr which is high enough to allow vapor transport of $CdCl_2$ species to CdTe.

Heat treatments were carried out in closed volume containers at reduced pressure with a $CdCl_2$ charge located near but not in physical contact with CdTe/CdS. The extent of CdTe grain coalescence, CdTe-CdS interdiffusion, and performance of CdTe/CdS devices was investigated as a function of heat treatment temperature and time. The $CdCl_2$ vapor heat treatments were carried out in two groups on 4 μm thick CdTe and 0.2 μm thick CdS from a single deposition: 1) temperatures from 410 °C to 480°C for ~20 minutes and 2) fixed temperature of 450 °C for times from 6 minutes to 20 minutes. The heat treatments were carried out in an evacuated quartz tube (~25 torr) inserted into a tube furnace with the $CdCl_2$ powder and CdS/CdTe samples at the same temperature. Grain size and morphology were determined from scanning electron micrographs. X-ray diffraction spectra of the (111) peak were taken to determine changes in lattice parameter (a_o) and peak width (FWHM). The shift in lattice parameter is interpreted as interdiffusion of CdS into CdTe, and an estimate of the molar concentration of S in the resulting Cd(TeS) layer was made (21).

The physical data for the two sample groups are shown in Table 2.8. For comparison, data for a sample from the same CdTe/CdS deposition heat treated with $CdCl_2$ on the CdTe surface is shown.

Comparing the surface treatment to the vapor treatment at 410°C, we find comparable changes in grain size and lattice parameter, however, the vapor treated sample exhibited a single phase surface of well defined grains while the surface treated sample exhibited a second phase overlying well defined CdTe grains. As temperature was increased, both the maximum and mean grain size increase with the same degree of S diffusion into the CdTe for 410 to 450°C. An SEM photograph of a vapor treated CdTe surface with grains as large as ~6 μm is shown in Figure 2.17. The sample treated at 480°C was non-uniform with grain separation along one side and increased S diffusion into CdTe. The time progression at 450°C reveals that grain size enhancement from 0.2 μm to ~1 μm occurs within the heatup time and continues for longer times. CdTe-CdS interdiffusion to ~4 % S in Cd(TeS) also occurs within the heatup time frame but does not progress with additional time.

Table 2.8. Physical data for CdTe/CdS films heat treated with $CdCl_2$ by surface application (S) and vapor treatment (V).

Sample	Heat Type	Treatment Temp (°C)	Time (min)	$CdCl_2$ Press. (Torr)	Grain Size Max (μm)	Mean (μm)	XRD a_o (Å)	FWHM (deg)	Est % S
738.111	(as-deposited)			-	0.2	<0.2	6.505	0.15	0
738.112	S	410	20	0.02	1.0	0.8	6.491	0.12	2
738.231	V	**410**	20	0.02	1.2	0.8	6.489	0.12	3
738.321	V	**425**	20	0.03	3.2	1.2	6.486	0.11	4
738.232	V	**450**	20	0.08	4.6	2.0	6.489	0.11	3
738.233	V	**480**	15	0.18	6.0	2.5	6.456	0.17	8
738.311	V	450	**6**	0.08	1.2	0.6	6.483	0.12	4
738.312	V	450	**10**	0.08	3.5	1.4	6.486	0.12	4
738.313	V	450	**15**	0.08	3.6	1.8	6.486	0.12	4
738.232	V	450	**20**	0.08	4.6	2.0	6.489	0.11	3

Devices were fabricated by evaporation of Cu/Au dots directly onto the heat treated surface. Device results are listed in Table 2.9 for all samples except the piece treated at 480°C for which the V_{oc} ranged from 100 - 500 mV. Surprisingly, results were similar for all other devices.

Table 2.9. Range of J-V parameters obtained on samples of Table 2.8.

Sample	Heat Treatment Type	Temp	Time	V_{oc} (mV) Max	Min	J_{sc} (mA/cm^2) Max	Min	FF (%) Max	Min
738.12	S	410	20	720	623	20.1	19.8	60.8	55.2
738.231	V	410	20	708	701	21.5	20.0	65.9	64.5
738.232	V	450	20	727	714	20.5	20.4	63.4	61.6
738.311	V	450	6	731	708	22.0	20.0	66.8	57.3
738.312	V	450	10	751	734	20.6	19.9	64.5	61.6
738.313	V	450	15	724	714	19.5	17.7	62.1	61.1
738.232	V	450	20	727	714	20.5	20.4	63.4	61.6

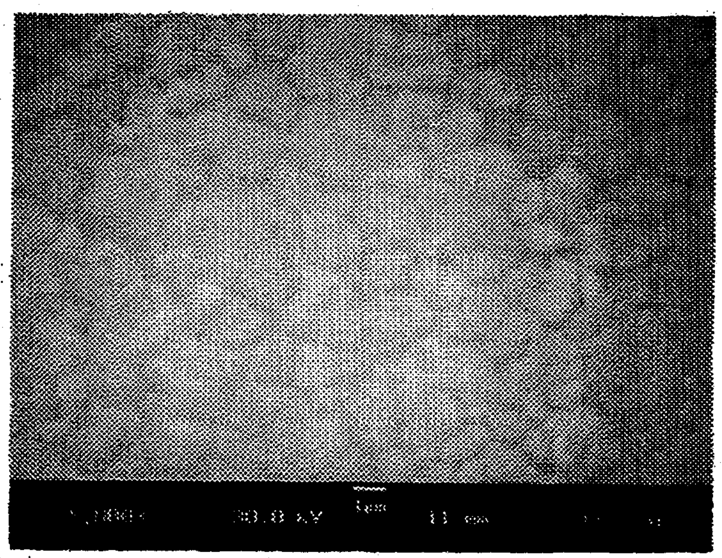

Figure 2.17. SEM photograph of CdTe surface of ITO/CdS/CdTe structure after $CdCl_2$ vapor treatment resulting in large grains.

The vapor treated devices exhibited little or no cross-over between the light and dark J-V curves, which may be an effect of the clean CdTe surface obtained with this method. The uniform device results coupled with its simplicity suggests that the vapor treatment is superior to the $CdCl_2$ dip or surface coat methods currently employed and offers an approach to large area CdTe/CdS processing.

Other halide systems may be found (e.g., KBr) to improve the crystallinity and properties of the CdTe/CdS. We performed a preliminary investigation of the interaction of these compounds and elements with CdTe/CdS with emphasis on grain modification and interdiffusion. In the case of $CdBr_2$ and KBr, the CdTe surface was coated with a solution of these salts in methanol. The samples were dried, leaving the precipitated coating. HCl was entrained in argon gas bubbled through a 70% solution of $HCl-H_2O$. The heat treatments were carried out at atmospheric pressure for 30 minutes. Table 2.10 summarizes the preliminary findings of this work for 2 μm thick CdTe. For reference, results for a $CdCl_2$ surface treated sample are given.

The decreased FWHM values after heat treatment are consistent with the grain size measurements. For the $CdBr_2$ treated sample at 500°C, the S diffusion into CdTe corresponds to 6% S content and the peak remained broad, suggesting non-uniform composition. The data thus far suggests that other halides and even HCl can be used to enhance grain size and offer other routes to post-processing of CdTe.

Table 2.10 Effects of heat treatment with different halide systems on structural properties of CdS/CdTe.

Treatment Technique	Sample Temp (°C)	Lattice Parameter (A)	FWHM (deg)	Maximum Grain Size (μm)
None	-	6.490	0.35-0.20	0.2
$CdCl_2$ on CdTe surface	400	6.480	0.18	1
HCl/Argon vapor	400	6.470	0.11	2
$HgCl_2$ vapor	400	6.481	0.13	2*
$CdBr_2$ on CdTe surface	400	6.465	0.11	0.2
$CdBr_2$ on CdTe surface	500	6.449	0.20	2
KBr on CdTe surface	400	-	-	<1

* Pitting observed on surface

Physical Characterization of $CdCl_2$ Treatment

CdTe/CdS cells fabricated using evaporated CdTe have achieved V_{oc} near 800 mV (e.g., 40723.12, V_{oc}=799 mV, NREL measurement). This limit in V_{oc} has been attributed to the properties of the grain boundaries, both in extent and in electronic properties, near the CdS/CdTe interface. Treatment conditions were found which produced significantly larger grains, yet the V_{oc} was nominally the same for devices made on the large grain CdTe. More complete measurements of the properties of the grains, grain boundaries and film structure are thus called for.

Experiments were performed to: 1) ascertain that the grain growth observed at the top surface of the CdTe layer accurately reflects the degree of grain growth at the CdS/CdTe interface and 2) determine the extent of CdS/CdTe interdiffusion accompanying the grain growth. The degree to which the top surface grain structure propagates into the film was measured by a comparison of polished and etched cross-sections of as-deposited and heat treated samples. In addition, ITO/CdS/CdTe samples were prepared on polished Si wafers and were polished into thin cross sections for TEM analysis. The extent of sulfur diffusion into CdTe was evaluated by: 1) SIMS profiling of the Si/ITO/CdS/CdTe sample; 2) EDS analysis of the cross-section; 3) optical transmission of CdS/CdTe structures; and 4) determination of the lattice parameter based on high angle x-ray diffraction peaks from the CdTe layer.

Cross sections were prepared by vacuum impregnation of the thin film samples with epoxy while supporting them perpendicular to the base of the potting cup with plastic c-clips. After hardening, the samples were polished on 0.05 micron alumina grit, then a three step process was used to reveal grain boundaries:

1) etch in 0.01% Br_2-methanol for 5 sec
2) exchange reaction in 0.1 M $CuCl_2$-H_2O at 65°C for 3 min
3) etch in 0.2 M KCN at 65°C for ~30 sec

Scanning electron micrographs of a CdS/CdTe structure heat treated at 410°C for 24 hours with $CdCl_2$ are shown in Figure 2.18. Figures 2.18a and 2.18b show the top surface of the CdTe and the cross section, respectively. The CdTe layer has pulled away from the CdS layer in the cross section due to epoxy deformation during processing of the potted sample. Most of the grains have recrystallized with their width greater than their depth. Consequently, only grain boundaries which are perpendicular to the heterojunction remain.

Similar structure is revealed in the TEM cross-section of CdS/CdTe on Si (Figure 2.19). On that sample, heat treated for 30 minutes, detail is revealed in the CdS and ITO layers as well. Preliminary findings are as follows (22):

1) grain size in the CdTe is nearly uniform throughout the thickness, contrary to the common belief that the grain size is much smaller close to the CdS/CdTe interface.

2) The TEM cross-section shows a high density of structural defects within the CdTe grains, such as stacking faults, twins, and dislocations.

3) The CdS/CdTe interface appears to be very planar.

4) The grain size in the ITO film does not seem to limit that in the CdS film, i.e., CdS grains larger than ITO grains.

5) The grain size in the CdS film does not seem to limit that in the CdTe film, i.e., CdTe grains larger than CdS grains.

EDS and SIMS measurements show diffusion of S into CdTe and Te into CdS. The latter was further demonstrated by optical and XRD measurements of CdS/CdTe structures after processing and subsequent removal of the CdTe layer. The CdTe and Cd(TeS) were selectively etched with Dichrol (KCr_2O_7:H_2SO_4) as reported by Clemminck, et al. (23). Cadmium sulfide and Cd(STe) chemically resist Dichrol, while CdTe and Cd(TeS) are etched. Two CdTe/CdS structures were examined, both having 2 μm thick CdTe and 0.15 μm thick CdS. In one case the CdS was not treated prior to CdTe deposition, but the other received a heat treatment with 0.05 μm thick $CdCl_2$ layer prior to CdTe deposition. The optical transmission and the x-ray diffraction spectrum of the window layer was measured before and after this processing.

Figure 2.20 shows the normalized transmission before and after processing and Dichrol etching for CdS which was not heat treated with $CdCl_2$. Figure 2.21 shows the same for CdS which received a 30 minute heat treatment at 400°C with $CdCl_2$ prior to CdTe deposition. In both figures, the transmission below 500 nm is higher after processing, corresponding to a loss in CdS thickness of approximately 30 - 40 nm. The CdS which received no $CdCl_2$ treatment (Figure 2.20) shows a broad optical cutoff, shifted to lower energy. The XRD spectrum of this sample after removal of the CdTe shows that the CdS lattice parameter increased (Figure 2.22). The shift in the CdS optical cutoff taken with increase in lattice parameter correspond to formation of Cd(STe) with ~ 4% Te. The CdS which received a $CdCl_2$ heat treatment (Figure 2.21) shows a sharp cutoff in the CdS transmission. After processing and removal of CdTe, the transmission remained sharp except at very low energy (~550 nm). Further, the lattice parameter did not change, indicating no detectable Te diffusion into the CdS.

Optical transmission and x-ray diffraction patterns were also obtained from CdS/CdTe samples having four CdTe thicknesses (0.4, 0.85, 1.7, and 4.45 μm), before and after heat treatment. Optical transmission measurements on these structures reveal the properties

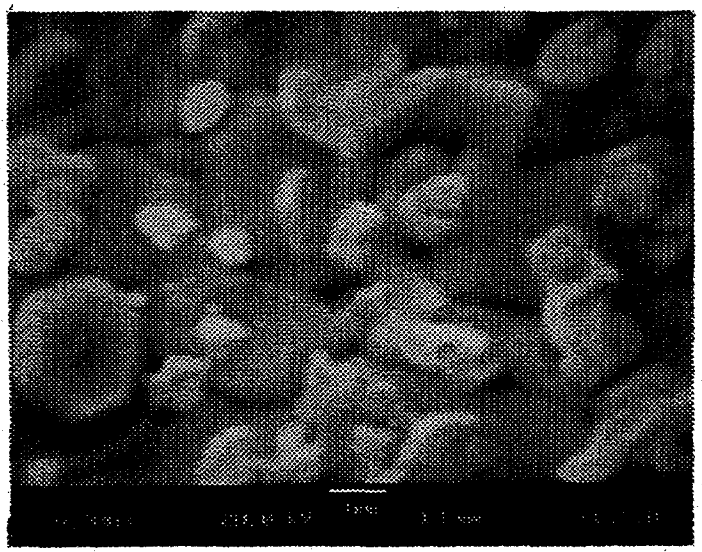

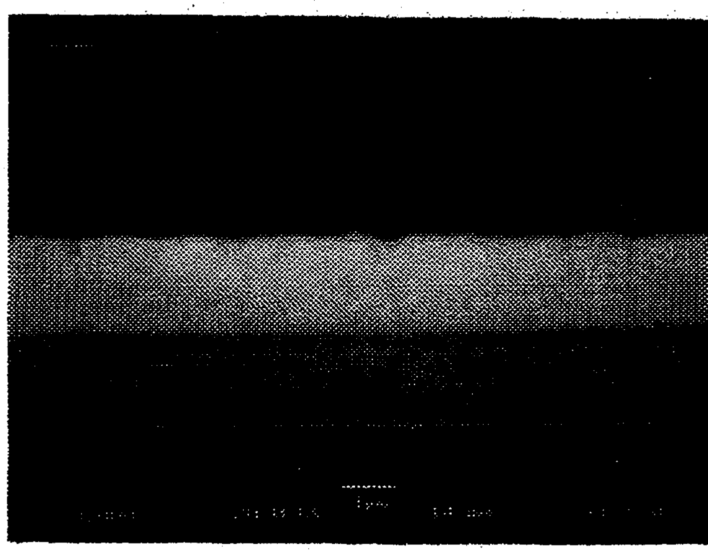

Figure 2.18 SEM photographs of ITO/CdS/CdTe after surface heat treatment with $CdCl_2$ at 410°C for 24 hours: a) CdTe surface and b) CdS/CdTe cross section.

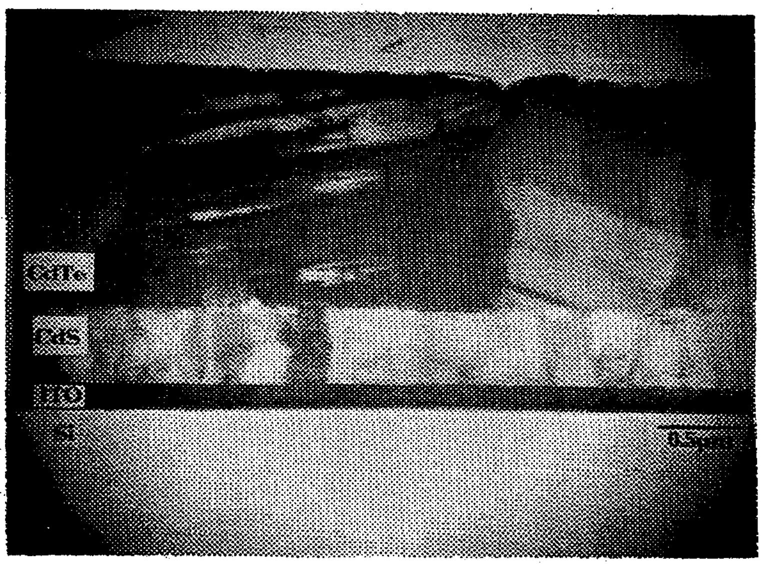

Figure 2.19 TEM photograph of Si/ITO/CdS/CdTe after heat treatment with $CdCl_2$ at 410°C for 30 minutes.

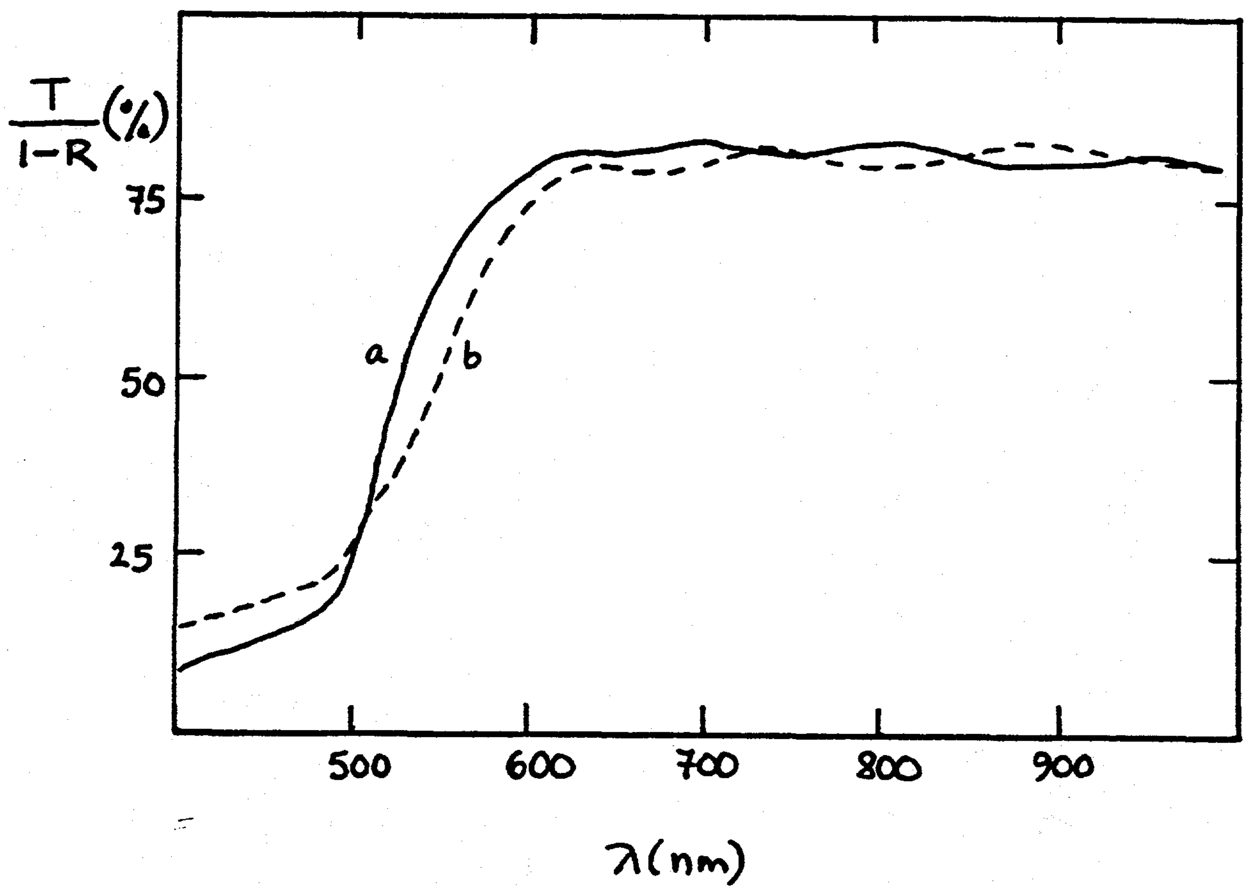

Figure 2.20 Normalized optical transmission, T/(1-R), of as-deposited SnO_2/CdS (a) and CdS after CdTe deposition, $CdCl_2$ surface treatment, and subsequent removal of the Cd(TeS) layer (b).

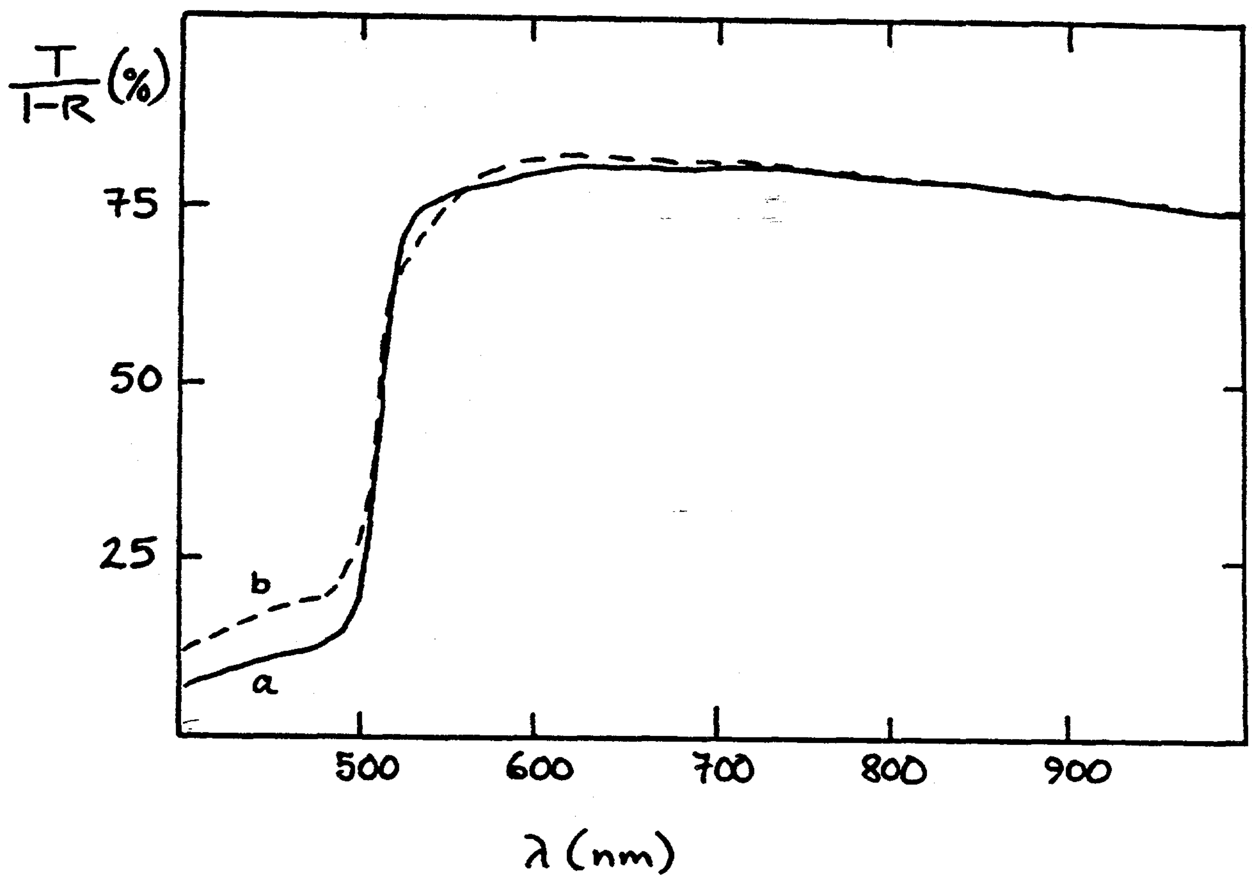

Figure 2.21. Normalized optical transmission, T/(1-R), of $CdCl_2$ surface treated SnO_2/CdS (a) and CdS after CdTe deposition, $CdCl_2$ surface treatment, and subsequent removal of the Cd(TeS) layer (b).

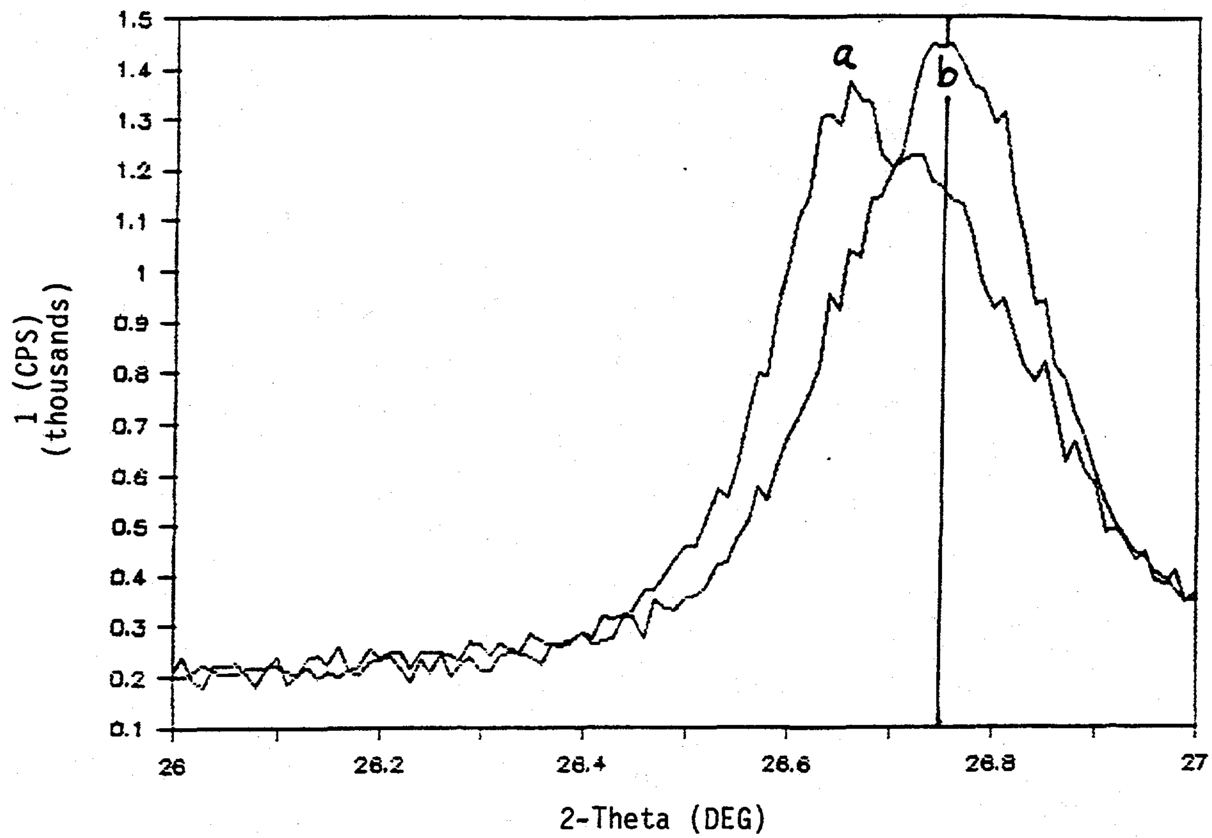

Figure 2.22 XRD spectrum of the 2-theta region of the CdS (002) peak after Cd(TeS) removal for the samples of Figures 2.18 and 2.19: a) no prior treatment of the CdS and b) $CdCl_2$ surface treatment of CdS prior to CdTe deposition. The vertical line indicates the position of the CdS (002) peak for as-deposited CdS films.

of the lowest bandgap component which, based on the data of Ohata is expected to decrease the bandgap for increasing sulfur content up to about 20% (8). The thinnest sample (0.4 μm) yielded a Cd(TeS) layer with a sulfur content of ~8%, while the thickest sample (4.45 μm) yielded a Cd(TeS) layer with sulfur content of 4%.

The diffraction measurement provides information integrated over the depth of the sample. After heat treatment the diffraction peaks shift towards lower lattice parameter with decreasing CdTe thickness, which is consistent with the optical data. The higher angle peaks exhibit peak splitting (other than the expected k-α_1-k-α_2 split) which was pronounced on the thinner samples, such as shown in Figure 2.23. The splitting suggests two regions of different composition, hence lattice parameter. To determine the location of the regions, a sample was thinned by etching to remove a layer.

The 1.7 μm thick sample was etched in Dichrol long enough to remove approximately 0.8 μm. The relative intensity of the higher lattice parameter (lower S content) component of the doublets was reduced after the etch, consistent with the <u>S-rich</u> component lying close to the CdS/CdTe junction (Figure 2.23). This implies that the CdTe region near CdS contains more S after heat treatment than the surface. For a Cd(TeS) alloy with 8% sulfur, the bandgap of the CdTe region near the junction will be

decreased by 70 meV, which may be expected to reduce the maximum obtainable V_{oc} of the device (24).

2.4 FABRICATION OF $CuInSe_2$ SUPERSTRATE SOLAR CELLS

Several approaches to fabricating $CuInSe_2$ thin film solar cells in a superstrate configuration are discussed. The $CuInSe_2$ films were grown on glass/ITO/CdS substrates by both three source evaporation and selenization using elemental Se. The ratio of the Cu/In in the $CuInSe_2$ film was varied from 0.5 to 1.3. The results are discussed in terms of device performance, $CuInSe_2$ film growth and alloy formation, and starting substrate.

The superstrate cells were made using glass substrates that were sputter coated with 400 nm of ITO having sheet resistance of 20 Ω/□. Both In-doped and undoped CdS were deposited with resistivities varying from 10 to 10^{-3} Ω/cm either by thermal evaporation or by solution growth. The growth of $CuInSe_2$ on CdS/ITO/glass substrates was examined for CdS thickness varying from 0.15 μm to 10 μm. The $CuInSe_2$ thickness varied from 1.5 to 2.0 μm and was deposited in a single layer by 3-source evaporation with substrate temperatures from 300 to 400°C. The Cu/In ratio in the final film was varied from 0.5 to 1.3 by changing the Cu and In incident flux during growth. The devices were completed by electron beam evaporated Pt as the back contact with an area of 0.057 cm^2. Ni, Cu and In were also evaluated as back contacts.

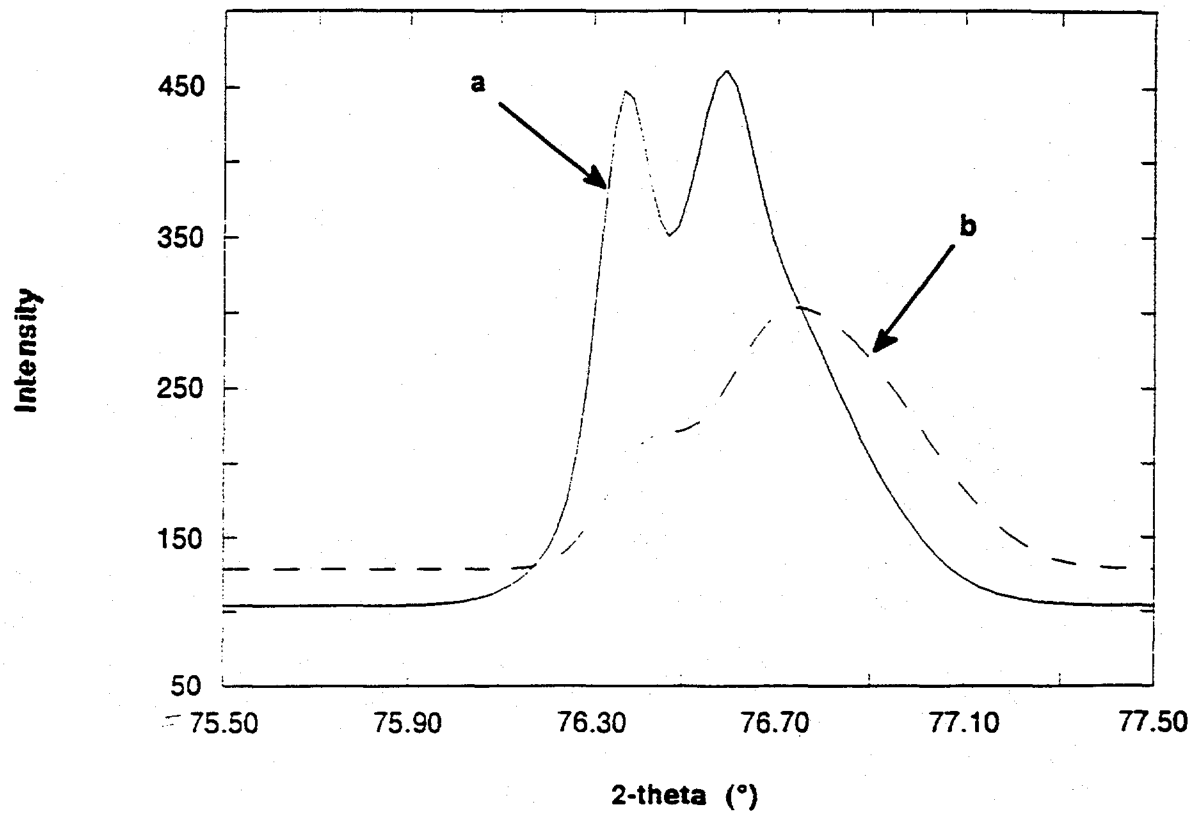

Figure 2.23 XRD spectrum of the 2-theta region of the CdTe (511) peak of an ITO/CdS/CdTe structure which initially had 0.2 μm CdS and 1.7 μm CdTe: a after $CdCl_2$ heat treatment and b) after removal of 0.8 μm of Cd(TeS).

As another approach for the growth of $CuInSe_2$, four different Cu-In-Se layered structures were deposited on CdS/ITO/glass substrates and selenized in Se vapor at 400°C. The structures examined were Cu/In, In/Cu, Se/Cu/In, and Se/In/Cu. The Se layer was deposited by thermal evaporation. The Cu and In layers were deposited by electron beam deposition to obtain the final appropriate composition. The composition and structure of these films were evaluated by EDS (energy-dispersive X-ray spectroscopy) and using an XRD (X-ray diffraction).

Three-source Evaporation

Figures 2.24 (a) and (b) show the grain structure of evaporated CdS with thicknesses of 0.5 and 8 μm. The grain boundaries were revealed by first reacting the CdS with CuCl which results in preferential formation of Cu_2S down the grain boundaries followed by a KCN etch to remove the Cu_2S. The grain size of the thin CdS is distributed in sub-micron size, approximately 10 times smaller than that of the thick CdS.

Figures 2.25 (a) and (b) show the X-ray diffraction patterns for the $CuInSe_2$ films deposited on CdS/ITO/glass substrate with CdS thickness of 0.5 μm and 8.6 μm. The $CuInSe_2$ was deposited at 300°C with the incidence flux of the Cu and In adjusted to give the film composition. For the thick CdS case, the $CuInSe_2$ is highly oriented along the (112) direction and has a surface morphology with grain structures greater than 0.5 μm. The high degree of orientation of the $CuInSe_2$ is inferred since the (112) peak of the $CuInSe_2$ overlaps with the (002) peak of the CdS.

However, there are no other $CuInSe_2$ peaks observed and the surface morphology suggests a well formed grain structure. For the thin CdS case, however, the $CuInSe_2$ is not as well oriented as indicated by the presence of (220) and (312) peaks in the XRD pattern. A second phase, $CuCd_2InSe_4$ (JCPDS #26-866), has formed indicating interdiffusion and alloy formation during film growth. There was twice as much Cd detected by EDS in the $CuInSe_2$ on thin CdS. Further, the composition of the two $CuInSe_2$ films deposited at the same time on the thick and thin CdS are significantly different with Cu/In ratios of 1.3 and 0.9 respectively.

For $CuInSe_2$ growth conditions where the Cu and In incident fluxes are set to grow $CuInSe_2$ films with a Cu/In ratio less than 0.8, no alloy formation has been detected for CdS from 0.5 to 10 μm and no Cd was detected by EDS. However, the ordered vacancy phase, $CuIn_2Se_{3.5}$, has been identified in these films. Thus, the $CuInSe_2$ growth conditions as well as the thickness and structure of the CdS influence the interdiffusion and film structure.

The effect of the Cu/In ratio was examined with respect to device performance for $CuInSe_2$ films deposited at 300°C on CdS films with thicknesses varied from 3 to 10 μm. Figure 2.26 shows the device

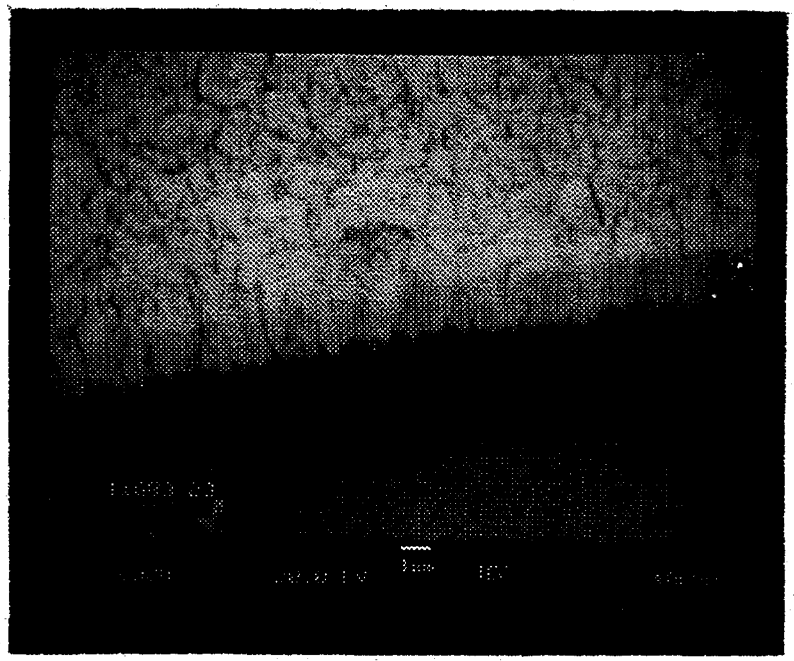

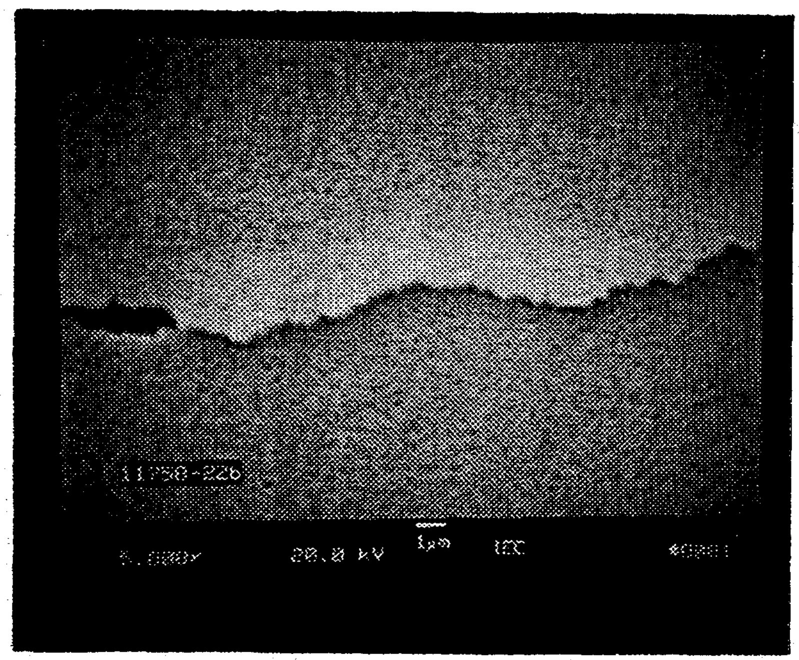

Figure 2.24 Grain structure of the evaporated CdS with thicknesses of (a) 0.5 μm and (b) 8.2 μm.

glass/ITO/CdS(0.5um)/CuInS2

Cu: Cd: In: Se=20.5: 5.9: 22.6: 51.0

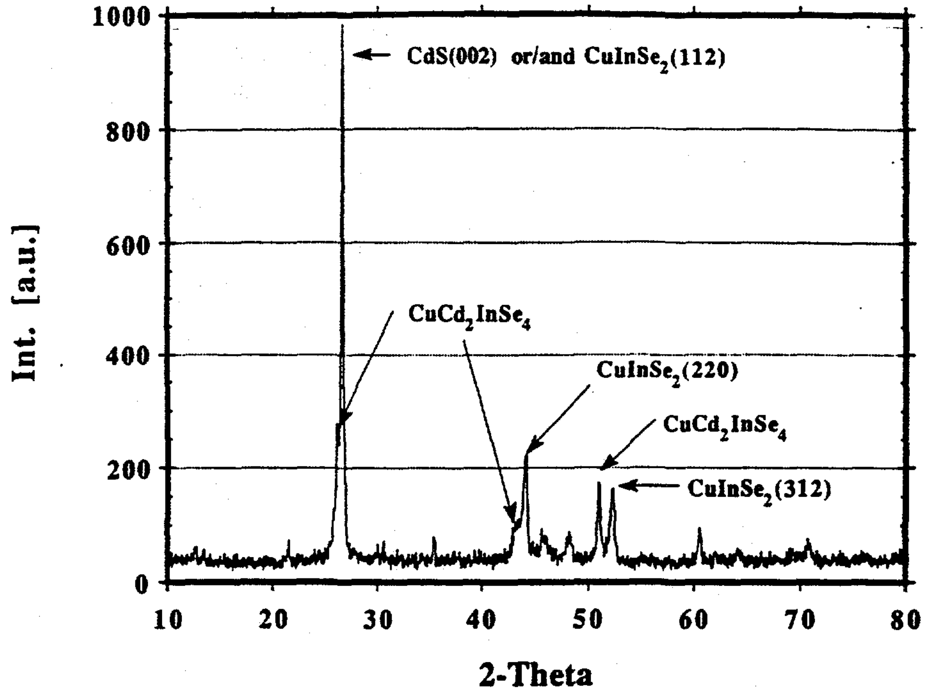

(a)

glass/ITO/CdS(8.6um)/CuInSe2

Cu: Cd: In: Se=27.3: 2.9: 21.2: 48.6

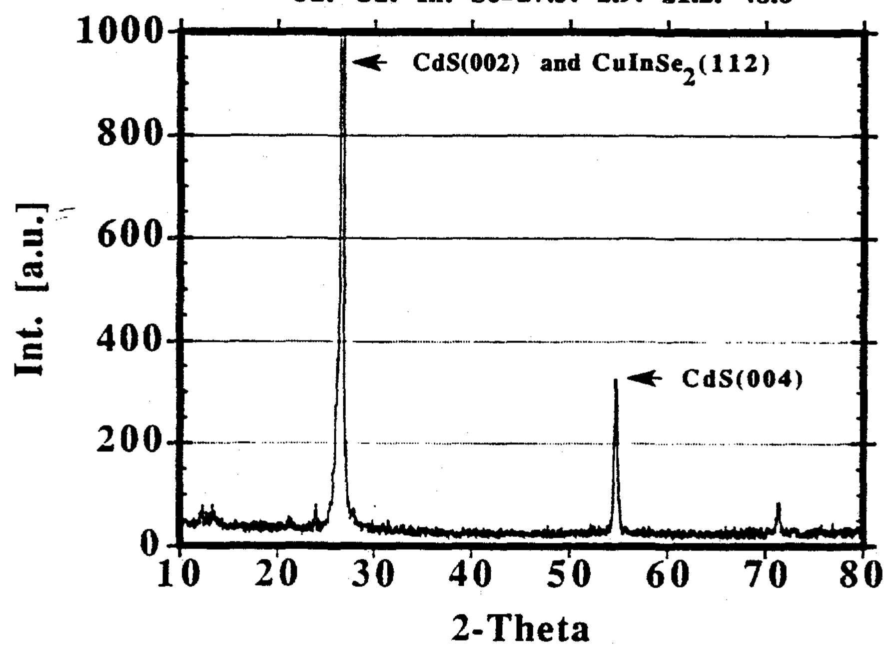

(b)

Figure 2.25 X-ray diffraction patterns for the $CuInSe_2$ films deposited on CdS/ITO/glass substrates with CdS thickness of (a) 0.5 μm and (b) 8.6 μm.

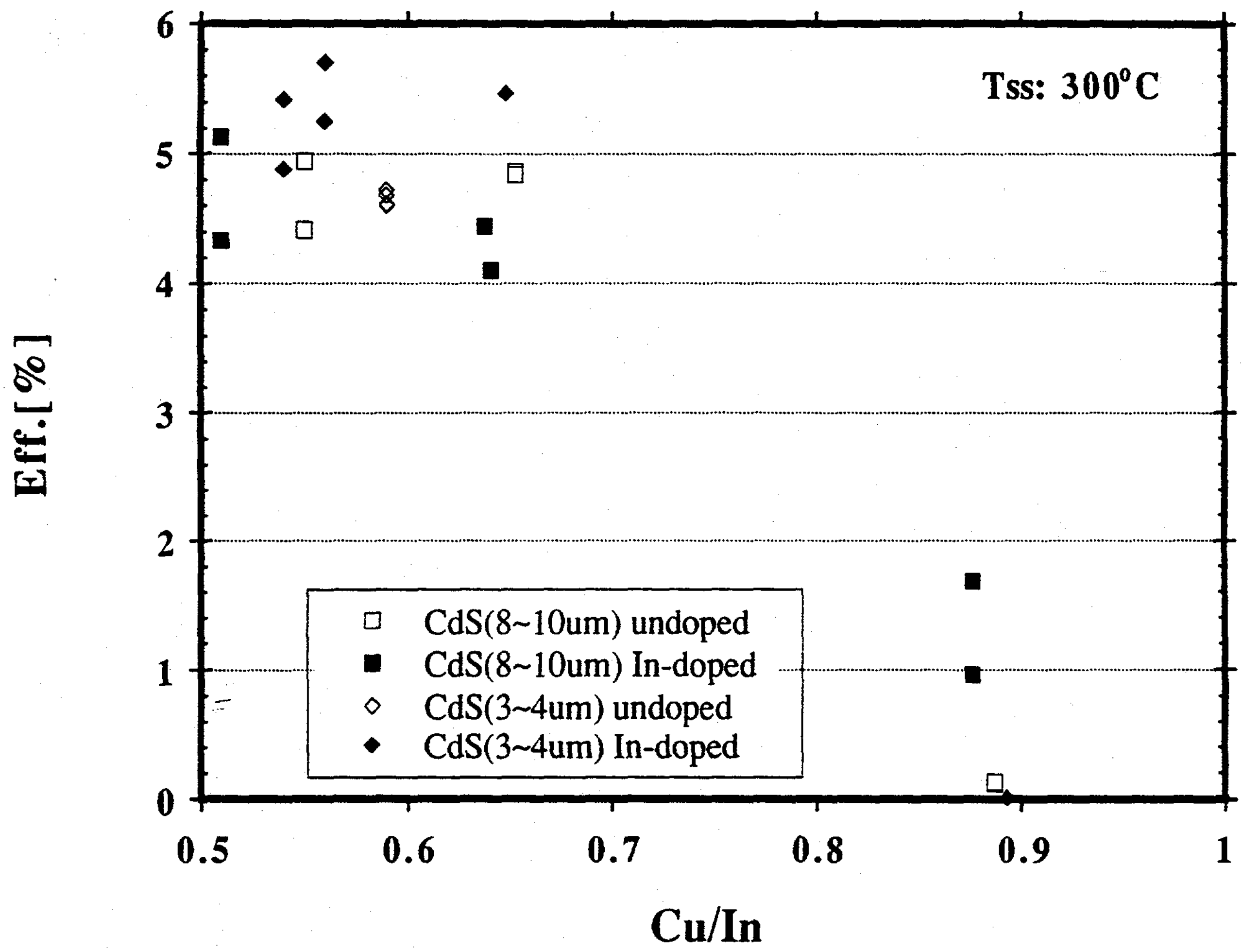

Figure 2.26 Device efficiency vs. Cu/In ratio. $CuInSe_2$ films were deposited at 300°C.

efficiency vs. Cu/In ratio. Reasonable conversion efficiencies were only obtained with Cu/In ratios between 0.5 and 0.7. For ratios of about 0.9 the device results were poor and for ratios greater than 1, the devices were shorted. We speculate that as the Cu/In ratio decreases, the In rich $CuIn_2Se_{3.5}$ phase reduces the diffusion of Cu. For Cu/In ratio greater than 0.9, there is increased interdiffusion resulting in alloy formation.

Table 2.11 shows the performances of superstrate devices deposited at 300, 350 and 400°C with the Cu/In ratio in the $CuInSe_2$ between 0.5 and 0.7. Both In-doped and undoped CdS with thickness between 0.15 and 10 μm were used. The V_{oc} is ~0.35V indicating that a reasonable junction is formed in these devices. The J_{sc} dropped dramatically at 400°C which suggests that the device has poor minority carrier transport properties or severe optical losses in the window layer caused by interdiffusion of the films. The In-doping improves the fill factor at 300 and 350°C which might be due to In compensation against Cu diffusion.

Figure 2.27 shows the dark and light I-V curves of the best device deposited on In-doped 3 μm CdS at 350°C. Although the strong light and dark crossover was observed, the light I-V characteristics are reasonable. The V_{oc} may be low because the Cu/In ratio is far from stoichiometry. To support this explanation, substrate devices, glass/Mo/$CuInSe_2$/CdS, were made where the $CuInSe_2$ was deposited by the 'standard' bilayer process [25]. For $CuInSe_2$ films with a Cu/In ratio of ~0.6, the device performance was similar to that of the superstrate cells.

For several samples, different back contact materials were compared to Pt. The I-V characteristics using Ni as a contact to the $CuInSe_2$ was comparable to that of Pt. With a Cu contact the I-V characteristics were unstable, had low V_{oc} and degraded with time. Devices with In also had low V_{oc}.

SELENIZATION

Of the four Cu-In-Se configurations investigated for the formation of $CuInSe_2$ by selenization in elemental Se, the CdS/Se/Cu/In and CdS/In/Cu structures had adhesion problems. Cu deposited on Se forms Cu_3Se_2 at room temperature, which results in weak adhesion. Indium deposited on CdS does not form a continuous film. This influences the subsequent Cu deposition and forms voids between CdS and In/Cu layers resulting in weak adhesion. After selenization, the films on these two structures peeled off. For the CdS/Cu/In structure, severe Cu penetration into the CdS during the selenization process was observed resulting in shorted devices.

For the CdS/Se/In/Cu films on a glass/ITO substrate, the XRD spectrum indicates that the In/Cu layers formed $CuIn_2$ and Cu_2In alloys with no Se reaction at room temperature. The films were

Table 2.11 Performance of the superstrate devices deposited at 300, 350 and 400°C.

Cu/In ratio 0.5~0.7 under ELH 87.5 mW/cm^2 illumination

Substrate Temperature[°C]	Thickness of CdS[μm]	In-doping	Voc [V]	Jsc [mA/cm^2]	FF [%]	EFF. [%]
300	7.8	yes	0.32	26	54	5.1
	8.1	no	0.30	29	49	4.9
	3.0	yes	0.32	29	54	5.7
	3.4	no	0.31	31	43	4.7
	1.0	yes	0.30	31	51	5.4
	0.4	yes	0.30	30	41	4.2
	0.5	no	0.18	4.1	20	0.2
	0.15	no	0.19	27	28	1.6
350	8.0	yes	0.33	29	56	6.0
	8.3	no	0.32	28	45	4.7
	3.5	yes	0.33	30	58	6.5
	3.1	yes	0.33	29	58	6.3
	3.6	no	0.30	23	21	1.6
	1.1	yes	0.28	28	24	2.1
	0.4	yes	0.32	28	39	4.0
	0.5	no	0.30	18	22	1.4
400	8.4	yes	0.28	7.5	40	1.0
	9.6	no	0.31	7.9	45	1.3
	3.2	yes	0.34	7.1	50	1.4
	3.6	no	0.36	8.3	43	1.5
	1.0	yes	0.36	7.5	53	1.6

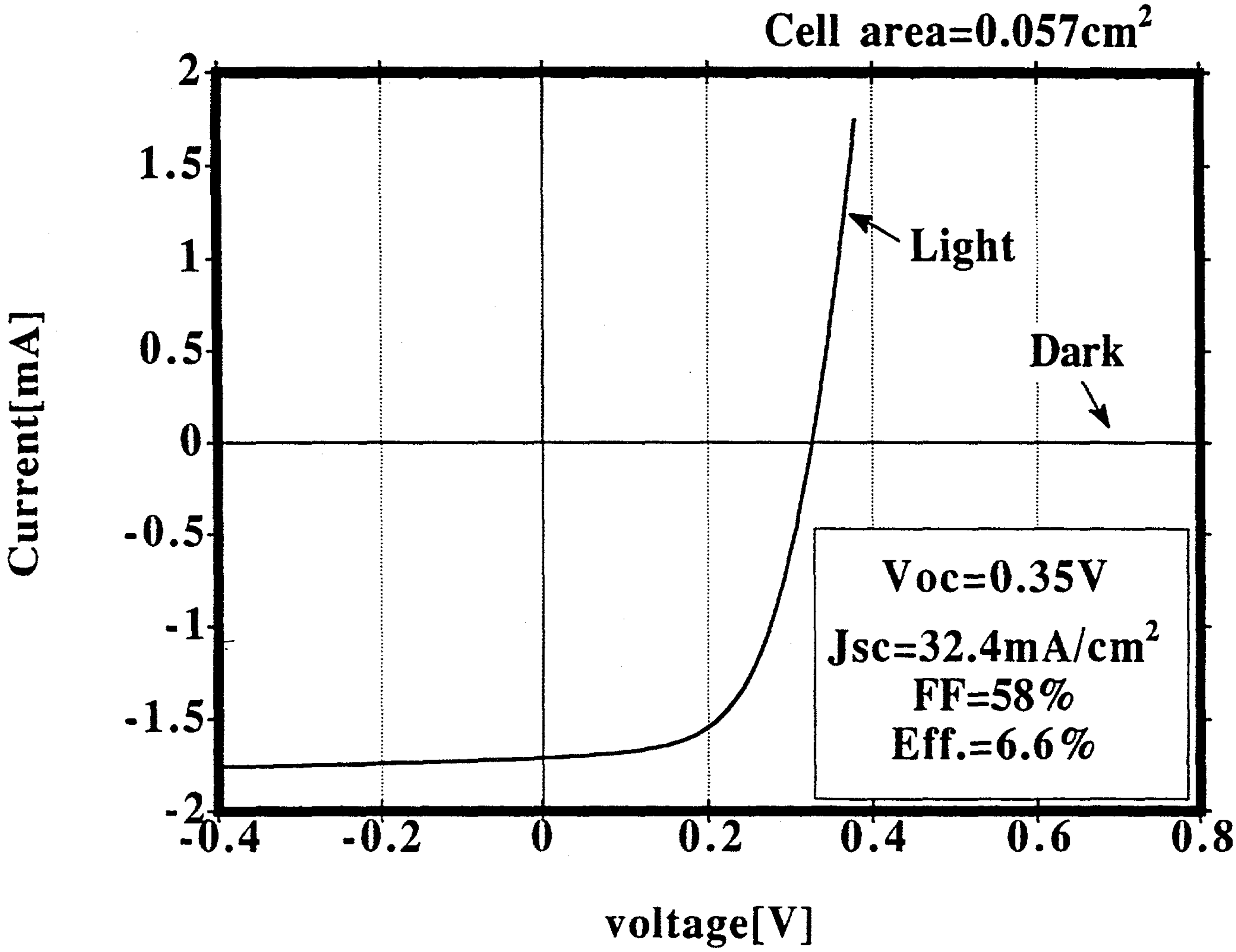

Figure 2.27 Dark and light I-V curves of the device deposited on In-doped 3 μm thick CdS at 350°C.

reacted in Se vapor at 400°C for 1 hour forming $CuInSe_2$ with a Cu/In ratio of 0.9. The cell performance obtained is V_{oc}=0.5V, J_{sc}=5.8 mA/cm^2 and FF=50%. The small J_{sc} is similar to that observed in the devices deposited by the 3-source evaporation at 400°C but with a V_{oc} of 0.5 V. Depth profiles of elements for this device were measured by SIMS and indicated that interdiffusion between CdS and $CuInSe_2$ is more pronounced than those deposited by evaporation. In addition, the device has two broad peaks (d=3.29 and 3.20) in the XRD spectrum indicating alloy formation. The peak positions are well fitted to those of CuInSeS (JCPDS #36-1311) and $CuInS_2$ (JCPDS #27-159), although not conclusive. Thus, the Se layer between the CdS and In/Cu layer appears to result in alloy formation with both the CdS and $CuInSe_2$.

In summary, $CuInSe_2$ superstrate devices were fabricated under various growth conditions using different thicknesses of both In-doped and undoped evaporated CdS as a substrate. Good ohmic contact to the $CuInSe_2$ was made by both Pt and Ni. The following observations were made:

1) Reasonable devices could be made only with $CuInSe_2$ films having a Cu/In ratio between 0.5 and 0.7. With Cu/In ratios greater than 0.9, interdiffusion and alloy formation dominate the film.

2) Even with the films that made reasonable devices, a $CuInSe_{3.5}$ phase, in addition to the $CuInSe_2$ phase, was detected.

3) Although all of the devices had low V_{oc}, the devices made from selenized films had the best open circuit voltages.

4) All of the devices had a strong light-to-dark crossover in the I-V characteristics. This is attributed to highly resistive and photoconductive CdS which could be caused by Cu diffusion. Both lowering the substrate temperature during $CuInSe_2$ film growth, using higher conductivity In-doped CdS and larger grain CdS helped reduce the light-to-dark I-V crossover and improve fill factor.

3.0 SOLAR CELL MEASUREMENTS AND ANALYSES

3.1 CURRENT-VOLTAGE ANALYSIS OF SOLAR CELLS

In determining the behavior of photovoltaic devices it is usual to collect current-voltage information over a wide range of light intensities and temperatures. Often, the output current of the device is measured as a function of the applied voltage, light intensity and temperature at over a thousand different points. Current-voltage analysis of these measurements usually consists of finding an equation or representation with a small number of parameters that will, within certain limits, reproduce the measured data set. The type of equation or representation used is not unique. However, given the form of the equation or representation, there should be enough flexibility so that the values and the number of parameters used are determined by accuracy that the equation reproduces the measured data set. This means that if we are to a priori use a given equation or representation it must contain a set of parameters both whose number and value are unknown before they are used as a substitute for the measured data. With a few simple modifications, the standard diode equation can satisfy these requirements.

The basic equation representing solar cell behavior is shown below.

$$J=J_O\left[\exp(V/V_T)-1\right]-J_{sc}$$

where J_{sc}, J_o, and V_T are fitting parameters.

Sometimes V_T is expressed as:

$$V_T=q/AkT$$

with A as a parameter.

This can be written with a light generated current and an offset voltage as shown.

With $J_L \equiv J_{sc}+J_o$ and $V_o \equiv V_T Ln(J_L/J_o)$, the fitting equations become:

$$J+J_L=J_L \ \exp[(V-V_o)/V_T]$$

or

$$V-V_o=V_T Ln[(J+J_L)/J_L]$$

with J_L, V_o, and V_T as fitting parameters.

Usually parametric terms R and G (usually referred to as series resistance and shunt conductance) are added to increase the accuracy of the representation equation.

$$J+J_L-GV = J_L \exp[(V-V_o-RJ)/V_T]$$

or

$$V-V_o - RJ = V_T \ Ln[(J+J_L-GV)/J_L]$$

In all current-voltage analysis, the parameters R and G are only fitting parameters. They have to be compared with quantitative models of solar cell operation to have any physical validity. The R parameter is used to obtain a more accurate fit or representation in the forward bias voltage part of the current-voltage characteristic while the G parameter does similar duty in reverse voltage bias. Realizing this, it is now apparent that both R and G are the first order linear terms of a more general parametric fitting or representation that can be used.

$$J+J_L-GV+A_2V^2+A_3V^3+...=J_L \quad \exp[(V-V_o-RJ+B_2J^2+B_3J^3+...)/V_T]$$

or

$$V-V_o-RJ+B_2J^2+B_3J^3+...=V_T Ln[(J+J_L-GV+A_2V^2+A_3V^3+...)/J_L]$$

With these equations, it is possible to determine the fewest parameters that will represent the measured data of a given current-voltage characteristic. For example, if including the quadratic and cubic terms beyond the linear term (say R) does not improve the accuracy of the representation, then only using a series resistance term is justified. However, it is necessary to determine this experimentally before limiting the order of the parameters in the equation representing the data. If this is not done, the changes in parameters from one current-voltage characteristic to the next may be primarily due to a better or worse fit of the data instead of reflecting changes in either light intensity, temperature, or processing parameters.

In the data reported, whenever only linear terms (series resistance R or shunt conductance G) are used, it has been determined that higher order (quadratic and cubic) terms do not improve the accuracy of the fit of the current-voltage data. Otherwise it is stated that additional non-linear terms are necessary to represent the measured data accurately. This is usually the case with the series resistance terms in $CuInSe_2$ devices at room temperature or below. It is sometimes true with shunt conductance terms in CdTe devices.

3.2 $CuInSe_2$ DEVICE ANALYSIS

The J-V behavior of a variety of $CuInSe_2/CdS$ solar cells has been measured over a wide range of temperature and light intensity.

This includes cells fabricated at IEC with the $CuInSe_2$ deposited by evaporation and selenization and another cell fabricated by Siemens Solar Industries (SSI). The data is analyzed to determine the diode behavior and other effects which determine the J-V characteristics and to compare the results for the different $CuInSe_2$ depositions.

For all the cells, the linear term R is sufficient to describe the data in forward bias only at the highest temperatures, as will be shown below. The cells have non-linear contributions in series with the main diode which are clearly observed at lower temperatures. The diode behavior is therefore determined from the results at V_{oc} where these series effects do not contribute. Except for the non-linear contributions, the devices all have the same diode behavior over the entire temperature and intensity ranges. This is consistent with the results of previous J-V analysis which has shown that the diode parameters agree with the model of Shockley-Read-Hall (SRH) recombination (26-28).

Experimental Results

Current-voltage curves of 4 devices were measured over the temperature range from 218 to 373K, and at four different light intensities (dark, ~5mW/cm^2, ~20mW/cm^2, and ~80mW/cm^2). This involved running forty separate current voltage traces and recording a total of 3,200 individual current voltage pairs for each cell. The voltage was stepped in increments of 0.04V from -0.62 to 0V and in 0.01V increments from 0 to 0.83V. The cells included three fabricated at IEC which have the $CuInSe_2$ deposited by: 1) three source evaporation, 2) selenization in elemental Se vapor and, 3) selenization of Cu/In layers in H_2Se. These cells were completed with evaporated (CdZn)S:In and ITO layers. The basic J-V parameters at 25°C for these cells and the cell fabricated by SSI are listed in Table 3.1. The J-V parameters J_{sc}, V_{oc}, $(dV/dJ)@V=V_{oc}$, $(dJ/dV)@V=0$, FF, and P_{max} are listed for each temperature and intensity in Appendix A.

Table 3.1. J-V parameters for 4 $CuInSe_2$ solar cells at 25°C under AM1.5 illumination.

Cell	$CuInSe_2$ deposition	V_{oc} (V)	J_{sc} (mA/cm^2)	FF (%)	Eff. (%)
IEC 32187-22-12	Evaporation	0.44	34	68	10.1
IEC 61079-23-5	Se selenization	0.43	33	65	9.5
IEC 89095-2-9	H_2Se selenization	0.45	35	65	10.2
SSI 16543-4-3	Siemens Solar	0.45	37	62	10.2

The current-voltage curves in the dark and at the highest intensity are shown for the SSI cell in Figure 3.1.

Below ~280K, the J-V curves deviate in forward bias from the ideal behavior seen at high temperatures, and at V_{oc} because the non-ohmic characteristics of the contacts becomes large enough to affect the solar cell response. This behavior has been reported previously for cells with evaporated $CuInSe_2$ (29,30) and has been attributed to a non-ohmic Mo/$CuInSe_2$ contact. All of the cells in this work show similar behavior below ~280-330K, depending on the sample.

Current-Voltage Analysis

The J-V results are analyzed according to a standard diode equation with linear terms:

$$J=J_o\{\exp[q(V-R_sJ)/AkT]-1\}-J_{sc}+GV \qquad (1)$$

where,

$$J_o=J_{oo}\exp(-\phi/AkT). \qquad (2)$$

At J=0, contributions in series with the main junction are eliminated and, since G is small, the diode equation gives

$$V_{oc}=\phi-(AkT/q)[\mathrm{Ln}(J_{oo})-\mathrm{Ln}(J_{sc})]. \qquad (3)$$

The barrier height, ϕ, diode factor A, and prefactor J_{oo} are uniquely determined by fitting the values of V_{oc} at all temperatures and light intensities simultaneously to equation 3. This gives a good fit for each of the four cells as shown for the SSI cell in Figure 3.2 where the lines are the fit to equation 3. The values of ϕ, A, and J_{oo} determined from the fit to equation 3 are listed for each cell in Table 3.2.

Table 3.2 Diode Parameters for the 4 $CuInSe_2$ Solar Cells

#	$CuInSe_2$ deposition	ϕ (eV)	A	J_{oo} (mA/cm^2)
32187-22-12	Evaporation	0.97	1.3	$2x10^8$
61079-23-5	Se selenization	0.97	1.6	$2x10^7$
89095-2-9	H_2Se selenization	0.96	1.6	$8x10^6$
16543-4-3	Siemens Solar	1.04	1.5	$1x10^8$

The J-V characteristics of the primary diode can be evaluated using Eq. 1 and the values in Table 3.2. The series contribution to the device behavior can then be evaluated by subtracting the diode contribution from the measured J-V data. Figures 3.3-3.6 show the

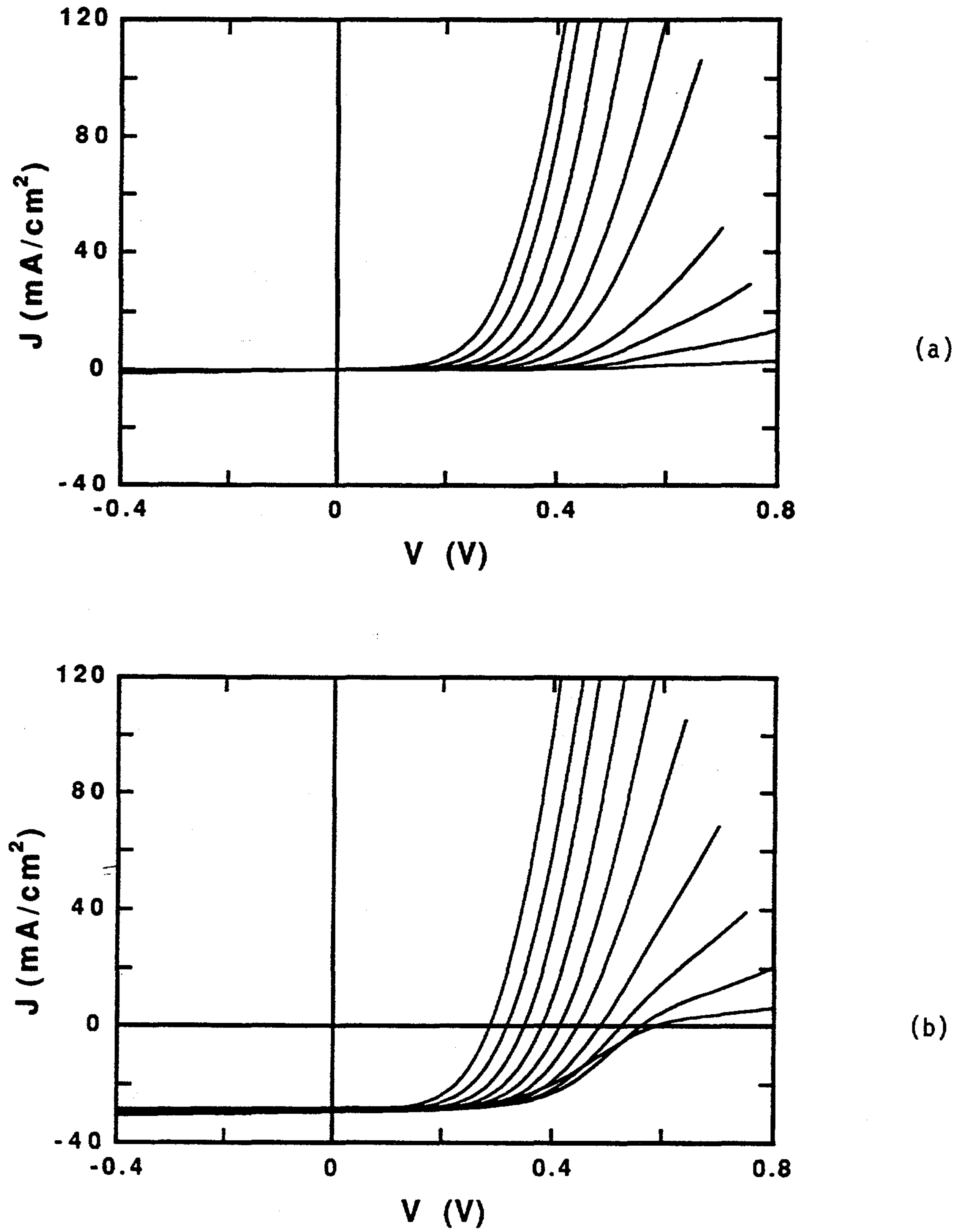

Figure 3.1 J-V results for the SSI cell at 373, 358, 343, 328, 313, 298, 278, 258, 238, and 218K, (a) in the dark and (b) under highest illumination.

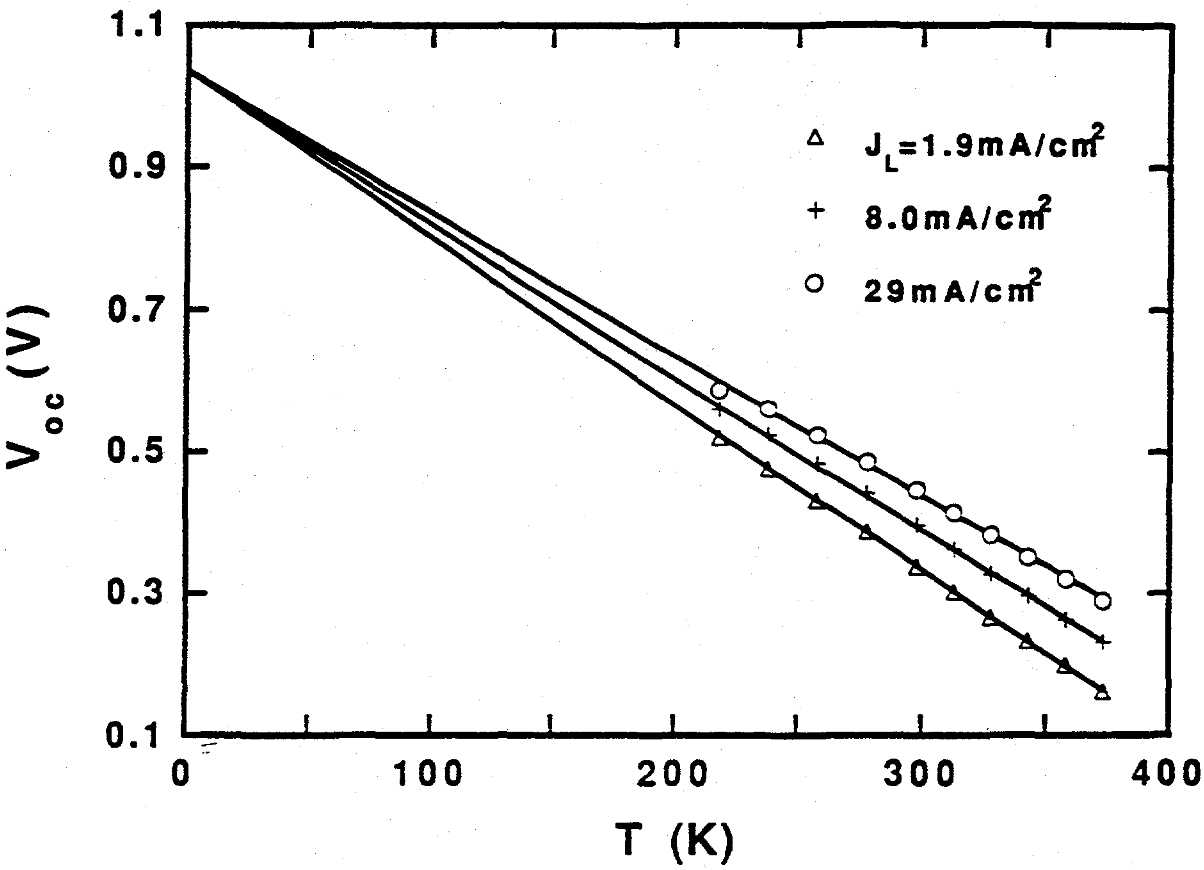

Figure 3.2 V_{oc} versus temperature for the SSI cell at 3 light intensities. The solid lines are a fit to equation 3.

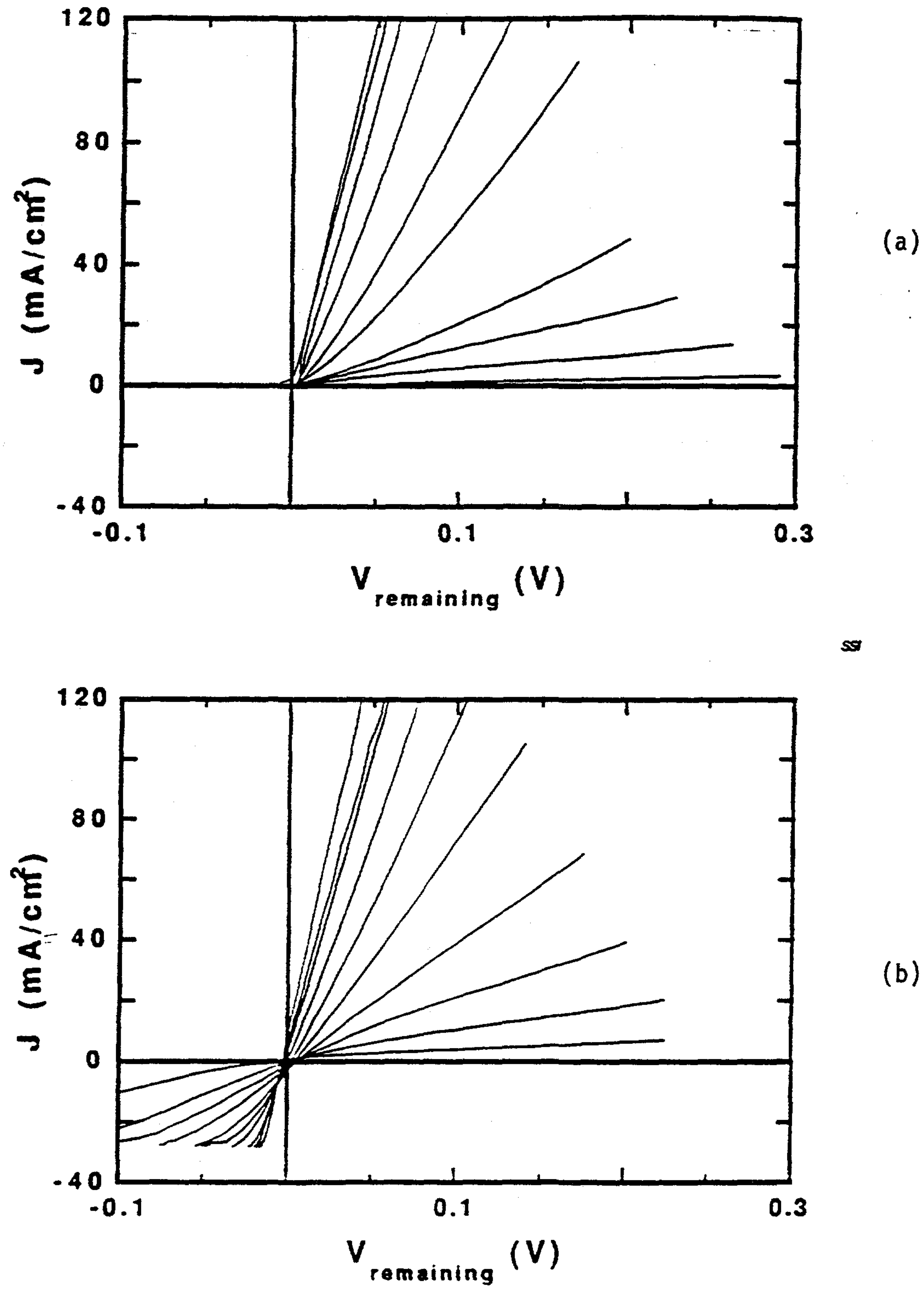

Figure 3.3 J-V characteristics for SSI cell 16543-4-3 after subtracting the contribution due to the primary diode for temperatures from 373 to 218K: a) dark and b) under ~80% AM1 illumination.

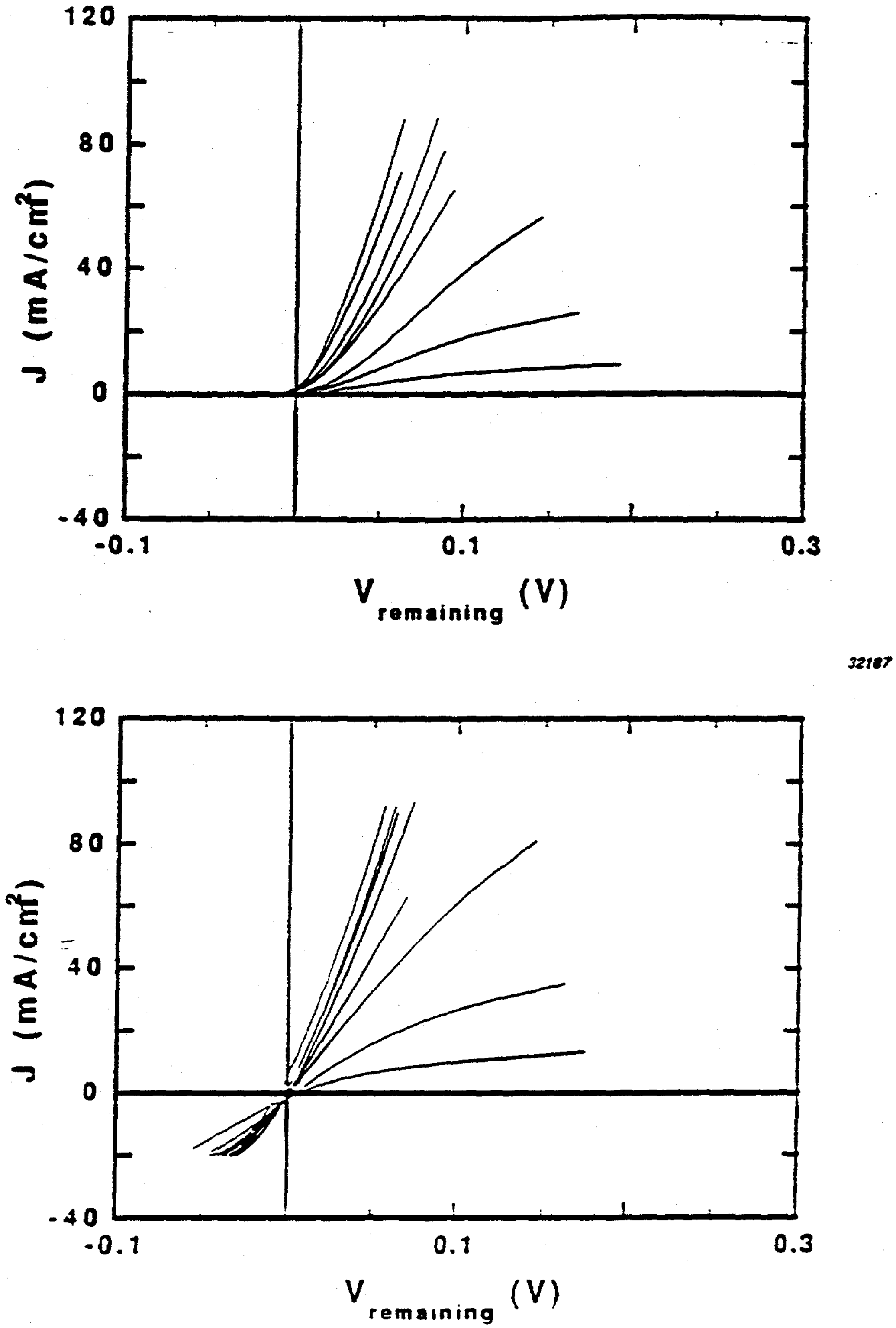

(a)

(b)

Figure 3.4 J-V characteristics for IEC cell 32187 after subtracting the contribution due to the primary diode for temperatures from 358 to 245K: a) dark and b) under ~80% AM1 illumination.

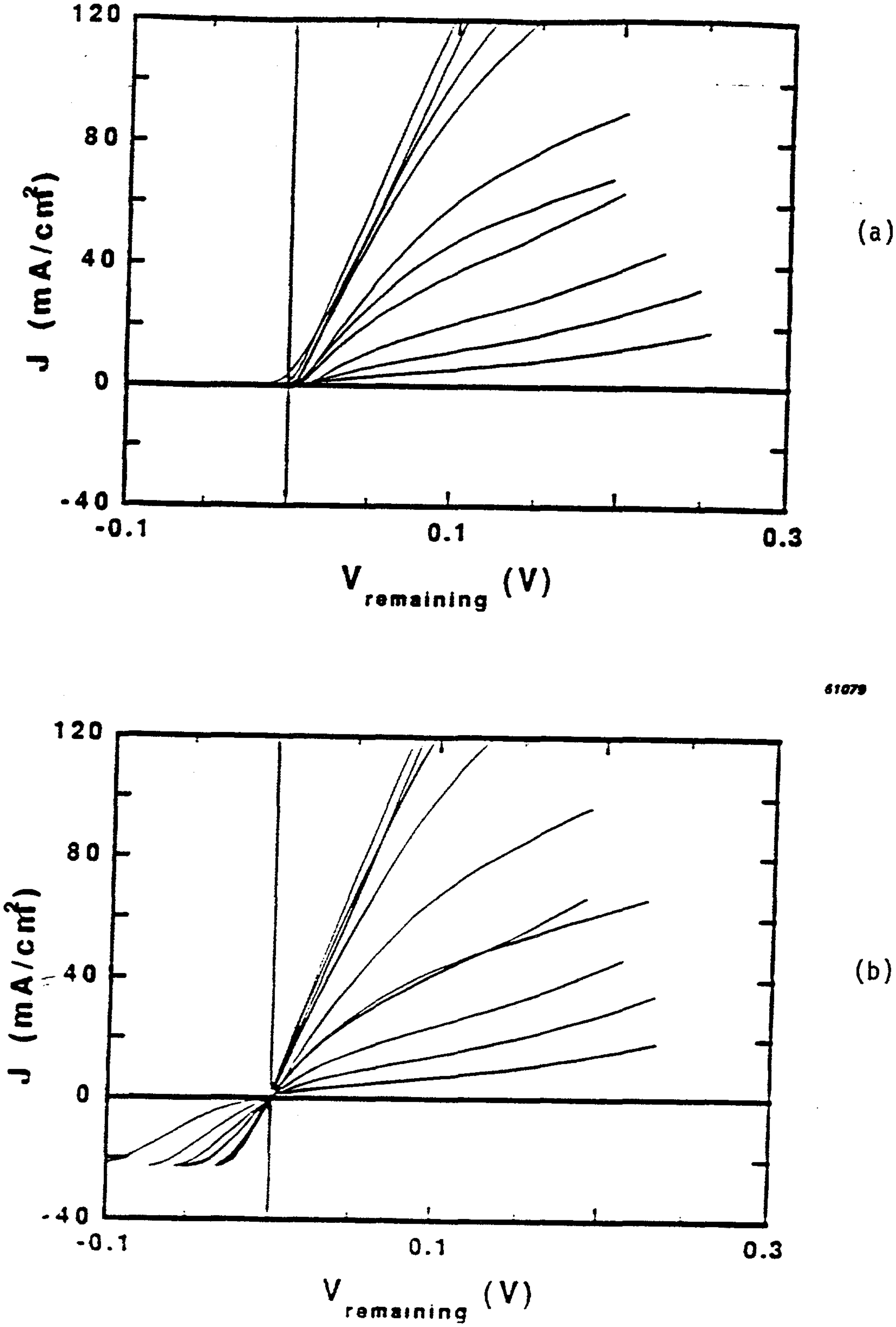

Figure 3.5 J-V characteristics for IEC cell 61079 after subtracting the contribution due to the primary diode for temperatures from 373 to 218K: a) dark and b) under ~80% AM1 illumination.

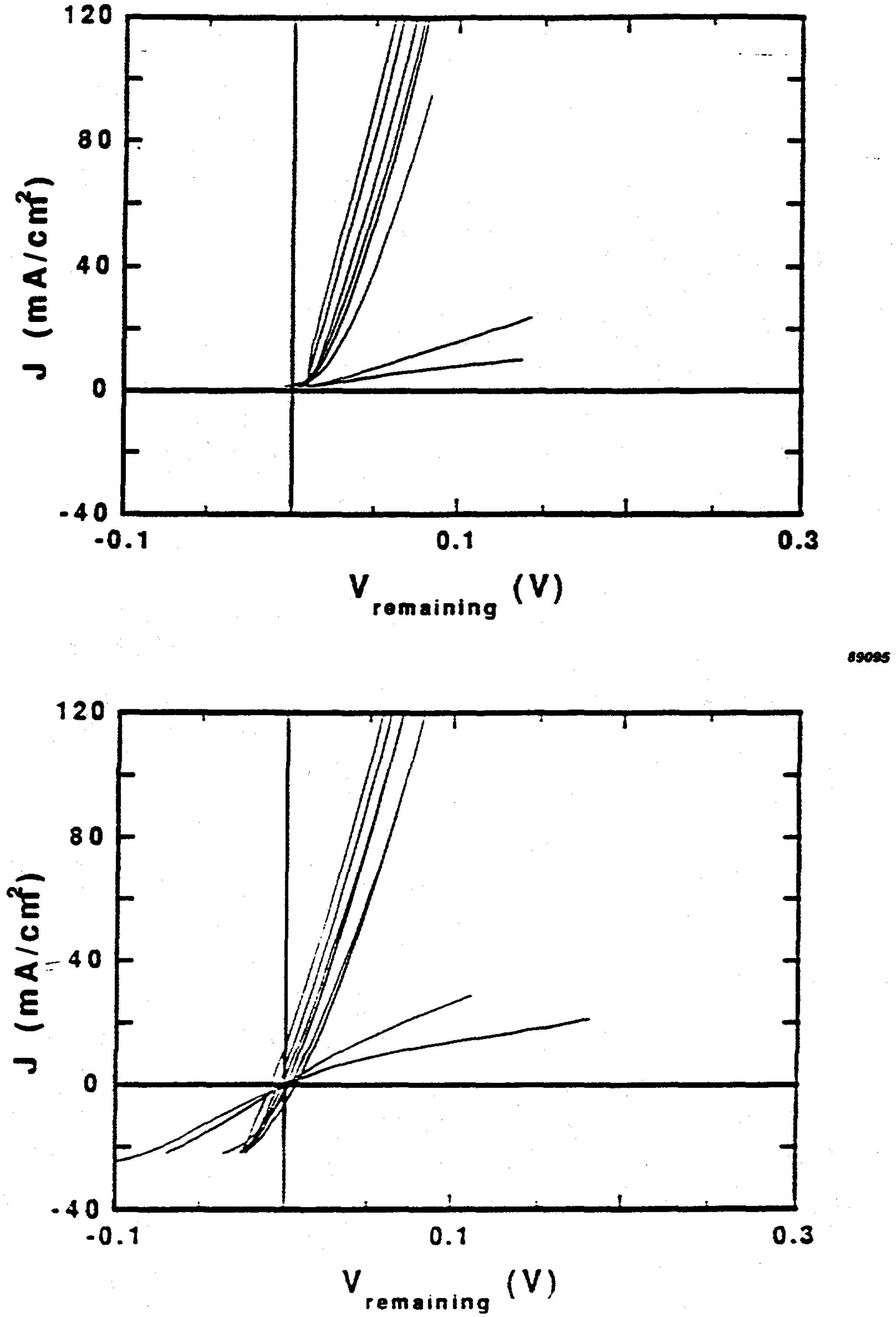

Figure 3.6 J-V characteristics for IEC cell 89095 after subtracting the contribution due to the primary diode for temperatures from 373 to 258K: a) dark and b) under ~80% AM1 illumination.

J-V characteristics when the contribution from the primary diode is subtracted from the measured J-V data for the four cells over the entire temperature range where

V(remaining)=V(diode)-V(measured)

At high temperatures, the J-V curves are linear indicating an ohmic series resistance contribution to the device behavior. Table 3.3 lists the value of R_s in the dark and under illumination for the four cells. At low temperatures, the J-V are non-linear and show a definite reverse diode-like behavior. Additionally, the difference in shape between the J-V curves in the dark and under illumination indicate a light dependent series contribution. Finally, there is a significant variation in the J-V data from cell to cell which could be related to the way the $CuInSe_2$ films were grown or to variations in the device processing.

Discussion and Future Work

The $CuInSe_2$ cell J-V data has been analyzed with the standard diode model, equation 1. At V_{oc}, where series effects in the device do not contribute, the analysis determines the behavior of the primary diode at the $CuInSe_2$/CdS junction and shows that all the cells behave the same. However, to describe the current-voltage behavior over the entire range of temperatures and light intensities, the non-ohmic contributions of the contacts must be taken into account.

At normal operating temperatures (near 25°C), the remaining non-ohmic contact behavior affects the J-V characteristics of all $CuInSe_2$ solar cells analyzed. This contact behavior, and not the diode behavior, appears to be a primary reason for cell to cell variability in the current voltage behavior.

The following conclusions can be made about the diode behavior:

1. All the cells, with the $CuInSe_2$ deposited by a variety of methods, have the same basic diode operation described by the standard diode equation with barrier height $\phi \approx 1.0$eV, A=1.3-1.7, and $J_{00} \approx$mA/cm^2. These values agree with the model of Shockley-Read-Hall recombination as described in references 26 and 27.
2. All the devices have non-linear contributions in series with the main diode which are clearly evident at temperatures below 280-330K and which can affect the J-V results at higher temperatures.
3. It is necessary to measure the J-V behavior of $CuInSe_2$ devices over a wide range of temperatures and light intensities, and to consider the effects of non-ohmic contacts, in order to analyze the diode characteristics of the $CuInSe_2$ devices.

Table 3.3 The linear series contribution after subtracting the primary diode

SSI	R_s(Dark) Ω-cm^2	R_s(~80% AM1) Ω-cm^2	Temperature K
SSI	0.5	0.5	373
32187	0.8	0.5	358
61079	0.8	0.6	373
89095	1.5	1.5	373

Further work is needed to locate the cause(s) and reduce the magnitude of non-ohmic contact resistances in the $CuInSe_2/CdS$ cells. This J-V data set and analysis will be expanded to include $CuInSe_2$ devices fabricated at several other laboratories. The complete data set is being established to be made accessible to any interested researchers for analysis and as input to device models.

3.3 CdTe DEVICE MEASUREMENTS AND ANALYSES

Stability and Reproducibility of Current-Voltage Measurements

The regular retesting of CdTe devices over time to determine the stability of the output assumes that the testing itself does not introduce degradation. This can happen if the testing process causes damage to the device, such as scratching from the test probes.

To test this assumption on IEC's CdTe devices, six samples with three different types of contacts to the CdTe were given six regular current-voltage tests within a two week period, either in July or January. Three of the samples were tested and retested during both periods. The results of the individual tests are shown in Appendix B.

In summary, there were substantial changes in output due to testing with devices that had either the Cu/Au (samples 40703-12, 40708-32, and 40721-12) or the ZnTe/Au (samples 40708-13 and 40724-32) contact. As can be seen in Appendix B, most of the change in output was due to reductions in fill factor. There was little change in the devices that had the harder and more robust ZnTe/Ni contact (sample 40724-31). It appears that the probes used for current-voltage testing scratch the surface of the soft contacts, causing lowered fill factors due to both contact removal and device shunting.

Because of this problem, all stability testing will be done with devices that either have hard contacts that resist probe damage, such as nickel or have permanent connections epoxied or soldered to the device to prevent physical damage to the contact.

CdTe Current-Voltage Analysis

Current-voltage measurements have been made on a University of South Florida CdTe solar cell (5-198-20-C) at 3 light intensities (dark, ~20% AM1, ~80% AM1) and 13 temperatures ranging from 218K to 373K. The dark and 80% AM1 J-V curves are shown in Figure 3.7 and a summary of the J-V data is given in Appendix A.

The device has a light dependent slope which can be seen in the values of $(dJ/dV)@J_{sc}$ (Appendix A) and in the J-V curves shown in Figure 3.7 indicating voltage dependent collection, $J_L(V)$. This type of behavior has been previously reported for evaporated CdTe devices fabricated at IEC (31).

A plot of V_{oc} vs. T for the two different light intensities is shown in Figure 3.8. The V_{oc}, J_{sc}, and temperature data fit the equation 3 with:

$$\phi \sim 1.4\text{eV} \quad A \sim 1.6 \quad J_{oo} \sim 5\times10^7 \text{ mA/cm}^2$$

These results also are very similar to the values obtained on CdTe devices made at IEC (31).

However, unlike IEC CdTe devices, this solar cell operates at temperatures as low as 250K before the J-V curve starts to collapse. Also, there is hysterisis in the J-V curves when either temperature or applied voltage is cycled.

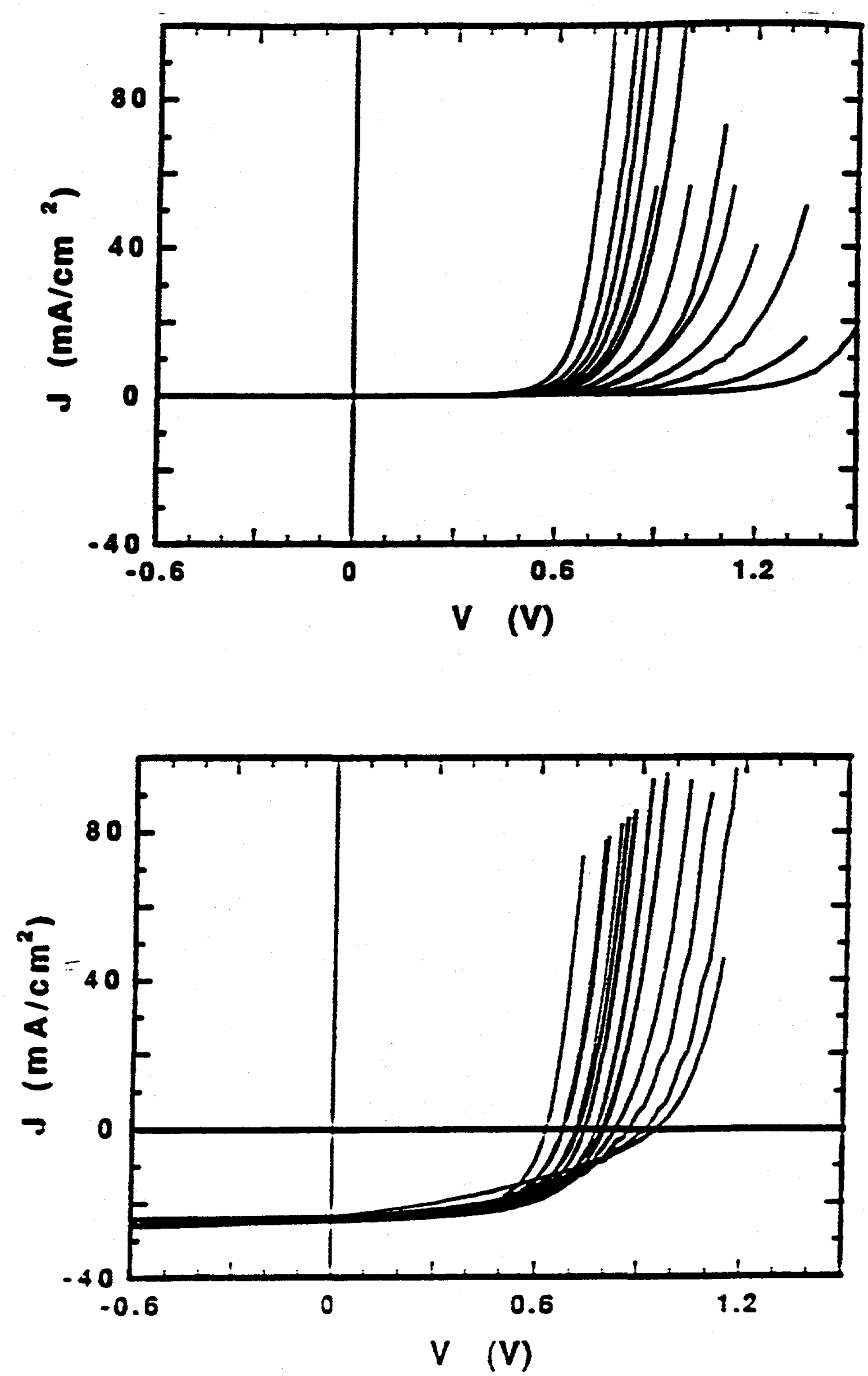

Figure 3.7 J-V curves as a function of temperature from 218 to 373K both in the dark (upper) and under illumination (lower) for the University of South Florida CdTe device #519B-20-C.

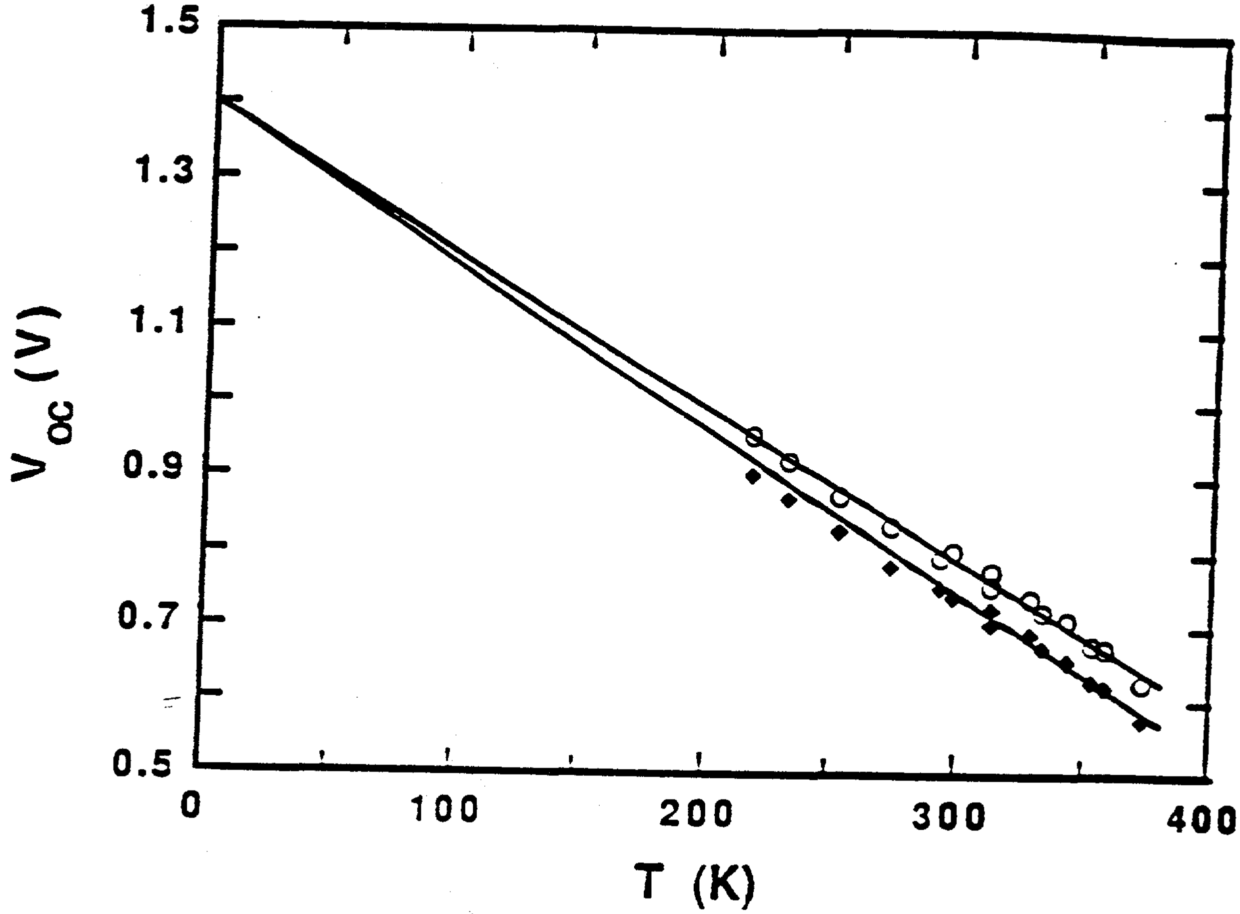

Figure 3.8 V_{oc} as a function of temperature at two illumination levels for the University of South Florida CdTe device #519B-20-C.

4.0 RESEARCH AND DEVELOPMENT COLLABORATION

INTRODUCTION

During the period of this report, IEC has collaborated with other research organizations in research dealing with all aspects of thin film polycrystalline solar cell research and development. What follows is a listing and description of that research. In addition to this, IEC is beginning a data base on detailed device measurements which is available to the polycrystalline thin film solar cell community via the Internet. An outline of the measurements and parameters of the data base at present is shown in Appendix A.

SIEMENS SOLAR INDUSTRIES

IEC has collaborated with Siemens Solar Industries in the evaluation of $CuInSe_2$ film formation by selenization with H_2Se in flowing gas reactors. This was done under a separate contract with Siemens. IEC has also done a detailed current-voltage analysis of one of their $CuInSe_2$ devices. The results are discussed in Section 3.2. Appendix A gives additional information.

UNIVERSITY OF ILLINOIS

IEC continued its ongoing collaboration with the University of Illinois to evaluate $CuInSe_2$ films deposited by their hybrid sputtering process. Recent modification to the sputtered $CuInSe_2$ films include improved uniformity and adhesion, and the use of Cu-Mo alloy substrates. $CuInSe_2$/CdS solar cells were fabricated using evaporated (CdZn)S:In, and ITO/Ni contacts. The best cell was 6801B-5 which had V_{oc}=0.426V, J_{sc}=35.3 mA/cm^2, FF=66.5% and efficiency=10.0% when measured at NREL. This is the highest efficiency to date using the hybrid sputtered $CuInSe_2$.

VILLANOVA

Optical measurements and x-ray diffraction analysis for Dr. Pali Singh of Villanova University, who is developing a galvanic approach to forming (ZnHg)Te films. The films were deposited on Hoya ITO substrates to a thickness of ~300 nm. After deposition, EDS analysis was performed at Villanova to confirm the presence of Zn, Hg, and Te in the films. X-ray diffraction scans showed a single non-ITO reflection which is attributed to the (111) plane of (ZnHg)Te. The Hg content in the films was estimated from shifts in the lattice parameter obtained from the d-spacing of the (111) peak compared to values obtained for ZnTe films. Table 4.1 summarizes the diffraction data for films measured to date. Optical transmission spectra indicated the presence of a shallow absorption edge.

Table 4.1. X-ray diffraction results for (ZnHg)Te films deposited on ITO substrates by galvanic deposition. In each series, the Hg content is estimated by the shift of a_o relative to the ZnTe sample for that series.

Sample	Measured 2-Theta (deg) (± 0.01 deg)	Estimated d (A) (± 0.002 A)	a_o (A)	% Hg[a]
ZT406	25.26	3.526	6.107	0
MZT394	24.71	3.603	6.240	38
MZT-1	24.58	3.622	6.273	47
P ZT-2	25.21	3.532	6.118	0
PMZT-4	24.91	3.574	6.191	21[b]
PMZT-1	24.66	3.610	6.253	39
PMZT-6	24.05	3.700	6.409	83

[a]) J.C.P.D.S. card files list the following lattice parameters: #15-746 ZnTe a_o = 6.1026 A; #8-26 HgTe a_o = 6.453 A.

[b]) (111) peak width yields a particulate size of 30 nm.

MICROCHEMISTRY (FINLAND)

This is a summary of results on processing CdS/CdTe material deposited by atomic layer epitaxy (ALE) by Microchemistry (MC). We focussed on two areas: comparing IEC's $CdCl_2$ heat treatment to theirs, and applying ZnTe:Cu layers by electrodeposition to their CdS/CdTe. Material measurements (x-ray diffraction (XRD) and optical spectroscopy) from MC samples were compared to ours. Solar cell performance was evaluated with illuminated JV measurements (scaled to 100 mW/cm^2, AM1.5) and spectral response (SR).

Processing

The IEC $CdCl_2$ heat treatment differs from the MC method in several details. We apply several drops of the saturated $CdCl_2/CH_3OH$ solution to the surface of the CdTe whereas MC soaks the sample in a saturated solution. We heat the sample at 410°C for 30 minutes to reach temperature, which may be very similar to the 20 minutes at 420°C used at MC except the ambient may differ. Finally, we rinse the $CdCl_2$ off with DI water while they boil in the DI water for 5 minutes, then rinse for another 5 minutes. The biggest difference is that we deposit the Cu/Au contact next, then dip in $BrCH_3OH$, whereas MC reverses the order of the contact and the dip. However, samples receiving the ZnTe:Cu layer at IEC have the $BrCH_3OH$ etch prior to ZnTe:Cu deposition. The details of the ZnTe:Cu electrodeposition are given in ref. 32. ZnTe:Cu deposition variables which we studied using your material were bath chemistry, CdTe surface etch, and Cu concentration.

Samples with prefix Y received $CdCl_2$ treatment at MC while those with prefix Z received $CdCl_2$ treatment at IEC.

Results

XRD scans revealed that MC CdTe had (111) and (220) orientations of comparable magnitude whereas IEC CdTe material is strongly (111) oriented. Figure 4.1 shows the (111) peak of a MC sample before and after $CdCl_2$ heat treatment at IEC. The lattice parameter, derived using only this peak, shifts by -0.011Å, which is only half as much as seen on our material. This suggests less S diffusion on their sample. However, the width of the peak increases from 0.12 to 0.15Å, while on our samples the (111) peak width decreases from about 0.20 to 0.15Å. The decrease in FWHM of the (111) peak found on our material is attributed to an increase in grain size, from 0.25 μm to ~ 1 μm. Without further analysis, we cannot determine whether MC CdTe becomes less oriented or has greater interdiffusion during $CdCl_2$ treatment.

After $CdCl_2$ treatment at IEC, the transmission of a MC sample exhibited sharpening and shift to longer wavelengths of the CdTe band edge, and increase in long wavelength transmission. This is very similar to behavior of our samples. Figure 4.2 compares three CdS/CdTe samples, two deposited at MC (one receiving the IEC $CdCl_2$ treatment), and one piece deposited and treated at IEC. To first order, they have the same CdTe bandedge, indicating similarity of both materials after either $CdCl_2$ treatments. Figure 4.3 is a log plot of the spectral response of three devices showing the long wavelength absorption tail. The samples receiving the IEC $CdCl_2$ treatment have slightly higher sub bandgap absorption. As we have shown (32) the long wavelength edge shifts to lower energy due to enhanced interdiffusion, or due to intentional grading to form a $CdTe_xS_{1-x}$ region. Also shown in Figure 4.3 is the data from an IEC cell having comparable CdS thickness to your cells. The all-IEC cell has the lowest band edge suggesting the greatest interdiffusion but the difference between the three is small, only about 20 meV.

The effect of MC and IEC $CdCl_2$ treatment on cell performance of MC-deposited CdS/CdTe was initially compared using Cu/Au contacts. Both were contacted with Cu/Au in the same run, tested, dipped in $BrCH_3OH$, then retested. Results for the best cell are given in Table 4.2.

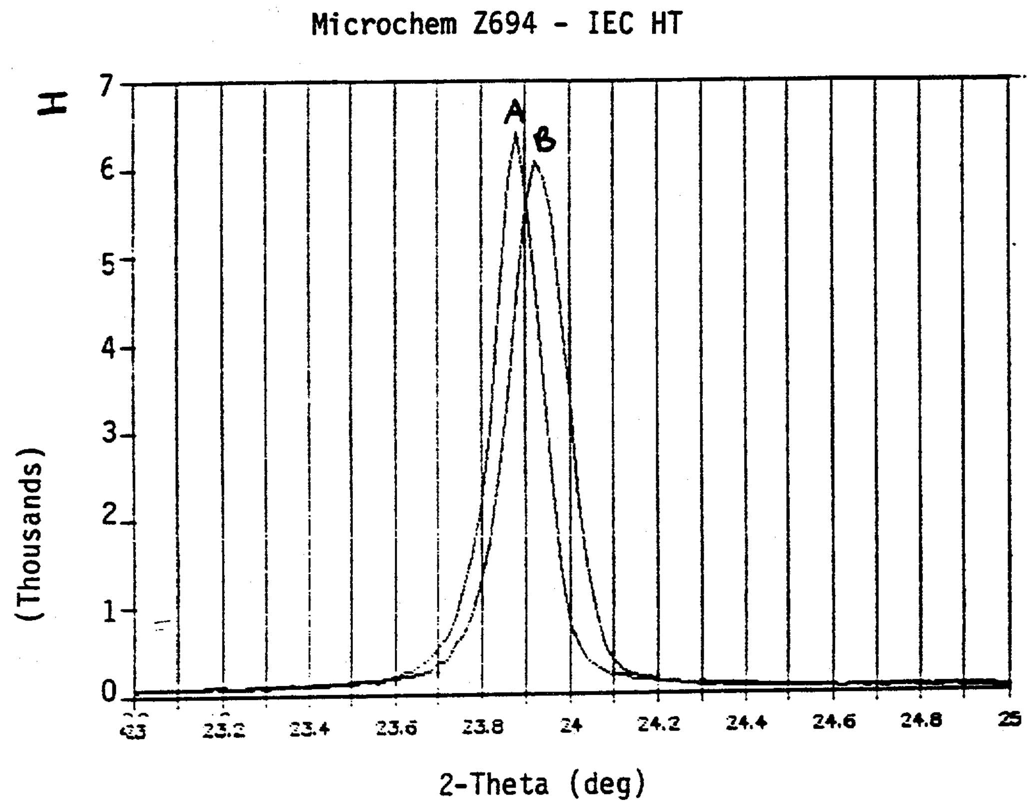

Figure 4.1 XRD scan of MC piece Z694A before (A) and after (B) $CdCl_2$ heat treatment at IEC, showing the shift in the (111) peak.

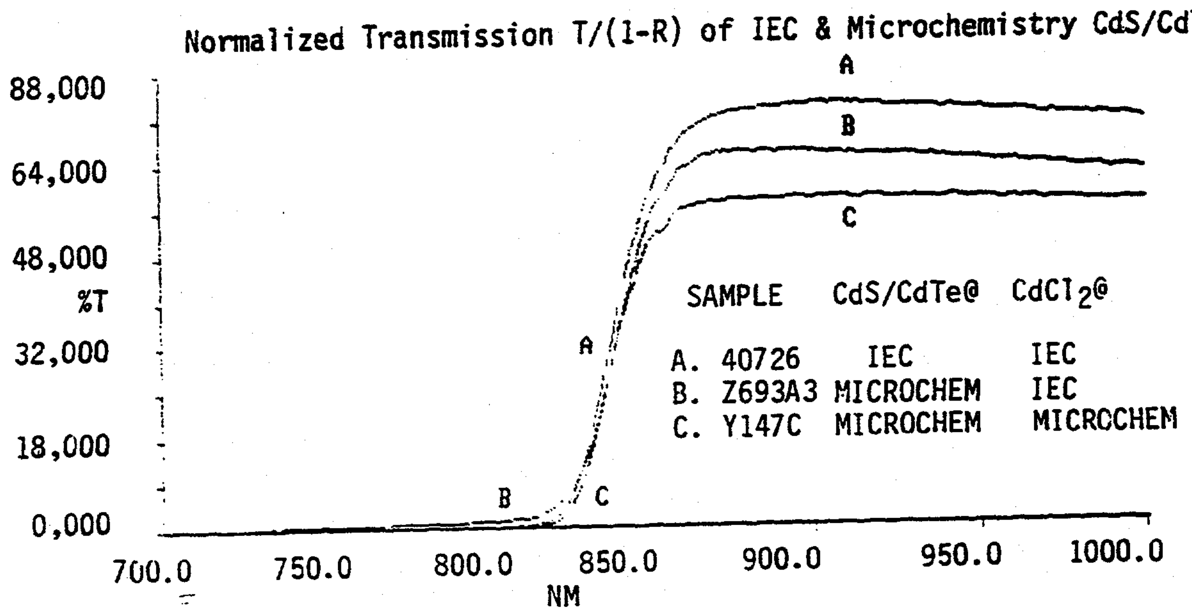

Figure 4.2 Normalized transmission of 3 CdS/CdTe films after $CdCl_2$ heat treatment showing the CdTe bandedge. Pieces received heat treatment at IEC (40726,Z693A-3) or at MC(Y147C).

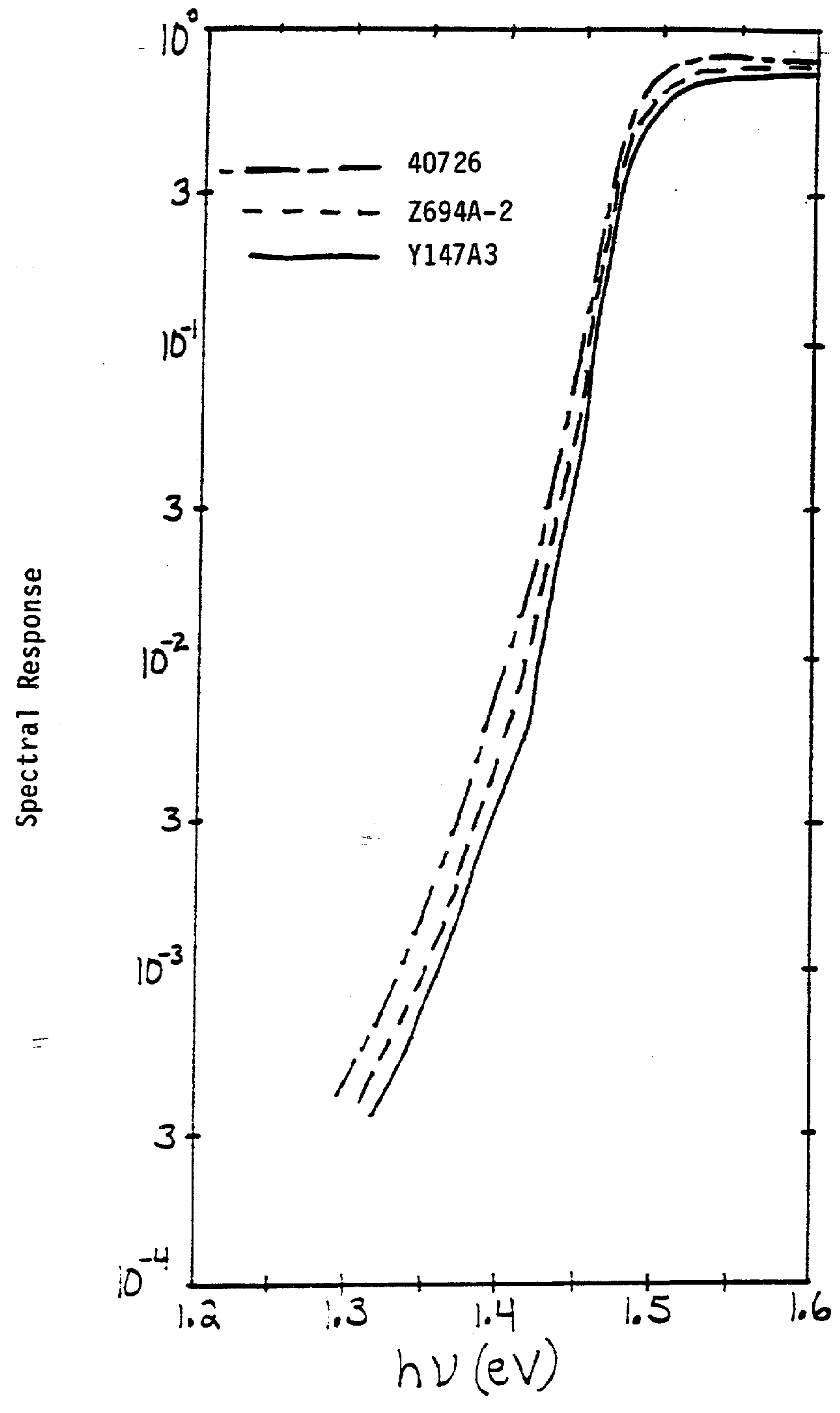

Figure 4.3 Absorption edge of 3 CdS/CdTe devices from low energy spectral response. 40726-deposition and heat treatment at IEC; Z694A-2-deposition at MC and heat treatment at IEC; Y147A-3-deposition and heat treatment at MC.

Table 4.2. Comparison of MC and IEC $CdCl_2$ treatment before and after $BrCH_3OH$ dip. Cu/Au contacts

Piece	$CdCl_2$	Cond.	V_{oc} (mV)	J_{sc} (mA/cm^2)	FF (%)	R_{voc} (Ω-cm^2)	η (%)
Y147A3-2	MC	init	713	16.5	66.4	8.0	7.8
		dip	794	16.3	67.8	6.9	8.8
Z694A2-8	IEC	init	671	18.0	65.0	4.8	7.9
		dip	754	17.4	65.1	4.4	8.6

Both pieces show a significant improvement in V_{oc} with the dip, typical of our cells. The MC-treated piece has higher V_{oc} and FF, (also higher resistance at V_{oc}) but lower J_{sc}. The spectral response of these two cells after dipping is shown in Figure 4.4. The Z piece has a higher response below 600 nm, suggesting either thinner <u>initial</u> CdS/CdS_yTe_{1-y} or greater interdiffusion hence consumption of CdS leading to a thinner <u>effective</u> CdS/CdS_yTe_{1-y} layer. This general difference in SR was observed between all Y and Z samples measured.

Table 4.3 contains cell performance from the best cell on each piece receiving electrodeposited ZnTe:Cu layers. Pieces were processed in pairs to evaluate a given process variable. The effect of bath chemistry was investigated using Y147C1 ($ZnCl_2$ bath) and Y147C2 ($ZnSO_4$ bath). The differences were insignificant, both yielding cells between 8.0 and 8.5% efficiency. The effect of CdTe surface etchant was studied using Y147A1 ($CrCH_3OH$) and Y147A2 (BDH etch, or bromine - dichrol - hydrazine etch). The BDH etch leaves a more Te-rich surface. The results showed very little difference between the two etchants with the BDH etched piece having about 1% higher FF on average.

The level of Cu in the solution had a strong influence on cell performance, with $2x10^{-4}$ M/l being nearly optimum while $4x10^{-4}$ M/l produces totally shunted devices. Results in Table 4.3 show little difference between 1 and $2x10^{-4}$ M/l of Cu.

The last two entries in Table 4.3 are for cells with Ni (as opposed to Au) as the metal contact to ZnTe:Cu.

Some general observations from Tables 4.2 and 4.3 follow:

1. The FF appears to be independent of whether the $CdCl_2$ treatment was done at IEC or MC, while the V_{oc} of pieces treated at MC seem to be slightly higher. However, $CdCl_2$ processing at both IEC and MC has yielded V_{oc} values around 790 mV, and FF values over 65%. However, neither of these is as high as reported on cells processed and measured at MC.

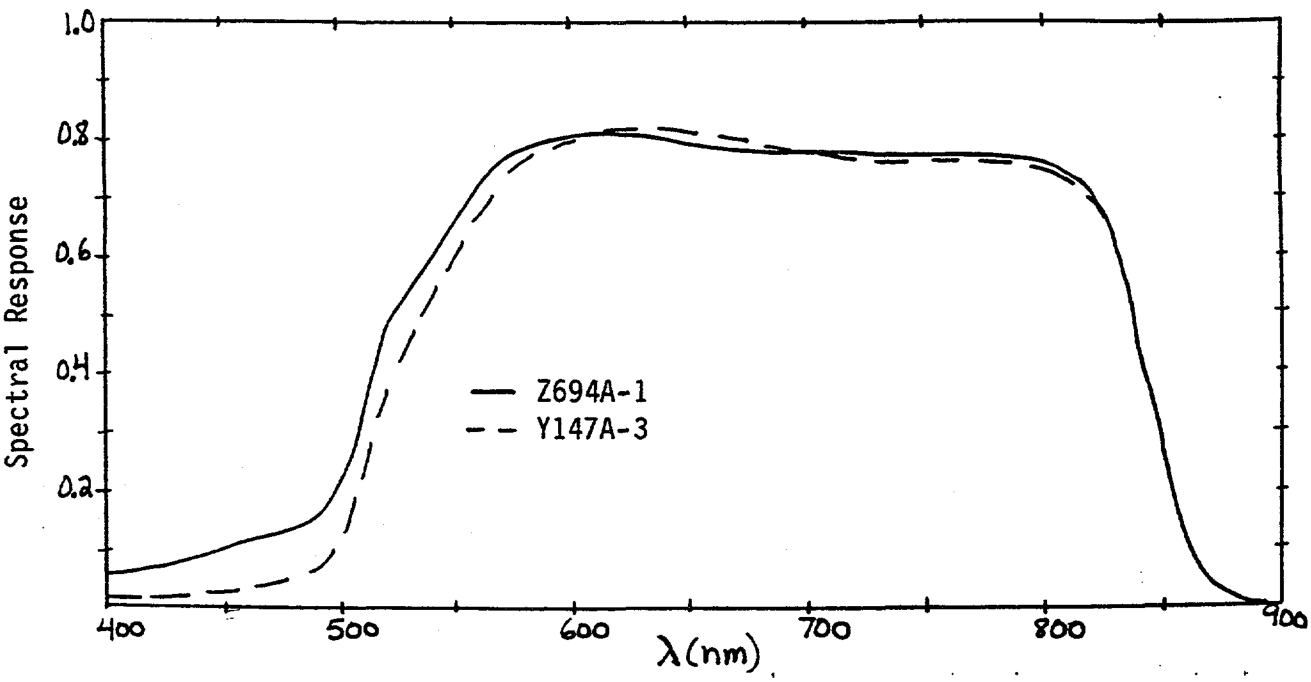

Figure 4.4 Spectral response at OV, ELH bias of MC CdS/CdTe.
Z694A-1 heat treatment at IEC.
Y147A-3 heat treatment at MC.

Table 4.3. Best cell performance of Microchemistry pieces processed at IEC with ZnTe:Cu layer. Scaled to 100 mW/cm^2. Prefix: Y-$CdCl_2$ HT @ Microchemistry; Z-$CdCl_2$ HT @ IEC. $BrCH_3OH$ pre-etch of CdTe, with sputtered Au contact, unless otherwise noted.

Piece	[Cu] $\times 10^{-4}$ M	V_{oc} mV	J_{sc} mA/cm^2	FF %	R_{voc} Ω-cm^2	η %	Comment
Y147C1	1	777	16.4	63.9	10.2	8.1	$ZnCl_2$ bath
Y147C2	1	787	16.5	65.1	8.4	8.5	
Y147A1	1	762	16.6	61.6	12.3	7.8	
Y147A2	1	750	17.1	63.2	8.6	8.1	BDH etch
Y147C3	1	753	15.7	62.2	9.9	7.3	
Y147C4	1	743	16.3	59.4	15.9	7.3	a
Z693A1	2	453	17.9	63.0	3.7	5.1	
Z694A1	1	790	18.0	64.9	8.4	9.3	
Z694A3	2	748	18.3	64.4	5.8	8.8	
Y146C2	2	746	18.2	61.7	11.9	8.4	Ni contact
Z693C2	2	706	19.3	65.2	5.6	7.9	Ni contact

a) complexing agent TEA in ZnTe:Cu was decreased by half in an attempt to increase activity of Cu.

---

2. The dark JV characteristic does not rise sharply beyond V_{oc}, and both light and dark JV shows significant curvature beyond V_{oc}. This was true for samples with or without ZnTe:Cu.

3. The J_{sc} values are consistently higher on Z pieces (processed at IEC) than on Y pieces (processed at MC). This appears to be related to the SR below 600 nm (Fig. 4.4). Either Z pieces have thinner initial CdS/CdS_yTe_{1-y} layers or they have greater interdiffusion, resulting in a thinner effective CdS layer after $CdCl_2$ treatment at IEC.

Conclusions

The $CdCl_2$ process and ZnTe:Cu contact developed at IEC using evaporated CdS/CdTe has been successfully applied to material deposited by a different method. Essentially equivalent performance was found. The IEC $CdCl_2$ heat treatment may cause greater interdiffusion between the CdTe and CdS than the MC $CdCl_2$ process, leading to higher J_{sc} but lower V_{oc} due to a reduced bandgap of the $Cd(Te_{1-y}S_y)$.

UNIVERSITY OF SOUTH FLORIDA

IEC has done a detailed set of device measurements on a CdTe solar cell furnished by the University of South Florida (sample 5-19B-20-C). Some of the analysis results of these measurements are discussed in Section 3.3. Appendix A gives additional information.

NATIONAL RENEWABLE ENERGY LABORATORY

Films and devices were provided to Larry Kazmerski and Fouad Abou-Elfotouh for analysis. Collaborative research effort was established with Mowafak Al-Jassim to characterize the effects of CdCl heat treatments on CdTe. Special CdS/CdTe devices on Si substrates were successfully prepared and characterized by cross-sectional TEM.

PHOTON ENERGY (GOLDEN PHOTON)

IEC fabricated CdS/CdTe devices on Photon Energy materials.

SOLAR CELLS, INC.

An exchange of materials and material evaluation of CdTe provided information on large area deposition of CdS.

EPV

Assistance on process development and device analysis and material characterization was provided.

5.0 REFERENCES

1. K. Zweibel, H.S. Ullal, R.L. Mitchell, and R. Noufi, Proc. 22nd IEEE Photovoltaic Specialists Conf., Las Vegas, NV, 1057 (1991).

2. B.N. Baron, R.W. Birkmire, J.E. Phillips, W.N. Shafarman, S.S. Hegedus, and B.E. McCandless, Annual Report under SERI Subcontract No. XN-0-10023-1 for the period 1/16/90 to 1/15/91 (March 1991).

3. R.W. Birkmire, W.N. Shafarman, R.D. Varrin, "Options for Fabrication and Design of $CuInSe_2$ Based Solar Cells," Proc. 21st IEEE Photovoltaic Specialists Conf., Kissimmee, FL, 529 (1990).

4. K.C. Mills, Thermodynamic Data for Inorganic Sulphides, Selenides and Tellurides, Butterworth (1974).

5. Gmelin Handbook of Inorganic Chemistry, **10**, Springer Verlag, (1988).

6. R.K. Pearson and G.R. Haugen, Int. J. of Hydrogen Energy, **6**(5), 509, (1981).

7. R.D. Varrin, Jr., Ph.D. Dissertation, University of Delaware (1991).

8. H. Dittrich, U. Prinz, J. Szot and H.W. Schock, Proceedings of the 9th European Community PV Conf., Freiburg, 163, (1989).

9. H. Oumous, A. Knowles, M.H. Badawi, M.J. Carter and R. Hill, Proc. 9th European Community PV Conf., Freiburg, (1989).

10. R.D. Varrin, Jr., S. Verma, R.W. Birkmire, B.E. McCandless and T.W.F. Russell, Proc. 21st Photovoltaic Specialists Conf., Kissimmee, Florida, (1990).

11. S. Verma, R.D. Varrin, Jr., R.W. Birkmire and T.W.F. Russell, Proc. 22nd IEEE Photovoltaic Specialists Conf., Las Vegas, (1991).

12. H. Dittrich, Institut fur Physikalische Elektronik, Univ. of Stuttgart, private communication.

13. W.B. Pearson, Pearson's Handbook of Crystallographicta for Intermetallic Phases, American Society for Metals, (1985).

14. J. Sullivan, Department of Engineering, Univ. of Delaware, private communication.

15. Brian E. McCandless, Robert W. Birkmire, Control of Deposition and Surface Properties of $CuInSe_2$ Thin Films for Solar Cells, Proc. 20th IEEE Photovoltaic Specialists Conf., Las Vegas, Nevada, (1988).

16. R.H. Mauch, et al. Proc. 22nd IEEE Photovoltaic Specialists Conf., 898, (1991).

17. B.E. McCandless and S.S. Hegedus, Proc. 22nd IEEE Photovoltaic Specialists Conf., 967 (1991).

18. Final report to NREL, Subcontract no. XM-0-18110-2 (1992).

19. CRC Handbook of Chemistry and Physics, R.C. Weast (Ed), 54th Edition, B75 (1974).

20. Ibid, p. D183.

21. W.N. Shafarman, R.W. Birkmire, D.A. Fardig, B.E. McCandless, A. Mondal, J.E. Phillips, and R.D. Varrin, Jr., Solar Cells, 30, 61-67 (1991).

22. Mowafak Al-Jassim, NREL, private communication.

23. I. Clemminck, M. Burgelman, M. Castelegn, J. DePoorter, and A. Vanvaet, Proc. 22nd IEEE Photovoltaic Specialists Conf., 1114 (1991).

24. K. Ohata, J. Saraie, and T. Tanaka, Jap. J. Appl. Phys. 12 (10), 1641 (1973).

25. R.A. Mickelsen and W.S. Chen, Appl. Phys. Lett. 36, 371 (1980).

26. M. Roy, S. Damaskinos, and J. E. Phillips, 20th IEEE Photovoltaic Specialists Conf., 1618, (1988).

27. K. Mitchell and H. Liu, 20th IEEE Photovoltaic Specialists Conf., 1461 (1988).

28. W. N. Shafarman and J. E. Phillips, 22nd IEEE Photovoltaic Specialists Conf., 934 (1991).

29. W. A. Miller and L. C. Olsen, IEEE Trans. Elec. Dev. ED-31, 654 (1984).

30. M. Roy and J. E. Phillips, 21st IEEE Photovoltaic Specialists Conf., 743, (1990).

31. D.A. Fardig and J.E. Phillips, Proceedings 22nd IEEE Photovoltaic Specialists Conf., 1146 (1991).

32. A. Mondal, B.E. McCandless, R.W. Birkmire, Proc. 22nd IEEE Photovoltaic Specialists Conf., 1126 (1991).

6.0 ABSTRACT

Results and conclusions of Phase II of a multi-year research program on polycrystalline thin film heterojunction solar cells are presented. The research consisted of the investigation of the relationships between processing, materials properties and device performance. This relationship was quantified by both an analysis of the materials processing used to make the device as well as analysis on modeling of the final device operation for $CuInSe_2$ formation by selenization, a clear understanding of the process is beginning to emerge.

Both H_2Se and elemental selenium are used to form copper indium diselenide. Equilibrium thermodynamic calculations were performed and show that the higher order Se_x species (Se_5, Se_6, Se_7) are important at temperatures below 800K whereas Se_2 becomes the predominant species at temperatures above 900K. A kinetic model is presented for the decomposition of H_2Se. The reaction is found to be first order at short times, but the reverse reaction of Se_x with H_2 assumes importance at higher conversions and longer times. The constants in the kinetic model are calculated from the data available in literature and our experiments.

Copper-indium bilayers have been selenized in 1) a tubular reactor with flowing H_2Se at atmospheric pressure and, 2) an evaporator using a Se source. In both systems, the selenizations were carried out at temperatures ranging from 150°C to 400°C for 60 minutes. Additionally, in the tubular reactor, copper-indium bilayers were selenized at 400°C for 1-45 minutes. The operating conditions in the tubular reactor were selected to ensure that the decomposition of H_2Se to Se_x species was less than 1%. The reaction pathways to $CuInSe_2$ formation using either H_2Se or Se proceed through the formation of a $Cu_{11}In_9$ alloy and the indium selenide phases (In_2Se and InSe). The only different precursors between the two reacting systems are the copper selenide phases which were observed in the selenization in the PVD reactor. The reaction with Se proceeds faster than the reaction with H_2Se.

Investigation of the relationship between CdTe post processing and the properties of the CdS and CdTe layers show that different optimization conditions are required for devices with different CdS thickness. For the $CdCl_2$ heat treatment step, reducing the treatment time improved yield and performance of devices with CdS less than 2000Å thick. Results for devices prepared with $CdCl_2$ vapor treatment show that the quantity of $CdCl_2$ and the delivery method are other important parameters to consider. The $CdCl_2$ heat treatment step recrystallizes the CdTe grains uniformly from the CdTe surface to the CdS/CdTe interface but produces non-uniform CdS and CdTe interdiffusion, the extent of which influences the device J_{sc}. Interdiffusion may also influence the V_{oc}, depending on the electronic properties of the resulting Cd(STe) and Cd(TeS) layers. Devices with CdTe films having 6 μm lateral grain size have been

fabricated but with no enhancement observed in the V_{oc}, which suggests that once grain size of ~1 μm is achieved, another V_{oc}-controlling mechanism dominates. Devices with very thin (<1000Å) CdS may also be sensitive to contamination or other properties associated with the TCO superstrate, since the junction is located closer to the TCO in those devices. With a post deposition process amenable to thin CdS in place, further improvement in device performance is likely to emerge from choice of a suitable TCO superstrate in conjunction with TCO/CdS preparation.

Several approaches to fabricating $CuInSe_2$ thin film solar cells in a superstrate configuration have been investigated. The $CuInSe_2$ films were grown on glass/ITO/CdS substrates by both three source evaporation and selenization using elemental Se. The ratio of the Cu/In in the $CuInSe_2$ film was varied from 0.5 to 1.3. The results are discussed in terms of device performance, $CuInSe_2$ film growth and alloy formation, and starting substrate.

I-V measurements over a wide range of temperatures and light intensities have been made on thin film $CuInSe_2$ based solar cells. These cells have been fabricated both at IEC and Siemens Solar Industries. The $CuInSe_2$ has been formed by several methods including elemental evaporation and selenization of Cu-In layers with H_2Se or elemental Se. The measurements have been analyzed and it has been found that all the devices have a non-linear series resistance which dominates the I-V behavior at lower temperatures. However, at higher temperatures and at V_{oc}, the behavior can be represented as a simple diode with an activation energy equal to the bandgap of the $CuInSe_2$ (~1.0eV) and with a diode quality factor between 1 and 2. This diode represents the behavior of the primary $CuInSe_2$/CdS junction, which is basically the same in all devices. But, when the standard diode behavior is subtracted from the I-V measurements to reveal the contribution of the non-linear series resistance, it is found that this contribution is different for each device.

I-V measurements over a similar range of light intensities and temperatures have been made on a University of South Florida CdTe solar cell. When a small voltage dependent current collection effect is accounted for, under illumination this device can also be represented by a simple diode with an activation energy of about 1.4eV and a diode quality factor of 1.6. This is very similar to results obtained from IEC's CdTe devices.

All of the I-V measurements are available to other researchers via the Internet or e-mail.

The regular retesting of CdTe devices over time to determine the stability of the output assumes that the testing itself does not introduce degradation. To test this assumption on IEC's CdTe devices, six samples with three different types of contacts to the CdTe were given repeated I-V tests. There were substantial changes in output due to testing with devices that had either the Cu/Au or the ZnTe/Au contact. There was little change in the devices that had the harder and more robust ZnTe/Ni contact. It appears that the probes used for current-voltage testing scratch the surface of the soft contacts, causing lowered fill factors due to both contact removal and device shunting.

APPENDIX A

The basic current-voltage test parameters are listed for seven different solar cells that were measured over the range of temperatures and light intensities shown. There are five $CuInSe_2$ devices made at IEC. Two of these (32187-22-12 and 32220-22-5) were made by elemental evaporation, one (61079-23-5) was made by the selenization of a Cu-In layer with elemental Se, and two (89091-2-6 and 89095-2-9) were made by the selenization of Cu-In layers with H_2Se. Device #16543-4-3 is a $CuInSe_2$ solar cell made by Siemens Solar and Device #5-19B-20-C is a CdTe solar cell made by the University of South Florida.

All or any of the J-V data collected from these devices is available. Contact: jep@brahms.udel.edu.

Institute of Energy Conversion
$CuInSe_2$ Device # 32187-22-12

Test #	Temp (K)	Ill. Level	# of J-V pts.	$(dJ/dV)@J_{sc}$ (mS/cm^2)
1	358	Dark	80	0.4
2	358	~20%AM1	78	1.3
3	358	~5%AM1	78	0.8
4	358	~80%AM1	77	3.3
5	343	Dark	83	0.3
6	343	~20%AM1	83	0.7
7	343	~5%AM1	83	0.6
8	343	~80%AM1	83	2.7
9	328	Dark	86	0.2
10	328	~20%AM1	81	0.9
11	328	~5%AM1	82	0.4
12	328	~80%AM1	80	1.8
13	313	Dark	89	0.1
14	313	~20%AM1	87	0.5
15	313	~5%AM1	89	0.3
16	313	~80%AM1	87	1.1
17	298	Dark	87	0.1
18	298	~20%AM1	84	0.4
19	298	~5%AM1	86	0.3
20	298	~80%AM1	79	2.3
21	281	Dark	95	0.0
22	281	~20%AM1	94	0.4
23	281	~5%AM1	94	0.2
24	281	~80%AM1	95	1.1
25	263	Dark	97	0.0
26	263	~20%AM1	97	0.3
27	263	~5%AM1	97	0.1
28	263	~80%AM1	96	
29	245	Dark	99	0.0
30	245	~20%AM1	99	
31	245	~5%AM1	99	0.1
32	245	~80%AM1	99	0.9

Institute of Energy Conversion
$CuInSe_2$ Device # 32187-22-12

Illumination Level~80%AM1

Temp (K)	J_{sc} (mA/cm^2)	V_{oc} (V)	FF (%)	P_{max} (mW/cm^2)	$(dV/dJ) @V_{oc}$ (Ω-cm^2)	$(dJ/dV) @J_{sc}$ (mS/cm^2)
358	23.61	.3128	55.40	4.09	2.9	3.3
343	23.54	.3440	58.47	4.73	2.8	2.7
328	23.45	.3710	60.96	5.30	2.7	1.8
313	23.40	.4002	63.40	5.94	2.6	1.1
298	22.12	.4244	64.32	6.04	2.9	2.3
281	23.46	.4579	65.42	7.03	3.1	1.1
263	23.68	.4952	65.29	7.66	3.7	
245	23.38	.5289	65.17	8.06	5.8	0.9

Illumination Level~20%AM1

Temp (K)	J_{sc} (mA/cm^2)	V_{oc} (V)	FF (%)	P_{max} (mW/cm^2)	$(dV/dJ@V_{oc})$ (Ω-cm^2)	$(dJ/dV) @J_{sc}$ (mS/cm^2)
358	5.81	.2655	54.77	0.85	8.6	1.3
343	5.80	.2902	57.91	0.97	8.3	0.7
328	5.84	.3189	60.08	1.12	8.8	0.9
313	5.95	.3514	62.58	1.31	7.9	0.5
298	5.79	.3832	64.65	1.43	8.3	0.4
281	5.81	.4140	65.78	1.58	8.4	0.4
263	5.88	.4532	67.90	1.81	9.1	0.3
245	5.86	.4934	69.46	2.01	11.4	

Illumination Level~5%AM1

Temp (K)	J_{sc} (mA/cm^2)	V_{oc} (V)	FF (%)	P_{max} (mW/cm^2)	$(dV/dJ) @V_{oc}$ (Ω-cm^2)	$(dJ/dV) @J_{sc}$ (mS/cm^2)
358	1.67	.2164	50.93	0.18	28.6	0.8
343	1.69	.2390	52.58	0.21	30.9	0.6
328	1.73	.2707	55.27	0.26	27.2	0.4
313	1.68	.2990	57.06	0.29	30.7	0.3
298	1.34	.3324	59.67	0.27	34.2	0.3
281	1.72	.3685	62.30	0.40	34.8	0.2
263	1.70	.4116	66.41	0.47	26.0	0.1
245	1.68	.4562	69.22	0.53	26.6	0.1

Institute of Energy Conversion
$CuInSe_2$ Device # 32220-22-5

Test #	Temp (K)	Ill. Level	# of J-V pts.	$(dJ/dV)@J_{sc}$ (mS/cm^2)
1	358	Dark	72	0.3
2	358	~20%AM1	72	1.5
3	358	~5%AM1	72	0.8
4	358	~80%AM1	72	3.8
5	343	Dark	79	0.2
6	343	~20%AM1	78	1.0
7	343	~5%AM1	78	0.5
8	343	~80%AM1	78	3.7
9	328	Dark	78	0.1
10	328	~20%AM1	77	0.6
11	328	~5%AM1	77	0.2
12	328	~80%AM1	78	1.9
13	313	Dark	87	0.1
14	313	~20%AM1	87	0.5
15	313	~5%AM1	87	0.2
16	313	~80%AM1	87	1.5
17	298	Dark	81	0.0
18	298	~20%AM1	83	0.4
19	298	~5%AM1	85	0.2
20	298	~80%AM1	78	1.1
21	281	Dark	94	0.0
22	281	~20%AM1	92	0.3
23	281	~5%AM1	94	0.2
24	281	~80%AM1	94	1.0
25	263	Dark	96	0.0
26	263	~20%AM1	96	0.2
27	263	~5%AM1	95	0.2
28	263	~80%AM1	96	0.6
29	245	Dark	98	0.0
30	245	~20%AM1	98	0.2
31	245	~5%AM1	98	0.1
32	245	~80%AM1	98	0.7

Institute of Energy Conversion
$CuInSe_2$ Device # 32220-22-5

Illumination Level~80%AM1

Temp (K)	J_{sc} (mA/cm^2)	V_{oc} (V)	FF (%)	P_{max} (mW/cm^2)	($dJ/dV@V_{oc}$) ($\Omega-cm^2$)	$(dJ/dV)@J_{sc}$ (mS/cm^2)
358	23.26	.3008	55.39	3.88	2.7	3.8
343	22.92	.3346	58.43	4.48	2.6	3.7
328	22.80	.3616	60.93	5.02	2.6	1.9
313	22.67	.3841	62.00	5.40	2.8	1.5
298	22.00	.4059	63.38	5.66	2.9	1.1
281	22.99	.4325	62.03	6.17	3.4	1.0
263	23.00	.4655	63.02	6.75	4.3	0.6
245	22.95	.4997	64.89	7.44	5.5	0.7

Illumination Level~20%AM1

Temp (K)	J_{sc} (mA/cm^2)	V_{oc} (V)	FF (%)	P_{max} (mW/cm^2)	($dV/dJ@V_{oc}$) ($\Omega-cm^2$)	$(dJ/dV)@J_{sc}$ (mS/cm^2)
358	5.86	.2485	54.02	0.79	8.8	1.5
343	5.85	.2788	57.50	0.94	8.6	1.0
328	5.84	.3076	60.17	1.08	8.3	0.6
313	5.84	.3333	61.13	1.19	8.6	0.5
298	5.67	.3628	63.51	1.31	8.2	0.4
281	5.77	.3868	61.94	1.38	9.7	0.3
263	5.76	.4237	63.67	1.55	10.6	0.2
245	5.76	.4680	67.83	1.83	11.9	0.2

Illumination Level~5%AM1

Temp (K)	J_{sc} (mA/cm^2)	V_{oc} (V)	FF (%)	P_{max} (mW/cm^2)	$(dV/dJ)@V_{oc}$ ($\Omega-cm^2$)	$(dJ/dV)@J_{sc}$ (mS/cm^2)
358	1.68	.1964	50.33	0.17	27.5	0.8
343	1.69	.2282	54.18	0.21	28.0	0.5
328	1.68	.2558	57.20	0.25	26.8	0.2
313	1.67	.2799	57.94	0.27	26.6	0.2
298	1.32	.3067	59.52	0.24	40.5	0.2
281	1.73	.3372	59.32	0.35	35.1	0.2
263	1.68	.3789	61.86	0.39	36.2	0.2
245	1.67	.4306	66.59	0.48	28.0	0.1

Institute of Energy Conversion
$CuInSe_2$ Device # 61079-23-5

Test #	Temp (K)	Ill. Level	# of J-V pts.	(dJ/dV) @J_{sc} (mS/cm^2)
1	373	Dark	65	1.8
2	373	~20%AM1	65	3.0
3	373	~5%AM1	65	2.0
4	373	~80%AM1	65	5.8
5	358	Dark	67	0.8
6	358	~20%AM1	67	1.8
7	358	~5%AM1	67	1.3
8	358	~80%AM1	67	3.7
9	343	Dark	72	0.5
10	343	~20%AM1	72	1.6
11	343	~5%AM1	72	0.7
12	343	~80%AM1	72	2.9
13	328	Dark	75	0.3
14	328	~20%AM1	75	1.1
15	328	~5%AM1	75	0.6
16	328	~80%AM1	80	2.7
17	313	Dark	80	0.2
18	313	~20%AM1	79	0.9
19	313	~5%AM1	80	0.3
20	313	~80%AM1	80	1.1
21	298	Dark	85	0.1
22	298	~20%AM1	85	0.6
23	298	~5%AM1	85	0.2
24	298	~80%AM1	85	1.9
25	278	Dark	85	0.1
26	278	~20%AM1	85	0.6
27	278	~5%AM1	85	0.2
28	278	~80%AM1	85	1.6
29	258	Dark	90	0.1
30	258	~20%AM1	90	0.7
31	258	~5%AM1	90	0.3
32	258	~80%AM1	90	1.3
33	238	Dark	95	0.0
34	238	~20%AM1	95	0.6
35	238	~5%AM1	95	0.2
36	238	~80%AM1	95	2.0
37	218	Dark	98	0.0
38	218	~20%AM1	98	0.4
39	218	~5%AM1	98	0.1
40	218	~80%AM1	98	1.9

Institute of Energy Conversion
$CuInSe_2$ Device # 61079-23-5

Illumination Level~80%AM1

Temp (K)	J_{sc} (mA/cm^2)	V_{oc} (V)	FF (%)	P_{max} (mW/cm^2)	$(dV/dJ)@V_{oc}$ (Ω-cm^2)	$(dJ/dV)@J_{sc}$ (mS/cm^2)
373	25.53	.2859	53.33	3.89	2.6	5.8
358	25.55	.3136	57.07	4.57	2.4	3.7
343	25.60	.3427	59.82	5.25	2.4	2.9
328	25.65	.3731	62.10	5.94	2.4	2.7
313	25.43	.4032	63.81	6.54	2.6	1.1
298	25.42	.4301	63.03	6.89	2.9	1.9
278	25.49	.4678	65.81	7.85	2.9	1.6
258	25.47	.5071	66.85	8.63	3.6	1.3
238	25.80	.5453	66.11	9.30	5.1	2.0
218	25.96	.5780	63.53	9.53	8.6	1.9

Illumination Level~20%AM1

Temp (K)	J_{sc} (mA/cm^2)	V_{oc} (V)	FF (%)	P_{max} (mW/cm^2)	$(dV/dJ)@V_{oc}$ (Ω-cm^2)	$(dJ/dV)@J_{sc}$ (mS/cm^2)
373	7.43	.2318	51.97	0.90	6.7	3.0
358	7.36	.2637	55.72	1.08	6.8	1.8
343	7.19	.2943	59.16	1.25	6.6	1.6
328	7.25	.3278	62.56	1.49	6.8	1.1
313	7.36	.3573	64.06	1.68	6.3	0.9
298	7.53	.3897	66.08	1.94	5.7	0.6
278	7.42	.4306	67.72	2.16	5.8	0.6
258	7.48	.4738	69.52	2.46	6.8	0.7
238	7.45	.5139	69.53	2.66	8.3	0.6
218	7.49	.5493	67.84	2.79	12.4	0.4

Illumination Level~5%AM1

Temp (K)	J_{sc} (mA/cm^2)	V_{oc} (V)	FF (%)	P_{max} (mW/cm^2)	$(dV/dJ)@V_{oc}$ (Ω-cm^2)	$(dJ/dV)@J_{sc}$ (mS/cm^2)
373	1.79	.1660	45.32	0.13	28.2	2.0
358	1.78	.2029	49.17	0.18	26.0	1.3
343	1.80	.2409	54.34	0.24	23.0	0.7
328	1.78	.2740	57.70	0.28	24.0	0.6
313	1.78	.3045	59.59	0.32	24.7	0.3
298	1.80	.3401	62.56	0.38	20.0	0.2
278	1.80	.3835	64.00	0.44	21.9	0.2
258	1.81	.4317	66.28	0.52	20.5	0.3
238	1.83	.4743	67.08	0.58	22.9	0.2
218	1.84	.5125	68.09	0.64	25.8	0.1

Institute of Energy Conversion
$CuInSe_2$ Device # 89091-2-6

Test #	Temp (K)	Ill. Level	# of J-V pts.	(dJ/dV) @J_{sc} (mS/cm^2)
1	358	Dark	70	2.4
2	358	~80%AM1	70	1.6
3	338	Dark	74	1.9
4	338	~80%AM1	75	5.1
5	318	Dark	75	1.6
6	318	~80%AM1	75	1.8
7	298	Dark	75	2.2
8	298	~80%AM1	75	3.1
9	278	Dark	85	4.0
10	278	~80%AM1	85	5.1
11	258	Dark	85	3.1
12	258	~80%AM1	85	5.0
13	238	Dark	85	3.0
14	238	~80%AM1	85	4.0
15	218	Dark	85	3.5
16	218	~80%AM1	95	5.3
17	198	Dark	95	2.9
18	198	~80%AM1	95	4.4

Illumination Level~80%AM1

Temp (K)	J_{sc} (mA/cm^2)	V_{oc} (V)	FF (%)	P_{max} (mW/cm^2)	(dV/dJ) @V_{oc} (Ω-cm^2)	(dJ/dV) @J_{sc} (mS/cm^2)
358	27.18	.2925	54.29	4.32	2.5	1.6
338	27.65	.3330	58.05	5.35	2.4	5.1
318	28.04	.3726	60.23	6.29	2.4	1.8
298	27.95	.4138	62.81	7.26	2.4	3.1
278	27.42	.4489	59.33	7.30	3.5	5.1
258	27.60	.4880	59.11	7.96	4.0	5.0
238	23.67	.5253	59.53	7.40	5.5	4.0
218	27.19	.5542	55.82	8.41	8.2	5.3
198	26.94	.5796	54.48	8.51	9.7	4.4

Institute of Energy Conversion
$CuInSe_2$ Device # 89095-2-9

Test #	Temp (K)	Ill. Level	# of J-V pts.	(dJ/dV)@J_{sc} (mS/cm^2)
1	373	Dark	65	2.4
2	373	~20%AM1	65	2.8
3	373	~5%AM1	65	2.5
4	373	~80%AM1	65	4.2
5	358	Dark	65	2.3
6	358	~20%AM1	65	2.3
7	358	~5%AM1	65	2.1
8	358	~80%AM1	65	3.1
9	343	Dark	72	2.2
10	343	~20%AM1	72	2.7
11	343	~5%AM1	72	2.5
12	343	~80%AM1	72	3.3
13	328	Dark	75	2.6
14	328	~20%AM1	75	2.7
15	328	~5%AM1	75	2.7
16	328	~80%AM1	74	3.5
17	313	Dark	75	2.5
18	313	~20%AM1	75	3.3
19	313	~5%AM1	75	1.9
20	313	~80%AM1	75	3.1
21	298	Dark	75	2.6
22	298	~20%AM1	75	2.5
23	298	~5%AM1	75	2.8
24	298	~80%AM1	75	2.8
25	278	Dark	75	0.9
26	278	~20%AM1	75	1.0
27	278	~5%AM1	75	1.0
28	278	~80%AM1	75	1.0
29	258	Dark	75	0.8
30	258	~20%AM1	85	0.9
31	258	~5%AM1	85	0.9
32	258	~80%AM1	84	1.1

Institute of Energy Conversion
$CuInSe_2$ Device # 89095-2-9

Illumination Level~80%AM1

Temp (K)	J_{sc} (mA/cm^2)	V_{oc} (V)	FF (%)	P_{max} (mW/cm^2)	$(dV/dJ)@V_{oc}$ (Ω-cm^2)	$(dJ/dV)@J_{sc}$ (mS/cm^2)
373	26.41	.2796	52.26	3.86	2.5	4.2
358	25.11	.3089	55.13	4.28	2.8	3.1
343	24.96	.3384	57.23	4.83	2.8	3.3
328	25.17	.3686	59.43	5.51	2.7	3.5
313	25.18	.3983	59.82	6.00	2.9	3.1
298	26.32	.4311	62.36	7.08	2.4	2.8
278	26.16	.4610	57.94	6.99	4.4	1.0
258	27.88	.5002	57.38	8.00	5.6	1.1

Illumination Level~20%AM1

Temp (K)	J_{sc} (mA/cm^2)	V_{oc} (V)	FF (%)	P_{max} (mW/cm^2)	$(dV/dJ)@V_{oc}$ (Ω-cm^2)	$(dJ/dV)@J_{sc}$ (mS/cm^2)
373	7.56	.2235	50.96	0.86	7.1	2.8
358	7.84	.2558	53.02	1.06	7.2	2.3
343	7.61	.2870	55.25	1.21	7.5	2.7
328	7.73	.3193	56.18	1.39	6.6	2.7
313	7.50	.3443	56.24	1.45	7.8	3.3
298	7.45	.3782	59.81	1.69	7.9	2.5
278	7.57	.4146	60.48	1.90	9.7	1.0
258	7.55	.4535	60.56	2.07	11.4	0.9

Illumination Level~5%AM1

Temp (K)	J_{sc} (mA/cm^2)	V_{oc} (V)	FF (%)	P_{max} (mW/cm^2)	$(dV/dJ)@V_{oc}$ (Ω-cm^2)	$(dJ/dV)@J_{sc}$ (mS/cm^2)
373	1.89	.1584	44.22	0.13	28.8	2.5
358	1.84	.1848	44.22	0.15	30.1	2.1
343	1.58	.2077	42.53	0.14	41.4	2.5
328	1.86	.2421	44.21	0.20	32.5	2.7
313	1.86	.2721	46.29	0.23	34.2	1.9
298	1.82	.3037	45.38	0.25	36.7	2.8
278	1.82	.3516	55.20	0.35	31.3	1.0
258	1.92	.3937	54.77	0.41	33.6	0.9

Siemens Solar
$CuInSe_2$ Device # SS16543-4-3

Test #	Temp (K)	Ill. Level	# of J-V pts.	(dJ/dV)@J_{sc} (mS/cm^2)
1	373	Dark	63	3.6
2	373	~20%AM1	63	3.7
3	373	~5%AM1	63	3.5
4	373	~80%AM1	62	4.6
5	358	Dark	65	0.9
6	358	~20%AM1	65	1.3
7	358	~5%AM1	65	1.7
8	358	~80%AM1	65	2.1
9	343	Dark	69	0.4
10	343	~20%AM1	69	0.8
11	343	~5%AM1	69	0.6
12	343	~80%AM1	69	1.4
13	328	Dark	75	0.3
14	328	~20%AM1	75	0.6
15	328	~5%AM1	75	0.4
16	328	~80%AM1	75	1.2
17	313	Dark	80	0.2
18	313	~20%AM1	80	0.7
19	313	~5%AM1	80	0.2
20	313	~80%AM1	80	1.3
21	298	Dark	81	0.1
22	298	~20%AM1	80	0.4
23	298	~5%AM1	81	0.2
24	298	~80%AM1	79	0.9
25	278	Dark	85	0.1
26	278	~20%AM1	85	0.4
27	278	~5%AM1	85	0.2
28	278	~80%AM1	85	
29	258	Dark	90	0.1
30	258	~20%AM1	90	0.4
31	258	~5%AM1	90	0.2
32	258	~80%AM1	90	1.1
33	238	Dark	95	0.1
34	238	~20%AM1	95	0.3
35	238	~5%AM1	95	0.1
36	238	~80%AM1	95	0.9
37	218	Dark	98	0.0
38	218	~20%AM1	98	0.3
39	218	~5%AM1	98	0.1
40	218	~80%AM1	98	1.4

Siemens Solar
$CuInSe_2$ Device # SS16543-4-3

Illumination Level~80%AM1

Temp (K)	J_{sc} (mA/cm^2)	V_{oc} (V)	FF (%)	P_{max} (mW/cm^2)	$(dV/dJ) @V_{oc}$ (Ω-cm^2)	$(dJ/dV) @J_{sc}$ (mS/cm^2)
373	29.32	.2882	56.01	4.73	2.1	4.6
358	29.31	.3190	58.15	5.44	2.2	2.1
343	29.44	.3499	60.38	6.22	2.0	1.4
328	29.46	.3813	61.23	6.88	2.1	1.2
313	29.13	.4132	61.84	7.44	2.4	1.3
298	29.18	.4454	62.02	8.06	2.8	0.9
278	29.02	.4861	61.08	8.62	3.7	
258	28.58	.5250	60.38	9.06	4.7	1.1
238	28.20	.5621	58.79	9.32	7.2	0.9
218	27.90	.5888	50.71	8.33	14.7	1.4

Illumination Level~20%AM1

Temp (K)	J_{sc} (mA/cm^2)	V_{oc} (V)	FF (%)	P_{max} (mW/cm^2)	$(dV/dJ) @V_{oc}$ (Ω-cm^2)	$(dJ/dV) @J_{sc}$ (mS/cm^2)
373	8.37	.2311	52.25	1.01	5.8	3.7
358	8.40	.2634	56.56	1.25	5.8	1.3
343	8.46	.2957	59.26	1.48	6.0	0.8
328	8.21	.3273	61.40	1.65	6.5	0.6
313	8.21	.3614	63.13	1.87	6.1	0.7
298	8.14	.3950	64.40	2.07	7.0	0.4
278	8.39	.4413	64.89	2.40	7.7	0.4
258	8.27	.4842	65.67	2.63	9.3	0.4
238	8.14	.5256	65.38	2.80	12.4	0.3
218	8.09	.5625	59.68	2.72	27.4	0.3

Illumination Level~5%AM1

Temp (K)	J_{sc} (mA/cm^2)	V_{oc} (V)	FF (%)	P_{max} (mW/cm^2)	$(dV/dJ) @V_{oc}$ (Ω-cm^2)	$(dJ/dV) @J_{sc}$ (mS/cm^2)
373	1.97	.1614	43.17	0.14	24.6	3.5
358	1.97	.1975	48.85	0.19	26.2	1.7
343	1.98	.2334	54.98	0.25	22.3	0.6
328	1.98	.2663	57.68	0.30	24.0	0.4
313	1.98	.3022	60.83	0.36	21.9	0.2
298	1.97	.3371	63.30	0.42	24.8	0.2
278	2.06	.3857	64.93	0.52	24.9	0.2
258	1.99	.4310	66.32	0.57	25.2	0.2
238	1.95	.4761	67.31	0.63	30.7	0.1
218	1.96	.5209	65.46	0.67	49.0	0.1

University of South Florida
CdTe Device # 5-19B-20-C

Test #	Temp (K)	Ill. Level	# of J-V pts.	(dJ/dV)@J_{sc} (mS/cm^2)	
1	298	Dark	96	0.0	(1)
2	298	Dark	95	0.0	
3	298	~80%AM1	83	0.6	
4	298	~80%AM1	84	1.2	(1)
5	298	~20%AM1	84	0.2	
6	313	Dark	83	0.0	
7	313	~20%AM1	80	0.2	
8	313	~80%AM1	79	1.3	
9	328	Dark	80	0.0	
10	328	~20%AM1	76	0.2	
11	328	~80%AM1	74	0.6	
12	343	Dark	76	0.0	
13	343	~20%AM1	71	0.3	
14	343	~80%AM1	70	0.5	
15	358	~80%AM1	65	0.7	
16	358	~20%AM1	66	0.0	
17	358	Dark	68	0.0	
18	373	~80%AM1	57	0.6	
19	373	~20%AM1	60	0.3	
20	373	Dark	61	0.0	
21	353	Dark	74	0.0	
22	353	~20%AM1	67		
23	353	~80%AM1	65		
24	333	Dark	74	0.0	
25	333	~20%AM1	74	0.2	
26	333	~80%AM1	72	1.4	
27	313	~80%AM1	76	1.2	
28	313	~20%AM1	76	0.2	
29	313	Dark	85	0.0	
30	293	Dark	97	0.0	
31	293	~20%AM1	86	0.3	
32	293	~80%AM1	83		
33	273	Dark	98	0.0	
34	273	~20%AM1	87	0.3	
35	273	~80%AM1	81	1.1	
36	253	Dark	95	0.0	
37	253	~20%AM1	87	0.5	
38	253	~80%AM1	86	2.2	
39	233	Dark	96	0.0	
40	233	~20%AM1	94	0.9	
41	233	~80%AM1	90	5.3	
42	218	Dark	99	0.0	
43	218	Dark	99	0.0	(1)
44	218	~80%AM1	79	8.4	(1)
45	218	~80%AM1	100	8.6	
46	218	~20%AM1	100	0.7	

University of South Florida
CdTe Device #5-19B-20-C

Illumination Level~80%AM1

Temp (K)	J_{sc} (mA/cm^2)	V_{oc} (V)	FF (%)	P_{max} (mW/cm^2)	$(dV/dJ)@V_{oc}$ (Ω-cm^2)	$(dJ/dV)@J_{sc}$ (mS/cm^2)	Test #	
373	23.64	.6268	62.74	9.30	2.4	0.6	18	
358	23.90	.6734	61.94	9.97	3.1	0.7	15	
353	23.93	.6779	60.00	9.73	3.3		23	
343	23.87	.7122	61.87	10.52	3.3	0.5	14	
333	23.79	.7230	58.38	10.04	3.7	1.4	26	
328	23.72	.7415	60.64	10.67	3.5	0.6	11	
313	23.89	.7762	60.29	11.18	4.2	1.3	8	
313	23.67	.7569	54.36	9.74	5.1	1.2	27	(2)
298	24.14	.8026	60.69	11.76	4.4	0.6	3	
298	24.08	.8035	62.95	12.18	3.9	1.2	4	(1)
293	23.81	.7949	58.34	1.04	5.1		32	
273	24.08	.8357	55.18	11.10	6.4	1.1	35	
253	24.76	.8754	50.99	11.05	7.9	2.2	38	
233	24.09	.9221	43.75	9.72	10.1	5.3	41	
218	23.62	.9546	37.02	8.35	12.3	8.6	45	
218	24.44	.9565	37.58	8.78	11.3	8.4	44	(1)

Illumination Level~20%AM1

Temp (K)	J_{sc} (mA/cm^2)	V_{oc} (V)	FF (%)	P_{max} (mW/cm^2)	$(dV/dJ)@V_{oc}$ (Ω-cm^2)	$(dJ/dV)@J_{sc}$ (mS/cm^2)	Test #	
373	7.38	.5764	61.47	2.61	8.9	0.3	19	
358	7.39	.6201	62.72	2.87	8.6	0.0	16	
353	7.36	.6285	60.92	2.82	10.7		22	
343	7.42	.6562	63.52	3.09	10.0	0.3	13	
333	7.43	.6750	59.77	3.00	10.8	0.2	25	
328	7.34	.6924	63.31	3.22	10.0	0.2	10	
313	7.37	.7254	63.45	3.39	11.3	0.2	7	
313	7.35	.7062	56.50	2.93	13.6	0.2	28	(2)
298	7.43	.7428	61.82	3.41	12.3	0.2	5	
293	7.39	.7551	62.49	3.49	13.9	0.3	31	
273	7.30	.7833	60.01	3.43	16.5	0.3	34	
253	7.53	.8296	56.96	3.56	18.2	0.5	37	
233	7.39	.8725	53.19	3.43	24.3	0.9	40	
218	7.24	.9031	49.13	3.21	30.7	0.7	46	

APPENDIX B

Durability Testing of CdTe Contacts

The basic J-V parameters are listed for each of the 354 I-V retests done on 40 cells with 3 different types of electrical contacts to the CdTe. Hysteris effects in the I-V retest is indicated by the comment "Uns. I-V".

Contact=ZnTe/Ni Sample=40724.31

Cell #	V_{oc} (V)	J_{sc} (ma/cm^2)	FF (%)	P_{max} (mW/cm^2)	Comment	Date Tested
1	0.670	19.2	65.8	9.7	Unst. I-V	14JUL92
	0.665	19.2	63.5	9.3	Unst. I-V	15JUL92
	0.667	19.2	63.1	9.2		16JUL92
	0.666	19.2	65.0	9.5	Unst. I-V	17JUL92
	0.669	19.3	61.9	9.2	Unst. I-V	21JUL92
	0.661	18.3	58.7	8.1	Unst. I-V	30JUL92
1	0.687	18.0	66.2	9.4	Unst. I-V	04JAN93
	0.673	17.9	65.4	9.0	Unst. I-V	05JAN93
	0.679	17.9	64.5	9.0	Unst. I-V	06JAN93
	0.677	17.6	65.2	8.9		07JAN93
	0.680	17.4	65.7	8.9	Unst. I-V	13JAN93
	0.678	17.3	66.4	8.9		14JAN93
2	0.646	19.2	65.9	9.4		14JUL92
	0.642	19.3	65.6	9.3	Unst. I-V	15JUL92
	0.642	19.3	65.8	9.3		16JUL92
	0.642	19.3	65.4	9.3		17JUL92
	0.645	19.7	65.5	9.5	Unst. I-V	21JUL92
	0.641	18.6	65.9	9.0	Unst. I-V	30JUL92
2	0.656	18.1	66.5	9.0		04JAN93
	0.646	18.1	66.0	8.8	Unst. I-V	05JAN93
	0.655	18.2	66.8	9.1		06JAN93
	0.642	17.8	66.4	8.7	Unst. I-V	07JAN93
	0.647	17.7	66.7	8.7	Unst. I-V	13JAN93
	0.644	17.7	66.3	8.6		14JAN93
3	0.646	19.4	66.6	9.5		14JUL92
	0.647	19.4	66.8	9.6		15JUL92
	0.645	19.5	66.1	9.5		16JUL92
	0.642	19.5	66.3	9.5		17JUL92
	0.640	18.0	67.0	8.8		21JUL92
	0.642	18.6	67.0	9.1	Unst. I-V	30JUL92
3	0.660	18.4	68.0	9.4		04JAN93
	0.666	18.3	68.3	9.5	Unst. I-V	05JAN93
	0.662	18.4	68.2	9.5		06JAN93
	0.660	18.1	67.6	9.3		07JAN93
	0.658	17.9	68.0	9.1		13JAN93
	0.658	17.7	67.5	9.0		14JAN93
6	0.639	19.0	64.2	8.9		14JUL92
	0.632	19.0	64.3	8.8		15JUL92
	0.635	19.0	65.9	9.1		16JUL92
	0.619	19.0	65.0	8.7		17JUL92
	0.625	17.8	65.9	8.4		21JUL92
	0.622	18.4	66.2	8.7		30JUL92
6	0.656	18.1	66.9	9.1	Unst. I-V	04JAN93
	0.640	18.0	66.4	8.7		05JAN93
	0.641	18.1	66.6	8.8		06JAN93
	0.635	17.9	66.4	8.6	Unst. I-V	07JAN93

Contact=ZnTe/Ni Sample=40724.31
(continued)

Cell #	V_{oc} (V)	J_{sc} (mA/cm^2)	FF (%)	P_{max} (mW/cm^2)	Comment	Date Tested
	0.624	17.4	66.2	8.2		13JAN93
	0.634	17.4	66.4	8.4		14JAN93
8	0.647	19.5	64.6	9.3		14JUL92
	0.650	19.4	64.7	9.3		15JUL92
	0.649	19.4	64.6	9.3		16JUL92
	0.636	19.4	64.7	9.1		17JUL92
	0.638	18.2	66.0	8.7		21JUL92
	0.645	18.9	66.2	9.2	Unst. I-V	30JUL92
8	0.670	18.6	66.5	9.5	Unst. I-V	04JAN93
	0.679	18.5	67.0	9.6	Unst. I-V	05JAN93
	0.665	18.6	66.3	9.3		06JAN93
	0.661	18.3	66.1	9.2	Unst. I-V	07JAN93
	0.651	17.9	66.6	8.9		13JAN93
	0.658	17.7	66.5	8.9		14JAN93

Contact=ZnTe/Au Sample=40708.13

Cell #	V_{oc} (V)	J_{sc} (mA/cm^2)	FF (%)	P_{max} (mW/cm^2)	Comment	Date Tested
1	0.593	15.7	47.2	5.0	Unst. I-V	04JAN93
	0.597	15.5	47.0	5.0	Unst. I-V	05JAN93
	0.607	15.7	50.0	5.4		06JAN93
	0.609	15.5	50.4	5.4		07JAN93
	0.610	15.5	50.6	5.4		12JAN93
	0.607	15.2	51.1	5.4		13JAN93
2	0.611	16.4	49.9	5.7	Unst. I-V	04JAN93
	0.606	16.6	54.2	6.2	Unst. I-V	05JAN93
	0.613	16.6	57.8	6.7		06JAN93
	0.612	16.5	55.8	6.4	Unst. I-V	07JAN93
	0.610	16.4	58.1	6.6	Unst. I-V	12JAN93
	0.607	16.1	58.0	6.5		13JAN93
3	0.637	19.7	46.8	6.7	Unst. I-V	04JAN93
	0.644	19.6	48.8	7.0	Unst. I-V	05JAN93
	0.639	19.4	49.1	7.0		06JAN93
	0.643	19.4	49.3	7.0		07JAN93
	0.642	19.3	50.5	7.1	Unst. I-V	12JAN93
	0.622	18.6	44.5	5.9		13JAN93
4	0.674	20.1	61.4	9.5		04JAN93
	0.669	19.9	59.1	9.0		05JAN93
	0.666	19.8	57.4	8.6		06JAN93
	0.656	19.5	54.7	8.0	Unst. I-V	07JAN93
	0.663	19.8	60.5	9.1	Unst. I-V	12JAN93
	0.652	19.3	57.8	8.3		13JAN93
5	0.660	19.9	52.2	7.8		04JAN93
	0.648	19.8	48.9	7.2		05JAN93
	0.649	19.4	49.3	7.1		06JAN93
	0.638	19.2	48.5	6.8	Unst. I-V	07JAN93
	0.652	19.0	48.5	6.9		12JAN93
	0.642	18.6	48.9	6.7		13JAN93
6	0.659	20.5	58.6	9.0		04JAN93
	0.650	20.5	59.3	9.0		05JAN93
	0.645	20.5	58.6	8.8		06JAN93
	0.637	20.2	57.7	8.5		07JAN93
	0.644	20.0	57.4	8.4		12JAN93
	0.668	19.6	60.0	9.0		14JAN93
7	0.677	20.3	60.4	9.5		04JAN93
	0.674	20.2	60.5	9.4	Unst. I-V	05JAN93
	0.672	20.2	59.8	9.3		06JAN93
	0.671	19.9	60.1	9.2		07JAN93
	0.671	19.6	59.4	8.9		12JAN93
	0.686	19.4	62.3	9.5		14JAN93
8	0.615	19.0	51.3	6.9		04JAN93
	0.593	18.9	50.9	6.5		05JAN93
	0.602	19.1	50.7	6.6		06JAN93
	0.605	18.9	50.4	6.6		07JAN93

Contact=ZnTe/Au Sample=40708.13
(continued)

Cell #	V_{oc} (V)	J_{sc} (mA/cm^2)	FF (%)	P_{max} (mW/cm^2)	Comment	Date Tested
	0.595	18.5	51.0	6.4		12JAN93
	0.606	18.2	50.9	6.4		14JAN93

Contact=ZnTe/Au Sample=40724.32

Cell #	V_{oc} (V)	J_{sc} (mA/cm^2)	FF (%)	P_{max} (mW/cm^2)	Comment	Date Tested
1	0.733	19.0	66.2	10.5	Unst. I-V	14JUL92
	0.733	18.9	66.1	10.5		15JUL92
	0.734	18.9	65.5	10.4	Unst. I-V	16JUL92
	0.730	19.0	66.0	10.5	Unst. I-V	17JUL92
	0.729	17.6	66.7	9.8	Unst. I-V	21JUL92
	0.727	18.2	66.2	10.0	Unst. I-V	30JUL92
1	0.724	17.8	65.0	9.6	Unst. I-V	04JAN93
	0.726	17.7	66.7	9.8	Unst. I-V	05JAN93
	0.727	17.7	65.2	9.6	Unst. I-V	06JAN93
	0.715	17.3	66.5	9.4	Unst. I-V	07JAN93
	0.720	17.3	66.0	9.4	Unst. I-V	13JAN93
	0.723	17.1	66.5	9.4		14JAN93
2	0.722	19.8	67.1	11.0		14JUL92
	0.721	19.7	67.1	10.9		15JUL92
	0.718	19.7	67.3	10.9		16JUL92
	0.719	19.9	66.7	10.9		17JUL92
	0.720	18.5	67.2	10.3	Unst. I-V	21JUL92
	0.718	19.1	67.1	10.5	Unst. I-V	30JUL92
2	0.715	18.7	66.9	10.2		04JAN93
	0.708	18.5	64.4	9.7	Unst. I-V	05JAN93
	0.716	18.5	66.4	10.1	Unst. I-V	06JAN93
	0.706	18.3	66.9	9.9	Unst. I-V	07JAN93
	0.709	18.0	66.7	9.8	Unst. I-V	13JAN93
	0.715	17.9	66.9	9.8	Unst. I-V	14JAN93
3	0.752	19.5	66.9	11.2	Unst. I-V	14JUL92
	0.754	19.5	66.4	11.2		15JUL92
	0.748	19.5	66.6	11.1		16JUL92
	0.751	9.6	66.8	11.2		17JUL92
	0.748	18.0	67.2	10.4	Unst. I-V	21JUL92
	0.748	18.7	66.8	10.7	Unst. I-V	30JUL92
3	0.745	18.4	66.6	10.5	Unst. I-V	04JAN93
	0.752	18.3	66.8	10.5	Unst. I-V	05JAN93
	0.747	18.3	66.3	10.4	Unst. I-V	06JAN93
	0.735	18.0	66.4	10.0	Unst. I-V	07JAN93
	0.740	17.8	66.8	10.1	Unst. I-V	13JAN93
	0.746	17.6	66.7	10.0	Unst. I-V	14JAN93
5	0.729	19.3	64.3	10.4	Unst. I-V	14JUL92
	0.737	19.3	63.8	10.4		15JUL92
	0.732	19.3	64.2	10.4		16JUL92
	0.732	19.4	64.0	10.4		17JUL92
	0.729	17.9	64.7	9.7	Unst. I-V	21JUL92
	0.729	18.6	64.8	10.1	Unst. I-V	30JUL92
5	0.731	18.4	64.1	9.8	Unst. I-V	04JAN93
	0.735	18.2	64.9	9.9	Unst. I-V	05JAN93
	0.730	18.3	64.5	9.8	Unst. I-V	06JAN93
	0.720	18.1	64.3	9.6	Unst. I-V	07JAN93

Contact=ZnTe/Au Sample=40724.32
(continued)

Cell #	V_{oc} (V)	J_{sc} (mA/cm^2)	FF (%)	P_{max} (mW/cm^2)	Comment	Date Tested
	0.726	17.7	64.5	9.5	Unst. I-V	13JAN93
	0.729	17.5	64.7	9.4	Unst. I-V	14JAN93
6	0.716	19.4	62.4	9.9	Unst. I-V	14JUL92
	0.721	19.4	62.4	10.0		15JUL92
	0.719	19.4	62.8	10.0		16JUL92
	0.714	19.5	61.7	9.8		17JUL92
	0.702	18.1	60.7	8.8		21JUL92
	0.705	18.8	61.5	9.3	Unst. I-V	30JUL92
6	0.703	18.5	61.7	9.2	Unst. I-V	04JAN93
	0.702	18.3	60.1	8.8	Unst. I-V	05JAN93
	0.700	18.5	60.6	9.0	Unst. I-V	06JAN93
	0.691	18.2	59.6	8.6	Unst. I-V	07JAN93
	0.693	17.7	59.0	8.3	Unst. I-V	13JAN93
	0.695	17.4	58.8	8.1	Unst. I-V	14JAN93
8	0.724	19.6	63.5	10.3	Unst. I-V	14JUL92
	0.727	19.6	64.0	10.4	Unst. I-V	15JUL92
	0.724	19.6	63.9	10.3		16JUL92
	0.723	19.6	64.0	10.4		17JUL92
	0.719	18.3	64.2	9.7	Unst. I-V	21JUL92
	0.719	19.0	64.5	10.1	Unst. I-V	30JUL92
8	0.716	18.8	64.1	9.8	Unst. I-V	04JAN93
	0.715	18.5	64.1	9.7	Unst. I-V	05JAN93
	0.713	18.5	62.4	9.4	Unst. I-V	06JAN93
	0.706	18.3	62.6	9.3	Unst. I-V	07JAN93
	0.712	17.7	63.3	9.1	Unst. I-V	13JAN93
	0.714	17.5	63.8	9.1	Unst. I-V	14JAN93

Contact=Cu/Au Sample=40703.12

Cell #	V_{oc} (V)	J_{sc} (mA/cm^2)	FF (%)	P_{max} (mW/cm^2)	Comment	Date Tested
3	0.670	22.3	54.5	9.3	Unst. I-V	04JAN93
	0.668	22.4	53.1	9.1	Unst. I-V	05JAN93
	0.675	22.0	54.0	9.1	Unst. I-V	06JAN93
	0.670	22.1	54.2	9.2		07JAN93
	0.678	22.0	54.7	9.3	Unst. I-V	12JAN93
	0.660	21.8	51.3	8.4	Unst. I-V	13JAN93
4	0.667	22.0	53.2	8.9	Unst. I-V	04JAN93
	0.684	22.0	53.8	9.3		05JAN93
	0.686	21.9	54.6	9.4		06JAN93
	0.675	21.9	54.9	9.3		07JAN93
	0.686	21.7	55.4	9.4	Unst. I-V	12JAN93
	0.682	21.6	54.6	9.2		13JAN93
6	0.673	19.1	53.7	7.9		04JAN93
	0.663	19.2	51.0	7.4	Unst. I-V	05JAN93
	0.633	19.0	43.9	6.0	Unst. I-V	06JAN93
	0.600	18.9	41.5	5.4	Unst. I-V	07JAN93
	0.623	18.8	43.1	5.8	Unst. I-V	12JAN93
	0.618	18.6	43.2	5.7	Unst. I-V	13JAN93
7	0.662	21.0	52.7	8.4	Unst. I-V	04JAN93
	0.667	21.0	53.2	8.5	Unst. I-V	05JAN93
	0.658	20.8	50.8	8.0	Unst. I-V	06JAN93
	0.655	20.8	51.3	8.0	Unst. I-V	07JAN93
	0.667	20.6	52.9	8.3	Unst. I-V	12JAN93
	0.657	20.4	51.9	7.9	Unst. I-V	13JAN93
8	0.687	21.0	55.2	9.1		04JAN93
	0.689	21.0	54.3	9.0		05JAN93
	0.680	21.0	53.7	8.7	Unst. I-V	06JAN93
	0.693	20.8	54.4	9.0		07JAN93
	0.693	20.6	55.0	9.0		12JAN93
	0.697	20.1	52.5	8.4		13JAN93

Contact=Cu/Au Sample=40708.32

Cell #	V_{oc} (V)	J_{sc} (mA/cm^2)	FF (%)	P_{max} (mW/cm^2)	Comment	Date Tested
1	0.715	17.8	68.3	9.9		04JAN93
	0.713	17.7	68.4	9.9	Unst. I-V	05JAN93
	0.712	17.6	68.4	9.8		06JAN93
	0.712	17.4	67.4	9.5		07JAN93
	0.714	17.3	68.2	9.6		12JAN93
	0.563	17.0	39.1	4.3		14JAN93
2	0.735	18.2	68.0	10.4		04JAN93
	0.726	18.1	67.5	10.1		05JAN93
	0.719	18.1	67.5	10.0		06JAN93
	0.722	18.0	65.9	9.8		07JAN93
	0.725	17.8	66.3	9.8		12JAN93
	0.718	17.7	66.5	9.7		14JAN93
3	0.682	18.1	68.1	9.6		04JAN93
	0.680	18.0	68.2	9.6		05JAN93
	0.682	17.9	67.4	9.4		06JAN93
	0.681	17.8	67.2	9.3		07JAN93
	0.682	17.7	68.0	9.4		12JAN93
	0.675	17.4	67.9	9.1		14JAN93
4	0.721	19.0	70.2	11.0		04JAN93
	0.719	18.9	69.9	10.9		05JAN93
	0.716	18.9	69.7	10.8		06JAN93
	0.718	18.7	69.8	10.7		07JAN93
	0.713	18.5	68.9	10.4		12JAN93
	0.711	18.3	69.7	10.3		14JAN93
5	0.669	19.1	67.8	9.9		04JAN93
	0.670	19.0	67.2	9.8		05JAN93
	0.672	19.0	66.1	9.6		06JAN93
	0.670	18.7	66.8	9.6		07JAN93
	0.668	18.5	66.9	9.4		12JAN93
	0.668	18.2	66.0	9.2		14JAN93
6	0.705	19.2	70.0	10.8		04JAN93
	0.707	19.1	69.7	10.8		05JAN93
	0.706	19.2	69.6	10.8		06JAN93
	0.705	18.9	69.7	10.6		07JAN93
	0.700	18.7	69.6	10.4		12JAN93
	0.704	18.4	69.4	10.3		14JAN93
7	0.682	20.1	68.9	10.8	Unst. I-V	04JAN93
	0.683	20.0	68.5	10.7		05JAN93
	0.686	20.0	67.7	10.6		06JAN93
	0.683	19.7	68.3	10.5		07JAN93
	0.684	19.5	67.7	10.3		12JAN93
	0.684	19.1	67.8	10.1		14JAN93
8	0.725	19.1	69.4	11.0	Unst. I-V	04JAN93
	0.720	19.1	69.0	10.8		05JAN93
	0.720	19.2	68.6	10.8		06JAN93
	0.718	18.9	68.4	10.6		07JAN93

Contact=Cu/Au Sample=40708.32
(continued)

Cell #	V_{oc} (V)	J_{sc} (mA/cm^2)	FF (%)	P_{max} (mW/cm^2)	Comment	Date Tested
	0.717	18.3	67.6	10.1		12JAN93
	0.715	18.0	67.2	9.9		14JAN93

Contact=Cu/Au Sample=40721.12

Cell #	V_{oc} (V)	J_{sc} (mA/cm^2)	FF (%)	P_{max} (mW/cm^2)	Comment	Date Tested
1	0.698	19.7	65.9	10.4		14JUL92
	0.693	19.7	64.8	10.1		15JUL92
	0.697	19.7	64.3	10.1	Unst. I-V	16JUL92
	0.684	19.8	63.8	9.9	Unst. I-V	17JUL92
	0.694	19.8	64.5	10.1		21JUL92
	0.687	18.9	63.6	9.4	Unst. I-V	30JUL92
1	0.696	18.5	60.8	9.0		04JAN93
	0.683	18.4	59.3	8.5	Unst. I-V	05JAN93
	0.680	18.4	59.1	8.4		06JAN93
	0.682	18.1	58.8	8.3	Unst. I-V	07JAN93
	0.681	18.1	59.3	8.4		12JAN93
	0.685	17.9	59.8	8.4		14JAN93
2	0.711	20.1	66.1	10.8	Unst. I-V	14JUL92
	0.705	20.1	64.7	10.5	Unst. I-V	15JUL92
	0.708	20.1	66.6	10.8		16JUL92
	0.702	20.1	66.1	10.7		17JUL92
	0.710	20.6	66.6	11.1		21JUL92
	0.701	19.6	66.4	10.4		30JUL92
2	0.714	18.9	64.8	10.0		04JAN93
	0.703	18.8	63.5	9.6	Unst. I-V	05JAN93
	0.698	19.0	63.3	9.6		06JAN93
	0.701	18.6	62.9	9.4		07JAN93
	0.691	18.6	63.5	9.3		12JAN93
	0.698	18.5	63.4	9.3		14JAN93
3	0.674	18.8	60.5	8.8	Unst. I-V	14JUL92
	0.675	19.0	61.9	9.0	Unst. I-V	15JUL92
	0.670	19.0	61.8	9.0	Unst. I-V	16JUL92
	0.660	19.0	61.2	8.8	Unst. I-V	17JUL92
	0.671	19.1	63.3	9.3	Unst. I-V	21JUL92
	0.664	18.3	62.7	8.7	Unst. I-V	30JUL92
3	0.685	17.8	60.5	8.4	Unst. I-V	04JAN93
	0.673	17.8	59.8	8.2	Unst. I-V	05JAN93
	0.669	17.9	58.6	8.0	Unst. I-V	06JAN93
	0.670	17.6	59.2	8.0	Unst. I-V	07JAN93
	0.666	17.6	59.1	7.9	Unst. I-V	12JAN93
	0.671	17.3	59.9	7.9		14JAN93
4	0.708	20.7	64.9	10.9		14JUL92
	0.707	20.7	64.8	10.9	Unst. I-V	15JUL92
	0.690	20.5	60.1	9.7	Unst. I-V	16JUL92
	0.693	20.7	61.0	10.0	Unst. I-V	17JUL92
	0.702	21.2	63.2	10.8	Unst. I-V	21JUL92
	0.691	20.1	62.7	10.0	Unst. I-V	30JUL92
4	0.709	19.5	61.6	9.7		04JAN93
	0.696	19.5	60.9	9.4		05JAN93
	0.692	19.6	59.2	9.2		06JAN93
	0.687	19.3	59.3	9.0	Unst. I-V	07JAN93

Contact=Cu/Au Sample=40721.12
(continued)

Cell #	V_{oc} (V)	J_{sc} (mA/cm^2)	FF (%)	P_{max} (mW/cm^2)	Comment	Date Tested
	0.684	19.2	58.1	8.7		12JAN93
	0.685	18.9	59.2	8.8		14JAN93
5	0.671	20.5	58.1	9.1	Unst. I-V	14JUL92
	0.660	20.3	55.9	8.5	Unst. I-V	15JUL92
	0.653	20.3	55.4	8.4	Unst. I-V	16JUL92
	0.655	20.3	55.4	8.4	Unst. I-V	17JUL92
	0.655	20.8	55.5	8.6	Unst. I-V	21JUL92
	0.654	19.8	57.6	8.5	Unst. I-V	30JUL92
5	0.650	19.4	55.6	8.0	Unst. I-V	04JAN93
	0.650	19.4	54.4	7.8	Unst. I-V	05JAN93
	0.646	19.5	54.2	7.8		06JAN93
	0.644	19.2	54.3	7.7		07JAN93
	0.645	19.0	55.5	7.8		12JAN93
	0.648	18.7	55.7	7.7		14JAN93
6	0.680	20.6	55.3	8.9	Unst. I-V	14JUL92
	0.671	20.6	54.8	8.7	Unst. I-V	15JUL92
	0.679	20.6	53.4	8.6	Unst. I-V	16JUL92
	0.673	20.7	54.3	8.6	Unst. I-V	17JUL92
	0.677	21.4	55.4	9.2	Unst. I-V	21JUL92
	0.668	20.2	53.9	8.3	Unst. I-V	30JUL92
6	0.660	19.6	52.3	7.7	Unst. I-V	04JAN93
	0.663	19.5	52.4	7.7	Unst. I-V	05JAN93
	0.658	19.6	52.8	7.8		06JAN93
	0.663	19.3	52.8	7.7	Unst. I-V	07JAN93
	0.658	19.0	53.7	7.7	Unst. I-V	12JAN93
	0.660	18.8	53.5	7.6	Unst. I-V	14JAN93
7	0.649	20.7	54.0	8.3	Unst. I-V	14JUL92
	0.661	20.8	54.3	8.6	Unst. I-V	15JUL92
	0.646	20.8	52.5	8.1		16JUL92
	0.657	20.8	54.0	8.4	Unst. I-V	17JUL92
	0.656	21.3	54.4	8.7	Unst. I-V	21JUL92
	0.651	20.2	54.5	8.2	Unst. I-V	30JUL92
7	0.632	19.8	52.0	7.4	Unst. I-V	04JAN93
	0.643	19.8	51.2	7.5		05JAN93
	0.635	20.0	51.1	7.4		06JAN93
	0.638	19.6	51.1	7.3	Unst. I-V	07JAN93
	0.497	16.9	34.9	3.3	Unst. I-V	13JAN93
	0.525	17.4	38.8	4.0	Unst. I-V	14JAN93
8	0.663	20.4	51.3	7.9	Unst. I-V	14JUL92
	0.653	20.4	49.7	7.6	Unst. I-V	15JUL92
	0.652	20.4	47.6	7.2	Unst. I-V	16JUL92
	0.651	20.4	48.5	7.4	Unst. I-V	17JUL92
	0.649	21.3	46.6	7.4	Unst. I-V	21JUL92
	0.645	20.0	50.4	7.4	Unst. I-V	30JUL92
8	0.632	19.6	51.0	7.2	Unst. I-V	04JAN93

Contact=Cu/Au Sample=40721.12
(continued)

Cell #	V_{oc} (V)	J_{sc} (mA/cm^2)	FF (%)	P_{max} (mW/cm^2)	Comment	Date Tested
	0.626	19.5	50.1	7.0	Unst. I-V	05JAN93
	0.622	19.7	49.8	7.0	Unst. I-V	06JAN93
	0.631	19.3	50.0	7.0	Unst. I-V	07JAN93
	0.625	18.9	50.6	6.8	Unst. I-V	13JAN93
	0.630	18.7	50.2	6.8	Unst. I-V	14JAN93

Document Control Page	1. NREL Report No.	2. NTIS Accession No.	3. Recipient's Accession No.
	NREL/TP-451-5755	DE93018213	

4. Title and Subtitle

Polycrystalline Thin Film Materials and Devices

5. Publication Date

August 1993

6.

7. Author(s)

R.W. Birkmire, J.E. Phillips, W.N. Shafarman, S.S. Hegedus, B.E. McCandless, T.A. Yokimcus

8. Performing Organization Rept. No.

9. Performing Organization Name and Address

Institute of Energy Conversion
University of Delaware
Newark, Delaware 19716-3820

10. Project/Task/Work Unit No.

PV331101

11. Contract (C) or Grant (G) No.

(C) XN-0-10023-1

(G)

12. Sponsoring Organization Name and Address

National Renewable Energy Laboratory
1617 Cole Blvd.
Golden, CO 80401-3393

13. Type of Report & Period Covered

Technical Report
16 January 1990 - 15 January 1993

14.

15. Supplementary Notes

NREL technical monitor: B. von Roedern

16. Abstract (Limit: 200 words)

This report describes results and conclusions of the final phase (III) of a three-year research program on polycrystalline thin-film heterojunction solar cells. The research consisted of the investigation of the relationships between processing, materials properties, and device performance. This relationship was quantified by device modeling and analysis. The analysis of thin-film polycrystalline heterojunction solar cells explains how minority-carrier recombination at the metallurgical interface and at grain boundaries can be greatly reduced by the proper doping of the window and absorber layers. Additional analysis and measurements show that the present solar cells are limited by the magnitude of the diode current, which appears to be caused by recombination in the space charge region. Developing an efficient commercial-scale process for fabricating large-area polycrystalline, thin-film solar cells from a research process requires a detailed understanding of the individual steps in making the solar cell, and their relationship to device performance and reliability. The complexities involved in characterizing a process are demonstrated with results from our research program on $CuInSe_2$ and CdTe processes.

17. Document Analysis

a. Descriptors

polycrystalline ; thin films ; photovoltaics ; solar cells

b. Identifiers/Open-Ended Terms

c. UC Categories

273

18. Availability Statement

National Technical Information Service
U.S. Department of Commerce
5285 Port Royal Road
Springfield, VA 22161

19. No. of Pages

136

20. Price

A07

Form No. 0069E (6-30-87)